UNIVERSITY OF CALIFORNIA
RIVERSIDE

# Anomalous Higgs Yukawa Couplings from Radiative Masses and Related Phenomena

A Dissertation submitted in partial satisfaction
of the requirements for the degree of

Doctor of Philosophy

in

Physics

by

Sean Patrick Fraser

August 2016

Dissertation Committee:

Dr. Ernest Ma, Chairperson
Dr. Jose Wudka
Dr. Hai-Bo Yu

The Dissertation of Sean Patrick Fraser is approved:

---

---

---

Committee Chairperson

University of California, Riverside

## Acknowledgments

I would like to express my gratitude to my advisor Dr. Ernest Ma, whose inspiration, guidance, patience, and support have made this work possible. I am also very grateful to Dr. Hai-Bo Yu and Dr. Jose Wudka for their advice and assistance. I thank each of them for taking the time to share their insights and expertise.

I would also like to express my thanks to Dr. Alexander Natale, Oleg Popov, Mohammadreza Zakeri, Corey Kownacki, and Nicholas Pollard for many enlightening discussions and collaborative works. I would also like to thank Dr. Subhaditya Bhattacharya and Dr. Daniel Wegman for very helpful group meetings, and Shakiba Haji Sadeghi, Tao Ren and Blake Pollard for useful conversations.

This thesis is based on material that was previously published with my co-authors in Refs. [1–6]. This work is also supported in part by the U. S. Department of Energy under Grant No. DESC0008541.

# ABSTRACT OF THE DISSERTATION

Anomalous Higgs Yukawa Couplings from Radiative Masses and Related Phenomena

by

Sean Patrick Fraser

Doctor of Philosophy, Graduate Program in Physics
University of California, Riverside, August 2016
Dr. Ernest Ma, Chairperson

The experimentally accessible branching fractions of the 125 GeV particle discovered in 2012 are consistent with the Higgs boson of the standard model (SM), but they are not yet conclusive due to large experimental uncertainties. Of particular interest are the inferred Yukawa couplings of the Higgs boson to a heavy quark or charged lepton. In the SM, this is given by a tree-level expression in which the Yukawa coupling is proportional to the fermion mass. We consider instead a radiative origin of fermion mass which occurs in one loop through dark matter. It is shown that the effective Higgs Yukawa coupling can have significant deviations from the SM, with potential consequences for Higgs production and decay. The radiative model also explains the muon anomalous magnetic moment, with predictions for rare lepton decays in parallel with a radiative model of neutrino mass based on the inverse seesaw. Also considered are three other possible extensions of the SM, with tree-level masses for charged fermions: A Higgs triplet model of radiative neutrino mass with dark matter and collider phenomenology, a vector dark matter model with relic density and direct detection analysis, and a supersymmetric model which relaxes the constraints

on the Higgs mass and accommodates the recent 750 GeV diphoton excess.

# Contents

# List of Figures

# List of Tables

# Chapter 1

# Introduction

## 1.1 Outline: Looking for New Physics

The standard model (SM) is a renormalizable theory because it is based on a local gauge symmetry. Phenomenologically, this symmetry is

$$SU(3)_C \times SU(2)_L \times U(1)_Y \tag{1.1}$$

The particle content and real gauge fields before spontaneous electroweak symmetry breaking are shown in Table 1.1, which assumes a minimal scalar sector consisting of a single Higgs doublet. No further symmetries are imposed other than the local gauge symmetry. The SM has been extremely successful in explaining the fundamental interactions of the observed particles and in confirming a wide range of experimental results. Even so, the SM cannot be a complete theory because neutrino mass and dark matter are not included. Throughout this thesis, several explanations of these will be given. All neutrino masses considered will be Majorana. The types of dark matter considered will be scalar, fermionic,

| Particle | | | | $SU(3)_C$ | $SU(2)_L$ | $Y$ |
|---|---|---|---|---|---|---|
| strong force | | $g_a$ | | **8** | **1** | 0 |
| weak isospin | | $W_a$ | | **1** | **3** | 0 |
| weak hypercharge | | $B$ | | **1** | **1** | 0 |
| $Q'_{iL}$ | $=$ | $\begin{pmatrix} u'_L \\ d'_L \end{pmatrix}$ | $\begin{pmatrix} c'_L \\ s'_L \end{pmatrix}$ | $\begin{pmatrix} t'_L \\ b'_L \end{pmatrix}$ | **3** | **2** | 1/6 |
| $u'_{iR}$ | $=$ | $u'_R$ | $c'_R$ | $t'_R$ | **3** | **1** | 2/3 |
| $d'_{iR}$ | $=$ | $d'_R$ | $s'_R$ | $b'_R$ | **3** | **1** | $-1/3$ |
| $L'_{iL}$ | $=$ | $\begin{pmatrix} \nu'_{eL} \\ e'_L \end{pmatrix}$ | $\begin{pmatrix} \nu'_{\mu L} \\ \mu'_L \end{pmatrix}$ | $\begin{pmatrix} \nu'_{\tau L} \\ \tau'_L \end{pmatrix}$ | **1** | **2** | $-1/2$ |
| $e'_{iR}$ | $=$ | $e'_R$ | $\mu'_R$ | $\tau'_R$ | **1** | **1** | $-1$ |
| $\Phi$ | $=$ | $\begin{pmatrix} \phi^+ \\ \phi^0 \end{pmatrix}$ | | | **1** | **2** | 1/2 |

Table 1.1: Particle content in the standard model.

and vector. The radiative mass models that will be studied are all inspired by the original scotogenic model [7], where the loop diagram responsible for neutrino mass has particles from the dark sector propagating in the loop.

The recent discovery [8, 9] of the 125 GeV particle at the Large Hadron Collider (LHC) is, on the one hand, a long-awaited confirmation of the Higgs boson in the SM. At the same time, it is also an opportunity for new discoveries, because the current experimental uncertainty of the measurement allows other models to be considered that are consistent with the data. Part I of this thesis is a unified discussion consisting of Chapters 2, 3, 4. The motivation is to reexamine the assumption previously made in radiative mass models that the effective Higgs Yukawa interactions are unaffected. The results are new, and may be important for the LHC era. Chapter 2 focuses on heavy quarks and leptons in a model of radiative fermion mass through dark matter. The purpose is to demonstrate that the

effective Higgs Yukawa coupling can have significant and measurable deviations from the SM, and that the new particles are within reach of the LHC. It will also be established that the radiative contribution to the muon magnetic moment has the correct sign and magnitude to explain the anomaly with the SM. Chapter 3 develops a new radiative implementation of the inverse seesaw for neutrino mass. This is adapted for use in Chapter 4, which adds a discrete flavor symmetry to encompass the entire lepton sector and incorporate real scalar dark matter.

The motivation for Part II of this thesis is to explore other extensions of the SM with tree-level masses for charged fermions. Chapter 5 uses a scalar Higgs triplet extension for radiative inverse seesaw neutrino mass. Chapter 6 uses an $SU(2)_N$ gauge extension for vector dark matter. Chapter 7 uses a $U(1)$ gauge extension of with supersymmetry, with an emphasis on explaining the recent preliminary LHC measurement of a diphoton excess. This bears some relation to the diphoton Higgs decay covered in Chapter 2.

Finally, the conclusion and bibliography are given in Part III. The remainder of this introductory chapter is a brief review of some relevant concepts and technical details.

## 1.2 Fermion Masses and Mixings

The measured fermion masses and mixing parameters [10] are shown in Table 1.2 and Table 1.3. Part I of this thesis fits into a larger theoretical framework that links flavor symmetry and dark matter [11] with the long-term goal of deciphering these patterns.
In the SM, the masses and mixing derive from the Higgs Yukawa interactions for the fermions listed in the previous Table 1.1. For quarks an additional color index is understood. The

| quarks | | | masses in GeV | | |
|---|---|---|---|---|---|
| $u$ | $c$ | $t$ | $3 \times 10^{-3}$ | 1.3 | 175 |
| $d$ | $s$ | $b$ | $6 \times 10^{-3}$ | 0.1 | 4.3 |

| $U_{CKM}$ | |
|---|---|
| $\theta_{12}$ | $13^\circ$ |
| $\theta_{23}$ | $2^\circ$ |
| $\theta_{13}$ | $0.2^\circ$ |
| $\delta_{CP}$ | $60^\circ$ |

Table 1.2: Quark masses and mixing parameters in the standard model.

| leptons | | | masses in GeV | | |
|---|---|---|---|---|---|
| $e$ | $\mu$ | $\tau$ | $5 \times 10^{-4}$ | 0.1 | 1.77 |
| $\nu_1$ | $\nu_2$ | $\nu_3$ | $\sim 10^{-8}$ | $\sim 10^{-8}$ | $\sim 10^{-8}$ |

| $U_{PMNS}$ | |
|---|---|
| $\theta_{12}$ | $34^\circ$ |
| $\theta_{23}$ | $45^\circ$ |
| $\theta_{13}$ | $8^\circ$ |
| $\delta_{CP}$ | $-108^\circ$ |

Table 1.3: Lepton masses and mixing parameters in the standard model.

primed fields denote fermions in an arbitrary interaction basis, as opposed to the physical mass basis. This is a general feature that will be encountered throughout this thesis. The particles that carry charge under the gauge group or other symmetries are not necessarily mass eigenstates because they can mix due to interactions. In terms of the primed fields, the Higgs Yukawa interactions are

$$\mathcal{L}_{Yukawa} = -f^e_{ij}\, \overline{L'_{iL}}\, \Phi\, e'_{jR} - f^d_{ij}\, \overline{Q'_{iL}}\, \Phi\, d'_{jR} - f^u_{ij}\, \overline{Q'_{iL}}\, \widetilde{\Phi}\, u'_{jR} + h.c. \tag{1.2}$$

where the couplings $f^e, f^d, f^u$ are $3\times3$ complex matrices in generation space, and the dual of the Higgs doublet is $\widetilde{\Phi} = i\sigma_2\Phi^*$. The hermitian conjugate terms in Eq. (1.2) for the charged leptons are shown in Fig. 1.1, with similar diagrams for the up and down type quarks. Mass terms for fermions and gauge bosons are not explicitly present in the SM Lagrangian because they do not respect the local gauge symmetry, but they will be generated when the

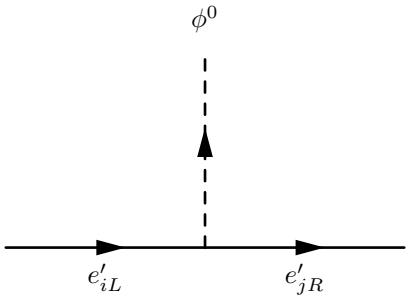


Figure 1.1: Higgs Yukawa interaction for charged leptons.

electroweak part of the gauge group is spontaneously broken. The virtue of breaking a local gauge symmetry spontaneously is that the theory remains renormalizable. This strategy will be used throughout this thesis for other scalars besides the Higgs. In the SM, the electroweak part of the gauge group is spontaneously broken down to the electromagetic gauge group $U(1)_Q$

$$SU(2)_L \times U(1)_Y \to U(1)_Q \tag{1.3}$$

where $Q = T_3 + Y$. This occurs when the neutral component of the Higgs doublet develops a nonzero vacuum expectation value (VEV). In the unitary gauge, this is

$$\langle \Phi \rangle = \begin{pmatrix} 0 \\ v/\sqrt{2} \end{pmatrix} \tag{1.4}$$

which allows the three scalar degrees of freedom contained in $\phi^+$ and $Im(\phi^0)$ to be gauged away. These scalar degrees of freedom are essentially absorbed by three combinations of the four originally real massless gauge fields $W_{1,2,3}$ and $B$, which are mixed into the massive vector bosons $W^{\pm}, Z$ and the massless photon $A$. The real part $Re(\phi^0)$ contains the SM Higgs $h$. The masses $m_h, m_W, m_Z$ are all of order the electroweak energy scale

$$v/\sqrt{2} = 174 \text{ GeV} \tag{1.5}$$

which is the only mass scale in the theory (apart from the non-perturbative QCD scale $\Lambda_{QCD} \sim 200$ MeV). The real part of $\phi^0$ generates the two terms

$$Re(\phi^0) = (v + h)/\sqrt{2} \tag{1.6}$$

The massive Higgs boson $h$ retains Yukawa interactions with the charged fermions, and the VEV generates complex mass matrices $M^{e,d,u} = f^{e,d,u}\ (v/\sqrt{2})$

$$\mathcal{L}_{Yukawa} \supset -\overline{e'_{iL}}\ M^e_{ij}\ e'_{jR} - \overline{d'_{iL}}\ M^d_{ij}\ d'_{jR} - \overline{u'_{iL}}\ M^u_{ij}\ u'_{jR} + h.c. \tag{1.7}$$

Arbitrary unitary rotations of the left-handed and right-handed fermion fields, for example $e''_{iL} = (U^e_L)_{ij}\, e'_{jL}$ and $e''_{iR} = (U^e_R)_{ij}\, e'_{jR}$, will keep the fermion kinetic terms diagonal. A specific set of unitary rotations $U^{e,d,u}_L$ and $U^{e,d,u}_R$ will diagonalize the mass matrices $M^{e,d,u}$ and so they will also diagonalize the coupling matrices $f^{e,d,u}$. For charged leptons

$$diag(m_e, m_\mu, m_\tau) = U^e_L\ f^e\ U^{e\,\dagger}_R\ (v/\sqrt{2}) \tag{1.8}$$

and similarly for quarks. This is the familiar SM result that the fermion mass is proportional to the Higgs Yukawa coupling in the physical mass basis. The replacement of $\phi^0$ with $\langle \phi^0 \rangle$ in Fig. 1.1 turns this three-point interaction into a two-point interaction. In the diagonal mass basis, it is a connection between only two massless fermions in the same generation. For example, the electron mass eigenstate has the infinite series of diagrams shown in Fig. 1.2. This infinte series can be formally summed to give

$$m_e\, \overline{e}e \quad = \quad m_e\, (\overline{e_L} e_R + \overline{e_R} e_L) \tag{1.9}$$

which is the statement that the inherently massless particles $e_L$ and $e_R$ have paired up to

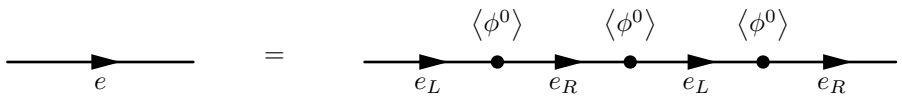


Figure 1.2: Electron mass as an infinite series with Higgs VEV.

become one massive Dirac particle $e = e_L + e_R$ in the presence of the Higgs VEV. Part I of this thesis is a fundamental modification of the Yukawa sector Eq. (1.2), and radiative versions of Fig. 1.1 will be studied in Chapters 2 and 4. Each two-point vertex in Fig. 1.2 will be replaced by an effective two-point vertex caused by radiative loops.

The unitary rotations that diagonallize the Yukawa couplings will not, however, diagonalize the charged current weak interactions. In the physical mass basis, the mismatch between left-handed rotations results in nondiagonal flavor mixing

$$\begin{aligned} \mathcal{L}_{Quarks} &\supset \frac{g}{\sqrt{2}}\, W_\mu^+\, \overline{u_{iL}}\, \gamma^\mu\, U_{CKM\,ij}\; d_{jL} \quad + \quad h.c. \\ \mathcal{L}_{Leptons} &\supset \frac{g}{\sqrt{2}}\, W_\mu^-\, \overline{e_{iL}}\, \gamma^\mu\, U_{PMNS\,ij}\; \nu_{jL} \quad + \quad h.c. \end{aligned} \tag{1.10}$$

which defines the unitary mixing matrices

$$\begin{aligned} U_{CKM} &= U_L^u\, U_L^{d\,\dagger} \quad \sim \quad \begin{pmatrix} 1 & 0.2 & 0 \\ -0.2 & 1 & 0 \\ 0 & 0 & 1 \end{pmatrix} \\ U_{PMNS} &= U_L^e\, U_L^{\nu\,\dagger} \quad \sim \quad \begin{pmatrix} \sqrt{2/3} & \sqrt{1/3} & 0 \\ -\sqrt{1/6} & \sqrt{1/3} & -\sqrt{1/2} \\ -\sqrt{1/6} & \sqrt{1/3} & \sqrt{1/2} \end{pmatrix} \end{aligned} \tag{1.11}$$

where the approximate structure shown corresponds to the mixing parameters given earlier in Tables 1.2 and Table 1.3. Beyond the SM, flavor symmetry may help to understand if there is a deeper reason for the mismatch between the left-handed field rotations which produce $U_{CKM}$ and $U_{PMNS}$. The following chapters will focus on the lepton sector, and the flavor symmetries $Z_3$ and $A_4$ will be used in Chapters 3 and 4, respectively. In the radiative models that will be considered, the field rotations are determined by the particle content and the full symmetry assignments. In Chapter 3, only $\nu'_{iL}$ will be rotated. In Chapter 5, only $e'_{iL}$ will be rotated. In Chapter 4, both $e'_{iL}$ and $\nu'_{iL}$ will be rotated.

## 1.3 Neutrinos

In the SM, neutrinos are massless becasue they are left-handed and do not have interactions with any right-handed fields. Of course, this must be remedied in light of the observed neutrino oscillations. A simple solution is to add three right-handed neutrinos $N_{iR}$ with $(SU(3)_C, SU(2)_L, Y) = (\mathbf{1}, \mathbf{1}, 0)$, that is, $N_{iR}$ are singlets under the full gauge group. The new Lagrangian terms are the usual kinetic terms for $N_{iR}$ and the Dirac Yukawa interaction

$$\mathcal{L}_{Dirac} = -f^{\nu}_{ij}\, \overline{L'_{iL}}\, \widetilde{\Phi}\, N_{jR} \quad + \quad h.c. \tag{1.12}$$

The diagram for the hermitian conjugate term is shown in Fig. 1.3. This will generate Dirac mass terms after spontaneous symmetry breaking, but they are not the only possible mass terms. Explicit mass terms are also allowed by the gauge symmetry using the conjugate

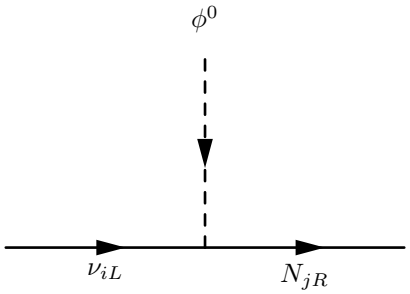


Figure 1.3: Higgs Yukawa interaction for left- and right-handed neutrinos.

fields $(N_{iR})^c$. These invariant Majorana mass terms are

$$\mathcal{L}_{Majorana} = -\mu_{ij}\ \overline{(N_{jR})^c}\ N_{iR} - \mu^*_{ij}\ \overline{N_{iR}}\ (N_{jR})^c \tag{1.13}$$

and the corresponding Feynman diagrams are shown in Fig. 1.4. The conventional direction of arrows illustrates that in the first term a right-handed particle goes in and a left-handed particle goes out, and in the second term a left-handed particle goes in and a right-handed particle goes out. Thus a pure Majorana particle constantly transforms on its own between left- and right-handed chiralities because of its Majorana mass. If both Dirac and Majorana mass terms are present, the general outcome will be six Majorana particles with different masses. For illustration, consider only one generation $N_L$ and $N_R$. The distinction between a pure Dirac particle $N_{Dirac} = N_L + N_R$ and a pure Majorana particle $N_{Majorana} = N_L + (N_L)^c$ is the existence of extra degrees of freedom from $N_R$. As a final comment, neutrinos in the


Figure 1.4: Majorana mass terms for right-handed neutrinos.

SM do not have Majorana mass terms $\overline{(\nu_{jL})^c}\,\nu_{iL} + h.c.$ because these terms do not conserve weak isopin or hypercharge. However, in other models these terms can be generated from the VEV of a Higgs triplet, as will be done in Chapter 5 although not at tree-level. The use of a Higgs triplet VEV to generate Majorana mass terms will also appear in Chapter 6 at tree-level, but applied instead to new fermions $n_{iL}$ rather than the SM $\nu_{iL}$, and also applied to new right-handed fermions $n_{iR}$.

## 1.4 Naturalness

Pure Dirac neutrinos require the arbitrary assumption $\mu_{ij} = 0$, but this can be remedied by the imposition of an exactly conserved global $U(1)_L$ symmetry, namely lepton number $L = +1$ for $L_{iL}, e_{iR}, N_{iR}$. This will forbid the Majorana terms since they break $L$ by two units. A shortcoming is that this does not give any insight into why the Dirac Yukawa couplings should be so much smaller for neutrinos compared to charged fermions. Closely related to this are pseudo-Dirac neutrinos which occur when $\mu_{ij}$ is small, which could be considered natural in the 't Hooft sense. A parameter is allowed to be small and is considered natural in the 't Hooft sense if taking that parameter to be small enhances a symmetry in the Lagrangain. The Majorana terms break $L$ by two units, but this breaking is small when $\mu_{ij}$ is small, so the global $U(1)_L$ symmetry is enhanced.

A pure Dirac particle that carries no $U(1)$ charges can be written as the superposition of two mass-degenerate Majorana particles. Genuine Majorana neutrinos occur when $\mu_{ij}$ is not too small and this degeneracy is removed. The well-known canonical seesaw mechanism occurs when one or more components $\mu_{ij} \sim M \gg v$, where $M$ is a new inherent

mass scale of the new physics responsible for the heavy Majorana neutrinos. Extremely small neutrino masses are then explained by a very large but otherwise arbitrary mass scale $M$. Light neutrino masses in the eV range can be obtained with $M \sim 10^9$ GeV and Dirac Higgs Yukawa couplings $f \sim 1$. This mechanism is used in Chapter 7. Various other cases $\mu_{ij} \sim \text{eV}, \text{keV}, \text{MeV}, \text{GeV}, \text{TeV}, \gtrsim 10^9 \text{GeV}$ are surveyed in Ref. [12]. These are tree-level neutrino masses. Radiative neutrino masses will be considered in Chapters 3, 4 and 5.

For charged leptons, it could be argued that the small Yukawa couplings are natural in the 't Hooft sense because in the limit when they are all zero the SM Lagrangian possesses an accidental symmetry [13] of unitary rotations. Even so, the numerical values and ordering are unexplained. Similarly for quarks, there is an accidental symmetry of unitary rotations in the zero mass limit. But this argument does not apply to the top quark. Its Higgs Yukawa coupling is of order 1, which by itself is not unusual because this gives a mass of the same order as the Higgs VEV. But then it is difficult to understand why the other quarks are so light. The radiative mass models in this thesis respond to these questions.

## 1.5 Quantum Corrections

Although they are not imposed, two global $U(1)$ symmetries exist at tree-level in the SM Lagrangian. They are therefore accidental symmetries. There is a global $U(1)_B$ symmetry for baryon number a global $U(1)_L$ symmetry for lepton number, where quarks have $B = +1/3$ and leptons have $L = +1$. A global symmetry has an associated conserved current that can be computed at the tree level, that is, at the classical level. There will also be corrections which occur at the one-loop level or higher, that is, at the quantum

level. At the quantum level, neither $B$ nor $L$ is conserved, but the combination $B - L$ is conserved. For this reason, the SM actually possesses only one true global symmetry, which is $U(1)_{B-L}$. So in the previous section, it is actually more precise to say that Majorana terms are forbidden by conservation of $B - L$ rather than by conservation of $L$. Even so, it is usually not a problem if a global symmetry becomes anomalous at the quantum level [14]

But for a local symmetry, that is, a gauge symmetry, its associated current must be conserved when the quantum corrections are included, otherwise the theory will not be renormalizable. This involves checking triangle loop diagrams with three external gauge bosons connected to fermions in the loop, and all the diagrams must add to zero so that there is no gauge anomaly. That is, the theory must be anomaly-free. It can be shown that the SM is anomaly-free, based on the its gauge symmetry and particle content. Throughout this thesis, either the gauge symmetry or the particle content will be enlarged, and the anomaly-free condition must be satisfied. In the simplest extensions, it is arranged so that any additional contributions from new left- and right-handed fermions cancel. In the earlier section 1.3, this was not an issue when adding the three right-handed neutrinos $N_{iR}$ because they are gauge singlets, which means they do not have gauge interactions and therefore do not contribute to the triangle diagrams.

Radiative mass models make use of the fact that any tree-level diagram receives quantum corrections from higher-order loop diagrams. Consider divergences that appear during renormalization. The original work of Symanzik [15, 16] illustrates that when a symmetry-breaking term is added to an initially symmetric Lagrangian, no new divergences are introduced with dimension greater than that of the symmetry-breaking term. In essence,

a soft-breaking term leaves a remnant of the initial symmetry, whereas a hard breaking term destroys the initial symmetry [17]. The general result is that soft symmetry-breaking terms do not destroy the renormalizability an initially symmetric theory [18]. This applies to the original scotogenic model of neutrino mass [7] and is also used in the following radiative mass models of quarks and leptons in Chapters 2, 3, 4 and 5.

Radiative corrections are also responsible for the SM contributions to the muon magnetic moment. The SM prediction is usually divided into three parts based on the particles appearing in the loop diagrams [10]. The QED part includes photons and leptons. The electroweak part includes the heavy $W^{\pm}$, $Z$ or Higgs particles. The hadronic part includes quarks and gluons, and is the main source of theoretical uncertainties. Currently there is a discrepancy between the theoretical prediction and the experimental measurement. Radiative mass models can generally give contributions of the rough form

$$\Delta a_{\mu} \sim C\frac{m_{\mu}^2}{M^2} \tag{1.14}$$

where $M$ is a physical high mass scale associated with the new physics and the value of $C \sim 1$ is very model-dependent [19].

Radiative mass models can also explain very small fermion masses with much larger Higgs Yukawa couplings compared to the SM due to the nature of the loop integrals. This is the subject of the next chapter, which also examines the corresponding effective interaction with the Higgs particle, which for charged leptons is $f_{\text{eff}}h\bar{l}l$. The result is that the deviation of the effective Higgs Yukawa coupling $f_{\text{eff}}$ from the SM expectation $m_l/v$ is not suppressed by the usual one-loop factor of $16\pi^2$ and may be large enough to be observable. Compare

this with the common approach of using higher-dimensional operators

$$-\mathcal{L} = f_l \overline{l_L} l_R \phi^0 \left(1 + \frac{\Phi^\dagger \Phi}{\Lambda^2}\right) \tag{1.15}$$

where $\Lambda^2 >> v^2$. This implies that the mass is $m_l = (f_l v/\sqrt{2})(1+v^2/2\Lambda^2)$ and the effective Higgs coupling is $f_{\text{eff}} = (f_l/\sqrt{2})(1+3v^2/2\Lambda^2) \simeq (m_l/v)(1+v^2/\Lambda^2)$. This approach is only valid for $v^2 << \Lambda^2$, which guarantees the effect to be small. The result of the following chapter is that both $m_l$ and $f_{\text{eff}}$ are infinite sums in powers of $v^2$ but each sum is finite. Their ratio is not necessarily small because some particles in the loop could be light.

# Part I

# Anomalous Higgs Yukawa Couplings

# Chapter 2

# Radiative Masses with $Z_2$ Symmetry

## 2.1 Tau Lepton

This chapter is the foundation of Part I, and is based on the work previously published in Ref. [1]. The main goal is to establish that the radiative mass mechanism can give large, measurable predictions for the effective Higgs Yukawa coupling in the case of heavy quarks and charged leptons, and the proper contributions for the anomalous magnetic moment in the case of the muon. A simple modification of the SM is used to illustrate the underlying strategy. The full symmetry group is based on that of the SM, but incorporates two discrete $Z_2$ symmetries

$$SU(3)_C \times SU(2)_L \times U(1)_Y \times Z_{2\,dark} \times Z_2 \tag{2.1}$$

The first $Z_{2\,dark}$ is used to stabilize dark matter and is therefore assumed to be exactly conserved. The main purpose of the second $Z_2$ is to forbid the Higgs Yukawa coupling at tree-level, but to permit its realization in one-loop. This is the essence of the radiative mechanism. To complete the loop, the second $Z_2$ symmetry will have to be softly broken by the Dirac mass term of the new neutral fermion $N = N_L + N_R$. The particle content is shown in Table 2.1. The particles $\Phi, \tau_L$ are the same as in the SM but $\tau_R$ is $(-)$ under the second $Z_2$. The tau neutrino is shown for completeness, but is not needed for this chapter. All other SM particles have $(Z_{2\,dark}, Z_2) = (+,+)$ and are therefore not affected by the imposition of the extra discrete symmetry. Since only the new particles have $(-)_{dark}$ under $Z_{2\,dark}$, they comprise the dark sector of this model. After any mixing effects have been included, the lightest neutral mass eigenstate among them is a candidate for dark matter. The new scalars are an electroweak doublet $\eta$ and charged singlet $\chi^+$. Note that each component of any electroweak doublet must have the same assignment under $Z_{2\,dark} \times Z_2$. The only new

| Particle | $(SU(3)_C, SU(2)_L, Y)$ | $Z_{2\,dark}$ | $Z_2$ |
|---|---|---|---|
| $\Phi = \begin{pmatrix} \phi^+ \\ \phi^0 \end{pmatrix}$ | $(\mathbf{1}, \mathbf{2}, +1/2)$ | $+$ | $+$ |
| $L = \begin{pmatrix} \nu_L \\ \tau_L \end{pmatrix}$ | $(\mathbf{1}, \mathbf{2}, +1/2)$ | $+$ | $+$ |
| $\tau_R$ | $(\mathbf{1}, \mathbf{1}, -1)$ | $+$ | $-$ |
| $N_L$ | $(\mathbf{1}, \mathbf{1}, 0)$ | $-$ | $-$ |
| $N_R$ | $(\mathbf{1}, \mathbf{1}, 0)$ | $-$ | $+$ |
| $\eta = \begin{pmatrix} \eta^+ \\ \eta^0 \end{pmatrix}$ | $(\mathbf{1}, \mathbf{2}, +1/2)$ | $-$ | $+$ |
| $\chi^+$ | $(\mathbf{1}, \mathbf{1}, +1)$ | $-$ | $+$ |

Table 2.1: Particle content in the $Z_2$ model for tau.

fermions are the electroweak singlets $N_L$ and $N_R$. They have no gauge interactions so they do not contribute to the gauge anomaly, hence this model is anomaly-free.

The SM Higgs Yukawa coupling is strictly forbidden because under $Z_{2\,dark} \times Z_2$ this term reads

$$\begin{aligned} & \overline{L_L} \;\; \widetilde{\Phi} \;\; \tau_R \\ Z_{2\,dark} &= (+)(+)(+) = (+)_{dark} \\ Z_2 &= (+)(+)(-) = (-) \end{aligned} \tag{2.2}$$

which is overall $(+)_{dark}(-) = (-)$ and therefore not allowed since all Lagrangian terms must be trivial singlets under the full symmetry group. Allowed Lagrangian terms are listed in Table 2.2. In $\mathcal{L}_{f_\eta}$ and $\mathcal{L}_{trilinear}$, the dual of $\eta$ is $\widetilde{\eta}$. Note that a Hermitian conjugate field or a dual field has the same $Z_2$ assignment as the original field, but this will not be the case for the other discrete symmetries $Z_3$ or $A_4$ encountered in the models considered in Chapters 3 and 4. The effective one-loop vertex for the Higgs Yukawa interaction with tau is shown in Fig. 2.1. The vital scalar interaction $\mathcal{L}_{trilinear} = \mu \; \widetilde{\eta}^{\,\dagger} \, \Phi \, \chi^- + h.c.$ is the

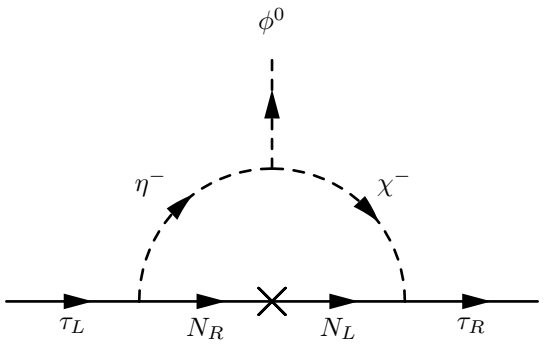


Figure 2.1: Radiative Higgs Yukawa interaction for tau.

| Terms that respect $Z_2$ | |
|---|---|
| $\mathcal{L}_{f_\eta}$ | $= -f_\eta \, \overline{L_L} \, \widetilde{\eta} \, N_R \qquad\qquad - f_\eta \, \overline{N_R} \, \widetilde{\eta}^\dagger \, L_L$<br>$= -f_\eta \, \left(\overline{\nu_L}\eta^{0*} - \overline{\tau_L}\eta^-\right) N_R - f_\eta \, \overline{N_R} \left(\nu_L \eta^0 - \tau_L \eta^+\right)$ |
| $\mathcal{L}_{f_\chi}$ | $= f_\chi \, \overline{N_L} \, \chi^+ \tau_R + f_\chi \, \overline{\tau_R} \, \chi^- N_L$ |
| $\mathcal{L}_{trilinear}$ | $= \mu \, \widetilde{\eta}^\dagger \, \Phi \, \chi^- \qquad\qquad + \mu \, \Phi^\dagger \, \widetilde{\eta} \, \chi^+$<br>$= \mu \left(\eta^0 \phi^+ - \eta^+ \phi^0\right) \chi^- + \mu \left(\eta^{0*} \phi^- - \eta^- \phi^{0*}\right) \chi^+$ |
| $\mathcal{L}_{scalars}$ | $= -m_\chi^2 (\chi^+ \chi^-) - \lambda_\chi (\Phi^\dagger \Phi)(\chi^+ \chi^-) - \lambda_{\eta\chi} (\eta^\dagger \eta)(\chi^+ \chi^-)$ |
| $\mathcal{L}_{2HDM}$ | $= +\mu_{SM}^2 (\Phi^\dagger \Phi) - m_\eta^2 (\eta^\dagger \eta)$<br>$-\lambda_{SM} (\Phi^\dagger \Phi)^2 - \lambda_\eta (\eta^\dagger \eta)^2$<br>$-\lambda_2 (\Phi^\dagger \Phi)(\eta^\dagger \eta)$<br>$-\lambda_4 (\Phi^\dagger \eta)(\eta^\dagger \Phi)$<br>$-\lambda_5 (\Phi^\dagger \eta)^2 - \lambda_5 (\eta^\dagger \Phi)^2$ |
| Terms that break $Z_2$ | |
| $\mathcal{L}_N$ | $= -m_N \left(\overline{N_L} \, N_R + \overline{N_R} \, N_L\right)$ |

Table 2.2: Lagrangian terms in the $Z_2$ model.

only connection to the Higgs doublet at the top of the loop before spontaneous electroweak symmetry breaking, and it is the primary connection to the Higgs particle after spontaneous electroweak symmetry breaking. As already mentioned, the loop requires the soft-breaking of $Z_2$ which allows $N_L$ and $N_R$ to pair up and become one Dirac particle $N = N_L + N_R$ with an invariant Dirac mass. Under $Z_{2,dark} \times Z_2$ this term reads

$$\begin{aligned} & \overline{N_L}\, N_R \\ Z_{2\,dark} &= (-)(-) = (+)_{dark} \\ Z_2 &= (-)(+) = (-) \end{aligned} \tag{2.3}$$

which is overall $(+)_{dark}(-) = (-)$ and therefore does not respect the discrete symmetries. This soft-breaking is indicated by the cross. Before spontaneous electroweak symmetry breaking, $\tau_L$ and $\tau_R$ are massless, and their chiralities do not change as they propagate along their respective fermion lines.

The two scalar doublets $\Phi$,$\eta$ in this model are a special case of general two Higgs doublet models (2HDM) with $\Phi_1$,$\Phi_2$, which have the same electroweak assignments as the SM Higgs doublet. By considering all possible combinations of $\Phi_1$,$\Phi_2$ and their duals, the most general scalar potential for these two doublets can be written in the customary

form [20]

$$
\begin{aligned}
-\mathcal{L}_{2HDM} \quad = \quad & m_{11}^2(\Phi_1^\dagger\Phi_1) + m_{22}^2(\Phi_2^\dagger\Phi_2) \\
& + m_{12}^2(\Phi_1^\dagger\Phi_2) + (m_{12}^2)^*(\Phi_2^\dagger\Phi_1) \\
& + \lambda_1(\Phi_1^\dagger\Phi_1)^2 + \lambda_2(\Phi_2^\dagger\Phi_2)^2 \\
& + \lambda_3(\Phi_1^\dagger\Phi_1)(\Phi_2^\dagger\Phi_2) \\
& + \lambda_4(\Phi_1^\dagger\Phi_2)(\Phi_2^\dagger\Phi_1) \\
& + \lambda_5(\Phi_1^\dagger\Phi_2)^2 + \lambda_5^*(\Phi_2^\dagger\Phi_1)^2 \\
& + \left[\lambda_6(\Phi_1^\dagger\Phi_2) + \lambda_6^*(\Phi_2^\dagger\Phi_1)\right](\Phi_1^\dagger\Phi_1) \\
& + \left[\lambda_7(\Phi_1^\dagger\Phi_2) + \lambda_7^*(\Phi_2^\dagger\Phi_1)\right](\Phi_2^\dagger\Phi_2)
\end{aligned}
\tag{2.4}
$$

Without loss of generality, the coefficients $m_{12}^2$ and $\lambda_{5,6,7}$ are complex, and all other coefficients are real. In our model, $\Phi_1 = \Phi$ is $(+,+)$ under $Z_{2\,dark} \times Z_2$, and $\Phi_2 = \eta$ is $(-,+)$. Thus the $m_{12}^2$ terms are forbidden because $(\Phi_1^\dagger\Phi_2)$ is overall $(-)_{dark}(+) = (-)$. Similarly, the $\lambda_6$ and $\lambda_7$ terms are forbidden because of the products in square brackets. Hence the new scalar terms in our model are the ones listed in Table 2.1, with change of notation. In passing, note that the elimination of terms compared to the general 2HDM now allows $\lambda_5$ to be real because its phase can be absorbed into one of the complex doublets.

Actually, the model of this chapter is close to a specific version of the 2HDM, the Inert Higgs doublet model, where the neutral component of $\Phi_2 = \eta$ does not get a VEV. In our case, this is because $\eta$ has $(-1)_{dark}$, and $Z_{2\,dark}$ is assumed to be exactly conserved.

## 2.2 Radiative Mass

The spontaneous breaking of electroweak symmetry

$$\Phi \to \begin{pmatrix} 0 \\ (v+h)/\sqrt{2} \end{pmatrix} \tag{2.5}$$

generates the radiative mass for tau, as shown schematically in Fig. 2.2. The Higgs VEV induces mixing of $\eta$ and $\chi$ into the the mass eigenstates $\zeta_1$ and $\zeta_2$, which then propagate in the loop. The Higgs mass $m_h$ receives the expected SM contributions in the usual way from the $+\mu_{SM}^2$ and $-\lambda_{SM}$ terms in $\mathcal{L}_{2HDM}$

$$\begin{aligned} \mathcal{L}_{2HDM} &= +\mu_{SM}^2(\Phi^\dagger\Phi) - m_\eta^2(\eta^\dagger\eta) \\ &\quad -\lambda_{SM}(\Phi^\dagger\Phi)^2 - \lambda_2(\eta^\dagger\eta)^2 \\ &\quad -\lambda_\eta(\Phi^\dagger\Phi)(\eta^\dagger\eta) \\ &\quad -\lambda_4(\Phi^\dagger\eta)(\eta^\dagger\Phi) \\ &\quad -\lambda_5(\Phi^\dagger\eta)^2 + \lambda_5(\eta^\dagger\Phi)^2 \end{aligned} \tag{2.6}$$

For $\eta^+$, its invariant mass from the $(\eta^\dagger\eta)$ term receives additional contributions from the $\lambda_\eta v^2$ term, but we absorb this into the $m_\eta^2$ parameter. The particle $\eta^0$ will not be needed

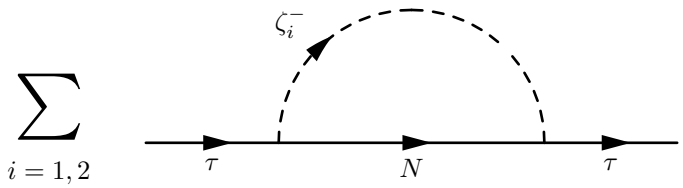


Figure 2.2: Radiative tau mass.

here, but its analogue will be referred to shortly in section 2.6. It has the same invariant mass from the $(\eta^\dagger\eta)$ term, and receives additional contributions from the $\lambda_4 v^2$ term, as well as the contributions from the $\lambda_5 v^2$ terms, which split the complex $\eta^0$ into its real and imaginary components. For $\chi^+$, its invariant mass receives additional contributions from the $\lambda_\chi v^2$ term

$$\mathcal{L}_{scalars} \supset -m_\chi^2(\chi^+\chi^-) - \lambda_\chi \frac{1}{2}(v+h)^2(\chi^+\chi^-) \tag{2.7}$$

but we absorb this into the $m_\chi^2$ parameter. The Higgs VEV also generates the important mixing term

$$\mathcal{L}_{trilinear} \supset -\frac{\mu v}{\sqrt{2}}\left(\eta^+\chi^- + \eta^-\chi^+\right) \tag{2.8}$$

We therefore have the mass-squared mixing matrix

$$\mathcal{L} \supset -(\eta^+, \chi^+)\begin{pmatrix} m_\eta^2 & \mu v/\sqrt{2} \\ \mu v/\sqrt{2} & m_\chi^2 \end{pmatrix}\begin{pmatrix} \eta^- \\ \chi^- \end{pmatrix} \tag{2.9}$$

which is diagonalized by rotating $\eta$,$\chi$ into the mass eigenstates $\zeta_{1,2}$ with masses $m_{1,2}$

$$\begin{pmatrix} \eta^- \\ \chi^- \end{pmatrix} = \begin{pmatrix} \cos\theta & -\sin\theta \\ \sin\theta & \cos\theta \end{pmatrix}\begin{pmatrix} \zeta_1^- \\ \zeta_2^- \end{pmatrix} \tag{2.10}$$

where the new parameters $m_1, m_2, \theta$ are related to $m_\eta, m_\chi, \mu$ by

$$\frac{\mu v}{\sqrt{2}} = \sin\theta\cos\theta(m_1^2 - m_2^2) \tag{2.11}$$

$$m_\eta^2 = \cos\theta m_1^2 + \sin\theta m_2^2 \tag{2.12}$$

$$m_\chi^2 = \sin\theta m_1^2 + \cos\theta m_2^2 \tag{2.13}$$

Now we need the Yukawa terms shown in the self-energy diagram Fig. 2.2. They come from

$$\begin{aligned} \mathcal{L}_{f_\eta} &= f_\eta \left( \overline{\tau_L}\, N_R\, \eta^- + \overline{N_R}\, \tau_L\, \eta^+ \right) \\ \mathcal{L}_{f_\chi} &= f_\chi \left( \overline{\tau_R}\, N_L\, \chi^- + \overline{N_L}\, \tau_R\, \chi^+ \right) \end{aligned} \tag{2.14}$$

The projection operators $P_{L,R} = \frac{1}{2}(1 \mp \gamma_5)$ can be separated from the fields $A$,$B$ using $\overline{A_L} B_R = \overline{A} P_R B$ and $\overline{A_R} B_L = \overline{A} P_L B$. Also expressing the fields $\eta$,$\chi$ in terms of the mass eignenstates $\zeta_{1,2}$, we have

$$\mathcal{L}_{f_\eta + f_\chi} = \sum_{i=1,2} \overline{\tau} \left[ a_i f_\eta P_R + b_i f_\chi P_L \right] N \zeta_i^- + \overline{N} \left[ a_i f_\eta P_L + b_i f_\chi P_R \right] \tau \zeta_i^+ \tag{2.15}$$

with the shorthand notation

$$\begin{array}{c|cc} & \zeta_1 & \zeta_2 \\ \hline a_i = & c & -s \\ b_i = & s & c \end{array} \tag{2.16}$$

and $c = \cos\theta$ and $s = \sin\theta$. Let the arrows in Fig. 2.2 dictate the flow of momentum. Then the momenta for $\tau, N, \zeta_i^-$ are $p, k, p-k$ respectively, and we set $p$ to zero. Then the loop integral for the self-energy is

$$-i m_\tau = i^4 \sum_{i=1,2} \int \frac{d^4 k}{(2\pi)^4} \left[ \frac{numerator}{(k^2 - m_i^2)(k^2 - m_N^2)} \right] \tag{2.17}$$

where the factor of $i^4 = 1$ is from the two propagators and the two vertices. and the

numerator is

$$\begin{aligned} numerator &= [a_i f_\eta P_R + b_i f_\chi P_L]\,[\not{k} + m_N]\,[a_i f_\eta P_L + b_i f_\chi P_R] \\ &= a_i b_i f_\eta f_\chi m_N (P_L^2 + P_R^2) \\ &= a_i b_i f_\eta f_\chi m_N \end{aligned} \tag{2.18}$$

In the first line, the term linear in $k$ integrates to zero, and the the projectors makes some terms vanish due to $P_{L,R}\not{k} = \not{k} P_{R,L}$ and $P_L P_R = P_L P_R = 0$. In the last two lines, $P_{L,R}^2 = P_{L,R}$ and $P_L + P_R = 1$. Then using $a_i$ and $b_i$, we have

$$\begin{aligned} -i m_\tau &= f_\eta f_\chi \int \frac{d^4k}{(2\pi)^4} \left[ \frac{sc\, m_N}{(k^2 - m_1^2)(k^2 - m_N^2)} + \frac{-sc\, m_N}{(k^2 - m_2^2)(k^2 - m_N^2)} \right] \\ &= f_\eta f_\chi \int \frac{d^4k}{(2\pi)^4} \left[ \frac{sc\, m_N\,(m_1^2 - m_2^2)}{(k^2 - m_N^2)(k^2 - m_1^2)(k^2 - m_2^2)} \right] \\ &= f_\eta f_\chi\; m_N\; (m_1^2 - m_2^2)\; sc\, I(m_1, m_2, m_N) \end{aligned} \tag{2.19}$$

The first line is the sum of two terms, each of which diverges, but their sum is finite, as shown in the second line by putting both terms over a common denominator. The Feynman parameters can be introduced in the usual way, and then the integral over $d^4k$ can be performed, which gives

$$\begin{aligned} I(m_1, m_2, m_N) &= \int \frac{d^4k}{(2\pi)^4} \frac{1}{(k^2 - m_N^2)(k^2 - m_1^2)(k^2 - m_2^2)} \\ &= \frac{-i}{16\pi^2} \int_0^1 dx dy dz \frac{\delta(1 - x - y - z)}{x m_1^2 + y m_2^2 + z m_N^2} \end{aligned} \tag{2.20}$$

Integrating over $x, y, z$ gives

$$\begin{aligned} I(m_1, m_2, m_N) &= \frac{-i}{16\pi^2} \frac{1}{m_1^2 - m_2^2} \left[ \frac{m_1^2}{m_1^2 - m_N^2} \ln \frac{m_1^2}{m_N^2} - \frac{m_2^2}{m_2^2 - m_N^2} \ln \frac{m_2^2}{m_N^2} \right] \\ &= \frac{-i}{16\pi^2} \frac{1}{m_N^2 (x_1 - x_2)} \left[ H(x_1) - H(x_2) \right] \\ &= \frac{-i}{16\pi^2 m_N^2} F(x_1, x_2) \end{aligned} \tag{2.21}$$

where $x_{1,2} = m_{1,2}^2 / m_N^2$ and

$$\begin{aligned} H(x) &= \frac{x}{x-1} \ln x \\ F(x_1, x_2) &= \frac{1}{x_1 - x_2} \left[ \frac{x_1}{x_1 - 1} \ln x_1 - \frac{x_2}{x_2 - 1} \ln x_2 \right] \\ F(x, x) &= \frac{1}{x-1} - \frac{\ln x}{(x-1)^2} \end{aligned} \tag{2.22}$$

Note $F(x_1, x_2) > 0$. Here $F(x, x)$ is the limit $x_1 \to x_2$, and $F(1, 1) \to 1/2$ . In terms of $F(x_1, x_2)$, the radiative mass is

$$-i m_\tau = f_\eta f_\chi m_N \sin\theta \cos\theta (m_1^2 - m_2^2) \frac{-i}{16\pi^2 m_N^2} F(x_1, x_2)$$

$$m_\tau = \frac{f_\eta f_\chi \sin\theta \cos\theta (m_1^2 - m_2^2)}{16\pi^2 m_N} F(x_1, x_2) \tag{2.23}$$

$$= \frac{f_\eta f_\chi \mu v}{16\pi^2 m_N \sqrt{2}} F(x_1, x_2) \tag{2.24}$$

The factors $-i$ cancels on both sides, so $m_\tau > 0$. In the last line we used Eq. (2.11).

## 2.3 Effective Higgs Yukawa Coupling

Fig. 2.3 shows the effective one-loop Higgs Yukawa coupling for tau. Schematically, the Higgs connects to the mass eigenstates $\zeta_i = \zeta_{1,2}$ in three different ways. They come

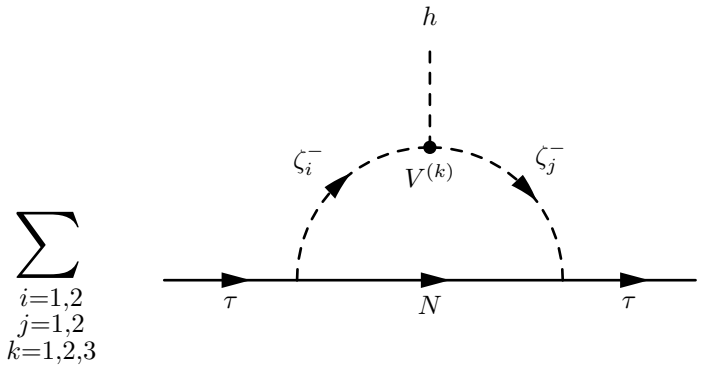


Figure 2.3: Effective Higgs Yukawa coupling for tau.

from the three types of Higgs interactions with $\eta$ and $\chi$

$$\begin{aligned}
\mathcal{L}_{trilinear} &\supset -\frac{\mu}{\sqrt{2}} h \left(\eta^+\chi^- + \eta^-\chi^+\right) \\
\mathcal{L}_{2HDM} &\supset -\lambda_\eta v h \eta^+\eta^- \\
\mathcal{L}_{scalars} &\supset -\lambda_\chi v h \chi^+\chi^-
\end{aligned} \tag{2.25}$$

In the physical mass basis, all three types of Higgs connections have the same form

$$\mathcal{L}_{(k)} \supset -V^{(k)} h \sum_{i,j} t_{ij}^{(k)} \left(\zeta_i^+ \zeta_j^-\right) \tag{2.26}$$

where $V^{(1,2,3)} = \left(\mu/\sqrt{2}, \lambda_\eta v, \lambda_\chi v\right)$ for the three Higgs connections. The coefficients $t_{ij}^{(k)}$ are combinations of $s = \sin\theta$ or $c = \cos\theta$ with various signs. For the primary $f^{(1)}$ contribution, going to the mass basis gives

$$\begin{aligned}
\mathcal{L}_{trilinear} &\supset -\frac{\mu h}{\sqrt{2}} \left[\eta^+\chi^- + \eta^-\chi^+\right] \\
&= -\frac{\mu h}{\sqrt{2}} \left[(c\zeta_1^+ - s\zeta_2^+)(s\zeta_1^- + c\zeta_2^-) + (c\zeta_1^- - s\zeta_2^-)(s\zeta_1^+ + c\zeta_2^+)\right] \\
&= -\frac{\mu h}{\sqrt{2}} \left[2sc\zeta_1^+\zeta_1^- - 2sc\zeta_2^+\zeta_2^- + (c^2 - s^2)(\zeta_1^+\zeta_2^- + \zeta_2^+\zeta_1^-)\right]
\end{aligned} \tag{2.27}$$

so that

$$t_{ij}^{(1)} \;=\; \begin{array}{c|cc} & \zeta_1 & \zeta_2 \\ \hline \zeta_1 & 2sc & c^2-s^2 \\ \zeta_2 & c^2-s^2 & -2sc \end{array} \tag{2.28}$$

For the other $f^{(2)}$ contribution in the mass basis, we have

$$\begin{aligned} \mathcal{L}_{2HDM} &\supset -\lambda_\eta v h \eta^+ \eta^- \\ &= -\lambda_\eta v h (c\zeta_1^+ - s\zeta_2^+)(c\zeta_1^- - s\zeta_2^-) \\ &= -\lambda_\eta v h \left[c^2\zeta_1^+\zeta_1^- + s^2\zeta_2^+\zeta_2^- - sc(\zeta_1^+\zeta_2^- + \zeta_2^+\zeta_1^-\right] \end{aligned} \tag{2.29}$$

so that

$$t_{ij}^{(2)} \;=\; \begin{array}{c|cc} & \zeta_1 & \zeta_2 \\ \hline \zeta_1 & c^2 & -sc \\ \zeta_2 & -sc & s^2 \end{array} \tag{2.30}$$

Similarly, for $\mathcal{L}_{scalars} \supset -\lambda_\chi v h \chi^+ \chi^-$, we have

$$t_{ij}^{(3)} \;=\; \begin{array}{c|cc} & \zeta_1 & \zeta_2 \\ \hline \zeta_1 & s^2 & sc \\ \zeta_2 & sc & c^2 \end{array} \tag{2.31}$$

Let the arrows in Fig. 2.3 dictate the flow of momentum. Assuming that $m_h^2$ is small compared to $m_N^2$ and $m_{1,2}^2$ the momenta for $\tau, N, \zeta_i^-, \zeta_j^-$ are $p, k, p-k, p-k$ respectively, and we set $p$ to zero. Then the loop integral for the effective Yukawa coupling is

$$-if_\tau \;=\; i^6 \sum_{i=1,2} \int \frac{d^4k}{(2\pi)^4} \left[\frac{numerator}{(k^2-m_i^2)(k^2-m_j^2)(k^2-m_N^2)}\right] \tag{2.32}$$

where the factor of $i^6 = -1$ is from the three propagators and the three vertices, and the numerator is

$$\begin{aligned} numerator &= -V^{(k)} t_{ij}^{(k)} \left[a_j f_\eta P_R + b_j f_\chi P_L\right] \left[\not{k} + m_N\right] \left[a_i f_\eta P_L + b_i f_\chi P_R\right] \\ &= -V^{(k)} t_{ij}^{(k)} \; f_\eta f_\chi m_N (a_j b_i P_R^2 + b_j a_i P_L^2) \end{aligned} \tag{2.33}$$

which has been partially simplified as before by the projection operators. The integral over $d^4k$ has already been done in $I(m_a, m_b, m_c)$ from Eq. (2.21). Note that the value of this integral does not depend on the order of the masses $m_a, m_b, m_c$. Using the fact that the $t_{ij}^{(k)}$ are symmetric in $ij$, we have for the effective Yukawa coupling

$$\begin{aligned} -i f_\tau &= -i^6 f_\eta f_\chi m_N \sum_{i,j,k} V^{(k)} t_{ij}^{(k)} \; (a_j b_i P_R + b_j a_i P_L) I_{ij} \\ &= +f_\eta f_\chi m_N \sum_{i,j,k} V^{(k)} a_i (t_{ij}^{(k)} I_{ij}) b_j \; (P_R + P_L) \\ &= f_\eta f_\chi m_N \frac{-i}{16\pi^2 m_N^2} \sum_{i,j,k} V^{(k)} a_i (t_{ij}^{(k)} F_{ij}) b_j \end{aligned} \tag{2.34}$$

where in the last line the projection operators add to one. Evaluating this using the $a_i, b_i$ and $t_{ij}^{(1)}$ for the primary Higgs Yukawa coupling gives

$$f_\tau^{(1)} = \frac{f_\eta f_\chi}{16\pi^2 m_N} \frac{\mu}{\sqrt{2}} \left[2s^2c^2 F_{11} + 2s^2c^2 F_{22} + (c^2 - s^2)^2 F_{12}\right] \tag{2.35}$$

The factors of $-i$ have canceled and $f_\tau^{(3)} > 0$ as it should be for the primary contribution since $m_\tau > 0$. The correction due to nonzero $m_h$ is a long expression for arbitrary $m_N, m_1, m_2$ but in the case $m_N = m_1 = m_2$ it easily found to be $m_h^2/(12m_N^2)$, which shows that it should be generally negligible.

Similar to the calculation of $f_\tau^{(1)}$, the other contributions to the Higgs Yukawa

coupling are

$$\begin{aligned} f_\tau^{(2)} &= \frac{f_\eta f_\chi}{16\pi^2 m_N}(\lambda_\eta v)\, sc\left[c^2 F_{11} - s^2 F_{22} - (c^2 - s^2)F_{12}\right] \\ f_\tau^{(3)} &= \frac{f_\eta f_\chi}{16\pi^2 m_N}(\lambda_\chi v)\, sc\left[s^2 F_{11} - c^2 F_{22} + (c^2 - s^2)F_{12}\right] \end{aligned} \tag{2.36}$$

Combining all three contributions and using the radiative mass Eq. (2.24) we have

$$\begin{aligned} \frac{f_\tau v}{m_\tau} &= \frac{\left[f_\tau^{(1)} + f_\tau^{(2)} + f_\tau^{(3)}\right] v}{m_\tau} \\ &= 2s^2c^2F_{11} + 2s^2c^2F_{22} + (c^2 - s^2)^2 F_{12} \\ &+ \frac{\lambda_\eta v}{\mu/\sqrt{2}} sc(c^2 F_{11} - s^2 F_{22} - (c^2 - s^2)F_{12}) \\ &+ \frac{\lambda_\chi v}{\mu/\sqrt{2}} sc(s^2 F_{11} - c^2 F_{22} + (c^2 - s^2)F_{12}) \end{aligned} \tag{2.37}$$

The factors of $16\pi^2$ and $f_\eta f_\chi v/m_N$ have cancelled. To make the meaning of this expression clear, define

$$\begin{aligned} F_+(x_1, x_2) &= \frac{F(x_1, x_1) + F(x_2, x_2)}{2F(x_1, x_2)} \\ F_-(x_1, x_2) &= \frac{F(x_1, x_1) - F(x_2, x_2)}{2F(x_1, x_2)} \\ r_{\eta,\chi} &= \lambda_{\eta,\chi}(m_N/\mu)^2 \end{aligned} \tag{2.38}$$

where $F_+(x_1, x_2) \geq 0$ and $F_+(x, x) = F_-(x, x) = 0$. After rearrangement, we find

$$\frac{f_\tau v}{m_\tau} = 1 + \frac{1}{2}(\sin 2\theta)^2 \left\{2F_+ + (x_1 - x_2)\left[\cos 2\theta(r_\eta - r_\chi)F_+ + (r_\eta + r_\chi)F_-\right]\right\} \tag{2.39}$$

In Fig. 2.4 we plot $(f_\tau v/m_\tau)^2$ as a function of $\theta$ for various $(r_\eta, r_\chi)$ for $x_1 = 3$, $x_2 = 1$ and

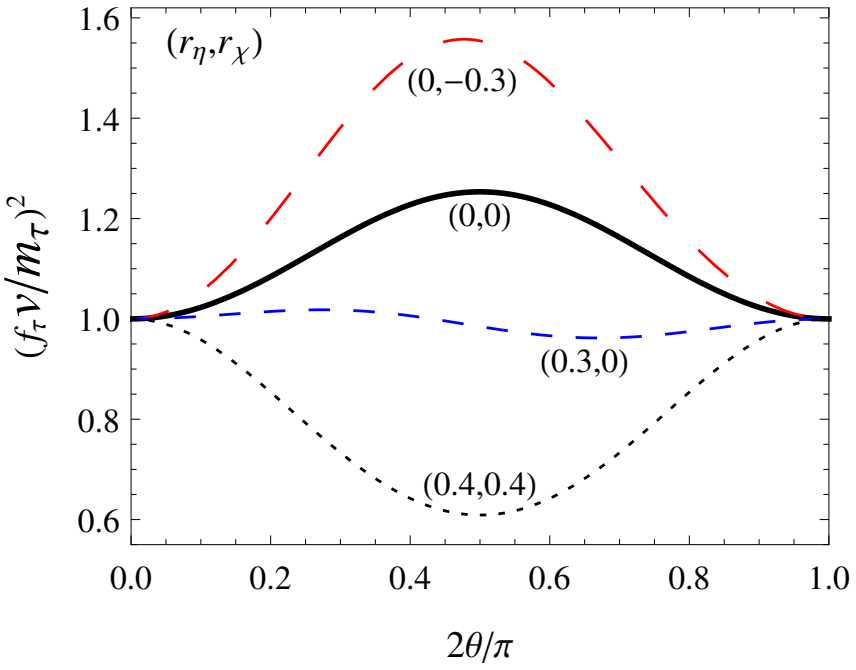


Figure 2.4: The ratio $(f_\tau v/m_\tau)^2$ versus $\theta$ with $x_1 = 3$, $x_2 = 1$, $\mu/m_N = 1$.

$\mu/m_N = 1$. It shows that a significant deviation from the SM is possible. This spans the range of the relatively large uncertainties in the LHC measurements from ATLAS [21] and CMS [22]

$$\begin{aligned} \mu(h \to \tau\tau)|_{\text{ATLAS}} &= 1.43^{+0.43}_{-0.37} \\ \mu(h \to \tau\tau)|_{\text{CMS}} &= 0.91 \pm 0.28 \end{aligned} \tag{2.40}$$

where the signal strength $\mu$ is the measured production cross section times branching fraction divided by the SM expectation

$$\mu = \frac{(\sigma \times BR)_{exp}}{(\sigma \times BR)_{SM}} \tag{2.41}$$

The parametrization used is explained as follows. The radiative mass formula Eq. (2.24) must be satisfied, but the couplings cannot be too large

$$\begin{aligned} \frac{f_\eta f_\chi}{4\pi} &= \left(\frac{m_\tau 4\pi\sqrt{2}}{vF(x_1,x_2)}\right)\left(\frac{m_N}{\mu}\right) \\ &= (0.4)\left(\frac{m_N}{\mu}\right) \end{aligned} \tag{2.42}$$

where is the last line we have chosen $x_1 = 3$ and $x_2 = 1$. Thus for this choice of $x_{1,2}$, we need $\mu/m_N \gtrsim 1$ so the couplings are not too large. However, $\mu$ must also satisfy the mass-mixing constraint Eq. (2.11)

$$\begin{aligned} \frac{\mu v}{\sqrt{2}} &= \sin\theta\cos\theta m_N^2(x_1 - x_2) \\ m_N &= \left(\frac{\mu}{m_N}\right)\frac{\sqrt{2}v}{(x_1 - x_2)\sin 2\theta} \end{aligned} \tag{2.43}$$

The four independent parameters are taken to be $(\mu/m_N)$, $x_1$, $x_2$ and $\theta$. This defines $m_N$ as a function of all four. For illustration, we have chosen to let $\theta$ vary, and have picked $\mu/m_N = 1$, $x_1 = 3$, $x_2 = 1$. As a final comment, these results are minor corrections to Ref. [1]. The above Eq. (2.35), Eq. (2.39) and Fig. 2.4 respectively correct the Ref. [1] Eq. (6) for factors of c and s, Eq. (10) for the coefficient 2 times $F_+$, and Fig. 3 for greater maximum value of $(f_\tau v/m_\tau)^2$.

## 2.4 Higgs Decay to $\gamma\gamma$

If this radiative model is the true description of the tau mass, then the new charged scalars will contribute to $h \to \gamma\gamma$. The amplitude for this decay is equal to the sum of all diagrams that have one Higgs and two photons connecting to an internal loop of any charged

particle. In the SM, the dominant contributions to the diphoton decay rate $\Gamma_{SM}$ are from the top quark and $W$ boson. Here there are additional contributions from $\zeta_{1,2}$ as shown in Fig. 2.5. The loop amplitudes for a fermion, gauge bosons, or scalar are well-known [23], and adapting these results we find the total decay rate to be

$$\Gamma_{\gamma\gamma} = \frac{G_F \alpha^2 m_h^3}{128\sqrt{2}\pi^3} \left| \frac{4}{3} A_{1/2}\left(\frac{4m_t^2}{m_h^2}\right) + A_1\left(\frac{4M_W^2}{m_h^2}\right) + f_1 A_0\left(\frac{4m_1^2}{m_h^2}\right) + f_2 A_0\left(\frac{4m_2^2}{m_h^2}\right) \right|^2 \tag{2.44}$$

where the couplings $f_{1,2}$ are

$$\begin{aligned} f_1 &= \frac{1}{4x_1}(\sin 2\theta)^2 (x_1 - x_2)\left\{1 + \frac{1}{2}(x_1 - x_2)[(r_\eta + r_\chi) + \cos 2\theta (r_\eta - r_\chi)]\right\} \\ f_2 &= \frac{1}{4x_2}(\sin 2\theta)^2 (x_1 - x_2)\left\{-1 + \frac{1}{2}(x_1 - x_2)[(r_\eta + r_\chi) - \cos 2\theta (r_\eta - r_\chi)]\right\} \end{aligned} \tag{2.45}$$

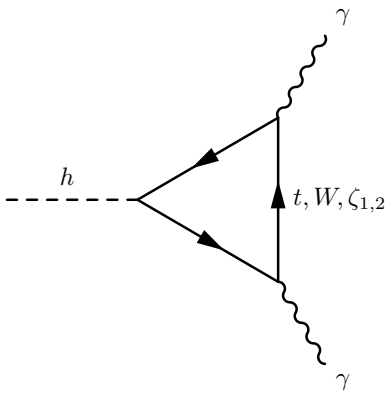


Figure 2.5: Higgs decay to two photons.

and the loop integral functions are

$$A_0(y) = -y[1 - yf(y)] \tag{2.46}$$

$$A_{1/2}(y) = 2y[1 + (1 - y)f(y)] \tag{2.47}$$

$$A_1(y) = -[2 + 3y + 3y(2 - y)f(y)] \tag{2.48}$$

$$f(y) = \arcsin^2(y^{-1/2}) \quad , \quad y \geq 1 \tag{2.49}$$

The ratio $\Gamma_{\gamma\gamma}/\Gamma_{SM}$ as a function of $\theta$ is shown in Fig. 2.6. We see that deviations of a few percent from the SM are predicted. This is consistent with the bounds from LHC

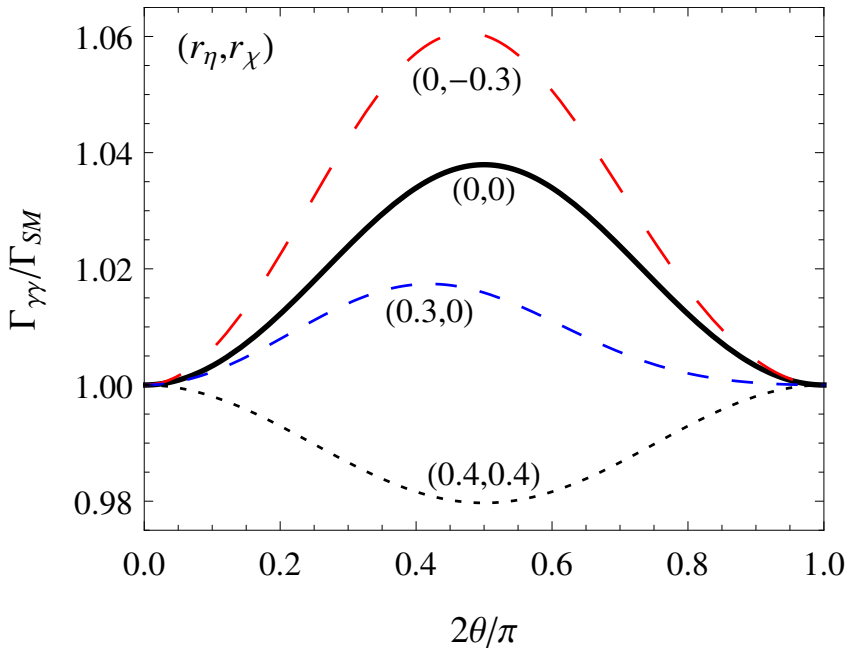


Figure 2.6: The ratio $\Gamma_{\gamma\gamma}/\Gamma_{SM}$ versus $\theta$ with $x_1 = 3$, $x_2 = 1$, $\mu/m_N = 1$.

measurements by ATLAS [21] and CMS [22]

$$\begin{aligned} \mu(h \to \gamma\gamma)|_{\rm ATLAS} &= 1.17^{+0.27}_{-0.27} \\ \mu(h \to \gamma\gamma)|_{\rm CMS} &= 1.12 \pm 0.24 \end{aligned} \tag{2.50}$$

## 2.5 Muon Anomalous Magnetic Moment

Consider now the case when the muon mass is radiative. The previous results of sections 2.1 and 2.2 are easily adapted, using a different $N$ and different $f_{\eta,\chi}$. Closely related to this is the electromagnetic interaction shown in Fig. 2.7, which essentially connects a photon to the charged scalar in the radiative mass diagram. This single diagram can be used to calculate the contributions to the muon magnetic moment $\Delta a_\mu = (g-2)/2$. However, it is important to emphasize that two other diagrams exist, where the photon attaches instead to either the ingoing or the outgoing muon. The divergent portions of these diagrams cancel the divergent portions of Fig. 2.7, but do not otherwise affect the finite portion of this diagram which is responsible for the contributions to the magnetic

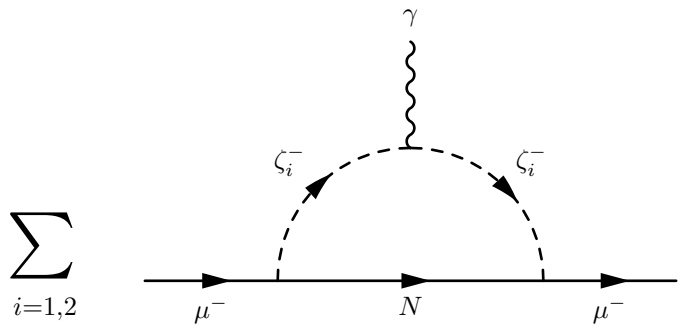


Figure 2.7: Main diagram for calculating $\Delta a_\mu$.

moment. The simplest approach is to examine the vertex correction

$$
\begin{aligned}
ie\Gamma^{\mu} &= i^6 \sum_i \int \frac{d^4k}{(2\pi)^4} \frac{ie(k_1^{\mu}+k_2^{\mu}) \times numerator}{(k_N^2-m_N^2)(k_1^2-m_i^2)(k_2^2-m_i^2)} \\
numerator &= [a_i f_\eta P_R + b_i f_\chi P_L]\,[\not{k}_N + m_N]\,[a_i f_\eta P_L + b_i f_\chi P_R] \qquad (2.51)
\end{aligned}
$$

and extract the relevant terms by expanding the numerator. After this, the Feynman parameters can be introduced in the usual way, and then the integral over $d^4k$ can be performed. The Gordan identity is used, since the spinor product $\overline{u_\mu(p')}\ [\dots]\ u_\mu(p)$ is understood on both sides of the above equation. This is carried out for a virtual photon with momentum $q^\mu$, in the limit $q^2 \to 0$. Following this procedure, the dominant contributions will come from the terms and $P_R m_N P_R$ and $P_L m_N P_L$, which correspond to $\mu_L \to \mu_R$ and $\mu_R \to \mu_L$ respectively. We find these dominant contributions to be positive, which is crucial to explain the the experimental measurement discussed below, and the total dominant contribution is given by

$$
\Delta a_\mu = \frac{m_\mu^2}{m_N^2}\left[\frac{G(x_1)-G(x_2)}{H(x_1)-H(x_2)}\right] \qquad (2.52)
$$

where

$$
\begin{aligned}
G(x) &= \frac{2x\ln x}{(x-1)^3} - \frac{x+1}{(x-1)^2} \\
H(x) &= \frac{x\ln x}{x-1} \qquad (2.53)
\end{aligned}
$$

The subdominant contributions will come from the terms and $P_R \not{k}_N P_L$ and $P_L \not{k}_N P_R$, which correspond to $\mu_L \to \mu_L$ and $\mu_R \to \mu_R$ respectively. They are subdominant because $\not{k}_N$ is

essentially converted by the spinors into the very small masses of the external leptons. We find the subdominant contributions are negative as expected [24] and given by

$$(\Delta a_\mu)' = \frac{-m_\mu^2}{16\pi^2 m_N^2}\left\{f_\eta^2\left[\cos^2\theta J(x_1)+\sin^2\theta J(x_2)\right]+f_\chi^2\left[\sin^2\theta J(x_1)+\cos^2\theta J(x_2)\right]\right\} \tag{2.54}$$

where

$$J(x)=\frac{x\ln x}{(x-1)^4}+\frac{x^2-5x-2}{6(x-1)^3} \tag{2.55}$$

The current discrepancy of the experimental measurement [25] versus the theoretical calculation [26] is

$$\Delta a_\mu = a_\mu^{\rm exp}-a_\mu^{\rm SM}=39.35\pm 5.21_{\rm th}\pm 6.3_{\rm exp}\times 10^{-10} \tag{2.56}$$

In Fig. 2.8, the shaded region is the range of this discrepancy, and the dashed limits correspond to the experimental and theoretical uncertainties combined in quadrature. Using the parameterization $x_1 = x_2 + 2$, we see that values of $m_N, m_1, m_2$ in roughly the TeV range can provide the required contributions to $\Delta a_\mu$.

The parametrization used is explained as follows. We must satisfy two conditions, the radiative mass formula Eq. (2.24)

$$\left(\frac{f_\eta f_\chi}{4\pi}\right)\left(\frac{\mu}{m_N}\right) = \frac{m_\mu 4\pi\sqrt{2}}{vF(x_1,x_2)} \tag{2.57}$$

and the mass-mixing constraint Eq. (2.11)

$$\sin 2\theta = \left(\frac{\mu}{m_N}\right)\left(\frac{v}{m_N}\right)\left(\frac{2}{x_1-x_2}\right)\frac{1}{\sqrt{2}} \tag{2.58}$$

In Fig. 2.8, we pick values of $x_1 - x_2 = 2$ and $(v/m_N) \lesssim 1$. Together, these will satisfy

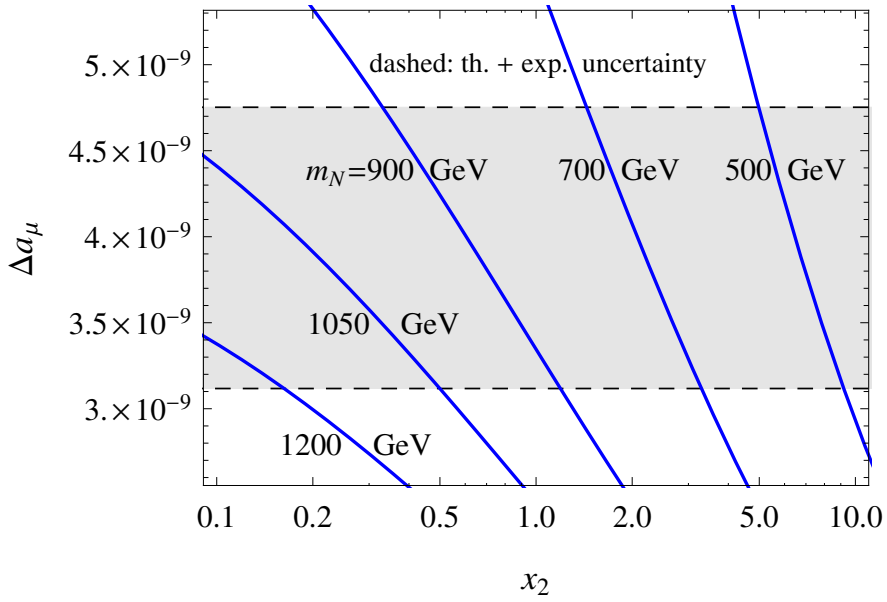


Figure 2.8: $\Delta a_\mu$ versus $x_2$ with $x_1 = x_2 + 2$ and various $m_N$.

the second condition by giving $\sin 2\theta \lesssim 1/\sqrt{2}$, as long as $(\mu/m_N) \lesssim 1$. This allows the couplings to be small for the first condition, since we have checked that the left-hand side varies between 0.01 and 0.1 for $x_1 = x_2 + 2$ and $x_2$ in the range of Fig. 2.8.

## 2.6 Bottom Quark and Higgs Production

Consider now the case when the bottom quark mass is radiative. The previous results of sections 2.1, 2.2, 2.3 and 2.4 are easily adapted. The new particle content is given in Table 2.3. The top quark is shown for completeness, but is not needed here. For quarks an additional color index is understood. The Higgs VEV will induce mixing of $\eta^{-1/3}, \chi^{-1/3}$ which also carry color. They mix into the physical particles $\zeta'_{1,2}$ with angle $\theta'$ and masses $m'_{1,2}$. All other SM particles, including muon and tau, have $(Z_{2\,dark}, Z_2) = (+,+)$ and are

| Particle | $(SU(3)_C, SU(2)_L, Y)$ | dark $Z_2$ | $Z_2$ |
|---|---|---|---|
| $\Phi = \begin{pmatrix} \phi^+ \\ \phi^0 \end{pmatrix}$ | $(\mathbf{1}, \mathbf{2}, +1/2)$ | $+$ | $+$ |
| $Q = \begin{pmatrix} t_L \\ b_L \end{pmatrix}$ | $(\mathbf{3}, \mathbf{2}, +1/6)$ | $+$ | $+$ |
| $t_R$ | $(\mathbf{3}, \mathbf{1}, +2/3)$ | $+$ | $-$ |
| $b_R$ | $(\mathbf{3}, \mathbf{1}, -1/3)$ | $+$ | $-$ |
| $N_L$ | $(\mathbf{1}, \mathbf{1}, 0)$ | $-$ | $-$ |
| $N_R$ | $(\mathbf{1}, \mathbf{1}, 0)$ | $-$ | $+$ |
| $\eta = \begin{pmatrix} \eta^{+2/3} \\ \eta^{-1/3} \end{pmatrix}$ | $(\mathbf{3}, \mathbf{2}, +1/2)$ | $-$ | $+$ |
| $\chi^{-1/3}$ | $(\mathbf{3}, \mathbf{1}, -1/3)$ | $-$ | $+$ |

Table 2.3: Particle content in the $Z_2$ model for bottom quark.

therefore not affected by the imposition of the extra discrete symmetry. Similar to the previous case, Fig. 2.9 generates both the the radiative mass for the bottom quark and its effective Higgs Yukawa coupling when the Higgs gets a VEV. A significant deviation of the effective Higgs Yukawa coupling is again possible, as shown in the previous Fig. 2.4. This

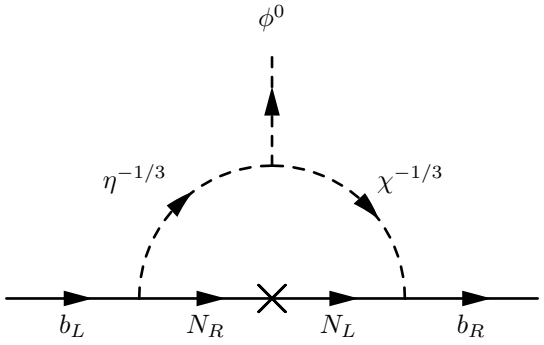


Figure 2.9: Radiative Higgs Yukawa interaction for bottom quark.

is consistent with the bounds from LHC measurements by ATLAS [21] and CMS [22]

$$\begin{aligned} \mu(h \to bb)|_{\text{ATLAS}} &= 0.52^{+0.4}_{-0.4} \\ \mu(h \to bb)|_{\text{CMS}} &= 0.84 \pm 0.44 \end{aligned} \tag{2.59}$$

The scalars $\eta^{-1/3}, \chi^{-1/3}$ are charged, so they will affect the Higgs diphoton decay rate as in the previous case, with an additional contribution from $\eta^{+2/3}$. Because these particles also carry color, they will also affect the gluon fusion rate for Higgs production $gg \to h$ shown in Fig. 2.10. To estimate the size of this effect, we will compute the reverse process of Higgs decay since the Higgs production cross section $\sigma_{gg} = \sigma(gg \to h)$ is directly related to the Higgs decay rate $\Gamma_{gg} = \Gamma(h \to gg)$ by integration over the parton distribution. The previous loop amplitudes Eq. (2.46) for a scalar and Eq. (2.47) for a fermion can be used by including the appropriate color factor [27]. At the parton level, the amplitude for this process is equal to the sum of all diagrams that have one Higgs and two photons connecting to an internal loop of any colored particle. In the SM, the dominant contributions to

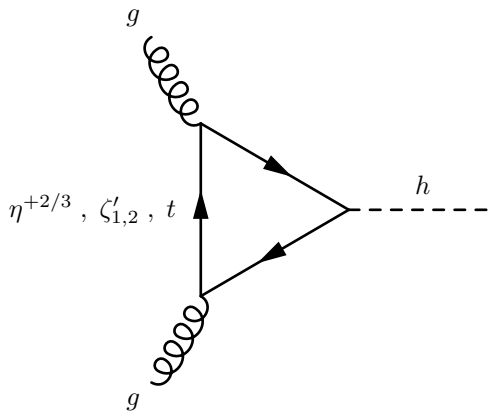


Figure 2.10: Higgs production from two gluons.

$\Gamma_{SM}$ are from the top quark and $W$ boson. Here there are additional contributions from $\zeta'_{1,2}$ and $\eta^{+2/3}$. For $\eta^{+2/3}$, we may refer to the previous reduced 2HDM Lagrangian in Table 2.1. The electroweak doublet $\Phi$ is still a color singlet, but the electroweak doublet $\eta$ is now a color triplet. This means the $\lambda_4$ and $\lambda_5$ terms are absent because the contracted indices in $\lambda_4(\Phi^\dagger\eta)(\eta^\dagger\Phi)$ and $\lambda_5(\Phi^\dagger\eta)^2 + \lambda_5(\eta^\dagger\Phi)^2$ do not not allow trivial singlets under $SU(3)_C \times SU(2)_L$. So after the Higgs gets a VEV, the mass of the colored $\eta^{+2/3}$ is simply given by ${m'_\eta}^2 = \cos\theta' {m'_1}^2 + \sin\theta' {m'_2}^2$ from Eq. (2.12). Using $r'_{\eta,\chi} = \lambda'_{\eta,\chi}(m_N/\mu')^2$ and $x'_{1,2,\eta} = {m'_{1,2,\eta}}^2/m_N^2$, the decay rate $\Gamma_{gg}$ is given by

$$
\begin{aligned}
\Gamma_{gg} &= \frac{G_F \alpha_S^2 m_h^3}{64\sqrt{2}\pi^3} \left| A_{1/2}\left(\frac{4m_t^2}{m_h^2}\right) + \left[ f'_1 A_0\left(\frac{4{m'_1}^2}{m_h^2}\right) + f'_2 A_0\left(\frac{4{m'_2}^2}{m_h^2}\right) + f'_\eta A_0\left(\frac{4{m'_\eta}^2}{m_h^2}\right) \right] \right|^2 \\
f'_1 &= \frac{1}{4x'_1}(\sin 2\theta')^2 (x'_1 - x'_2)\left\{ 1 + \frac{1}{2}(x'_1 - x'_2)[(r'_\eta + r'_\chi) + \cos 2\theta'(r'_\eta - r'_\chi)] \right\} \\
f'_2 &= \frac{1}{4x'_2}(\sin 2\theta')^2 (x'_1 - x'_2)\left\{ -1 + \frac{1}{2}(x'_1 - x'_2)[(r'_\eta + r'_\chi) - \cos 2\theta'(r'_\eta - r'_\chi)] \right\} \\
f'_\eta &= \frac{r'_\eta}{4x'_\eta}(\sin 2\theta')^2 (x'_1 - x'_2)^2
\end{aligned}
\tag{2.60}
$$

The ratio $\Gamma_{gg}/\Gamma_{SM}$ as a function of $\theta'$ is shown in Fig. 2.11 for $x'_1 = 3$ and $x'_2 = 1$ with $\mu'/m_N = 1$ for various $(r'_\eta, r'_\chi)$. We see that Higgs production from gluon fusion may be significantly affected.

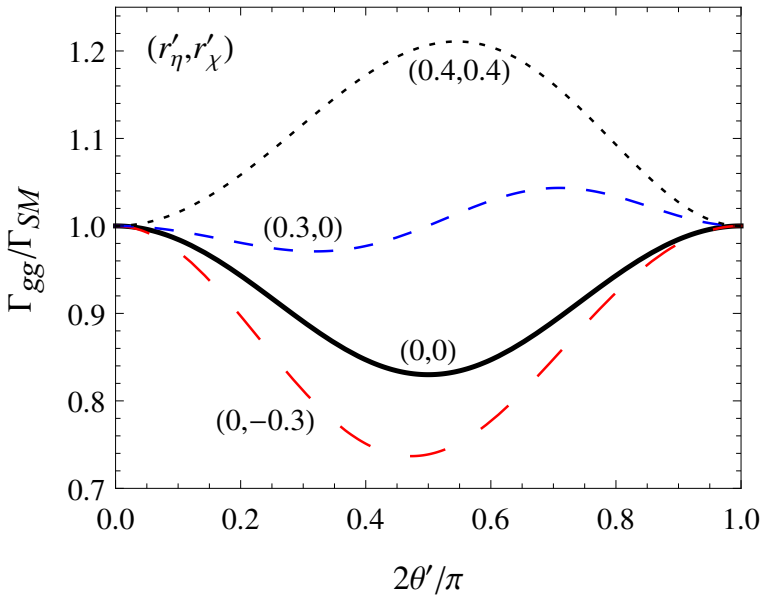


Figure 2.11: The ratio $\Gamma_{gg}/\Gamma_{SM}$ versus $\theta'$ with $x'_1 = 3$, $x'_2 = 1$, $\mu'/m_N = 1$.

To summarize, this chapter has established that the radiative mass mechanism can give large, measurable predictions for the effective Higgs Yukawa coupling in the case of heavy quarks and charged leptons, and the proper contributions for the anomalous magnetic moment in the case of the muon.

# Chapter 3

# Scotogenic Inverse Seesaw Neutrino Mass

## 3.1 Radiative Mass

This chapter discusses a model of neutrino mass that is a radiative implementation of the inverse seesaw [28–30]. It is based on the work previously published in Ref. [2] and will be adapted for use in the next chapter. For background, a concise summary of most Majorana neutrino mass models can be understood from the Weinberg operator, which is the unique effective dimension-five operator [31] given by

$$\mathcal{L}_5 = \frac{(\overline{\widetilde{L_{iL}}}\Phi)(\widetilde{\Phi}^\dagger L_{jL})}{\Lambda} + h.c. \tag{3.1}$$

where $\Lambda$ is a large effective mass. This describes Majorana neutrino masses in terms of the SM particle content with all new heavy particles integrated out. At tree-level, it was shown in Ref. [32] that there are three possible ways to obtain the Weinberg operator, and they

are classified by the heavy particle used. Type I uses a heavy singlet neutral Majorana fermion. This is the canonical seesaw, which will appear in Chapter 7. Type II uses a heavy triplet Higgs scalar. A radiative version of this type will be studied in Chapter 5. Type III uses a heavy triplet Majorana fermion. Going beyond the level of effective operators and specifying all particle interactions at one-loop, it was also shown in Ref. [32] that there are three generic one-loop mechanisms that lead to the Weinberg operator. The model discussed in this chapter is a new realization of the third such mechanism.

The full symmetry group of the model is the SM gauge group with the addition of a discrete symmetry

$$SU(3)_C \times SU(2)_L \times U(1)_Y \times Z_{2\,dark} \tag{3.2}$$

The discrete symmetry $Z_{2\,dark}$ is assumed to be exactly conserved because its purpose is to stabilize dark matter. The particle content is listed in Table 3.1. All the new particles are odd under $Z_{2\,dark}$. There is one left-handed neutral fermion $N_L$ which is an electroweak

| Particle | | | | | $(SU(3)_C, SU(2)_L, Y)$ | $Z_{2\,dark}$ |
|---|---|---|---|---|---|---|
| $L_{iL}$ | $=$ | $\begin{pmatrix}\nu_{eL}\\ e_L\end{pmatrix}$ | $\begin{pmatrix}\nu_{\mu L}\\ \mu_L\end{pmatrix}$ | $\begin{pmatrix}\nu_{\tau L}\\ \tau_L\end{pmatrix}$ | $(\mathbf{1},\mathbf{2},-1/2)$ | $+$ |
| $l_{iR}$ | $=$ | $e_R$ | $\mu_R$ | $\tau_R$ | $(\mathbf{1},\mathbf{1},-1)$ | $+$ |
| $\Phi$ | $=$ | $\begin{pmatrix}\phi^+\\ \phi^0\end{pmatrix}$ | | | $(\mathbf{1},\mathbf{2},+1/2)$ | $+$ |
| $E_{L,R}$ | $=$ | $\begin{pmatrix}E^0\\ E^-\end{pmatrix}_{L,R}$ | | | $(\mathbf{1},\mathbf{2},-1/2)$ | $-$ |
| | | $N_L$ | | | $(\mathbf{1},\mathbf{1},0)$ | $-$ |
| $s_i$ | $=$ | $s_1$ | $s_2$ | $s_3$ | $(\mathbf{1},\mathbf{1},0)$ | $-$ |

Table 3.1: Particle content for radiative neutrino mass.

singlet, so it does not contribute to the gauge anomaly. There are also two electroweak fermion doublets $E_{L,R}$. Since $E$ is vector-like, the left- and right-handed contributions to the gauge anomaly cancel, hence this model is anomaly-free. Although not listed, lepton number may be defined as $L = +1$ for $E_{L,R}$, $N_L$ and the SM leptons. There are also three real scalars $s_{1,2,3}$ which are electroweak singlets.

The allowed Lagrangian terms are listed in Table 3.2 before spontaneous symmetry breaking. The SM charged fermions have the usual Higgs Yukawa interactions and will obtain masses as in the SM after electroweak symmetry breaking. The conservation of lepton number allows the hard Yukawa terms in $\mathcal{L}_D$ but forbids the similar hard Yukawa terms $\overline{E_L}\ \widetilde{\Phi}\ (N_L)^c + h.c.$. For the fermions $E_{L,R}$ the general mass terms $m_A\overline{E_L}E_R$ and $m_B\overline{E_R}E_L$ are allowed, but adding their hermitian conjugates simply leads to $m_E = (m_A + m_B)$. Since the model does not include any right-handed fermion singlets, $N_L$ only has Majorana mass terms, which softly break lepton number and so these terms may be naturally small. This soft-breaking of the lepton number symmetry allows completion of the loop as shown in Fig. 3.1 for a single neutrino $\nu_L$ and a single scalar mass eigenstate $s$. In general, the original states $s_i$ and $s_j$ listed in the Lagrangian terms will mix after electroweak symmetry breaking due to $\mathcal{L}_{\Phi,s}$. Note that $E_L$ is not needed to complete the loop, but it is needed to provide a large invariant mass $m_E$ for the inverse seesaw mechanism. It is also used to cancel the gauge anomaly from $E_R$.

After spontaneous electroweak symmetry breaking, the Higgs VEV mixes $E_R$ and $N_L$. Together with the Majorana terms for $N_L$, the complete fermion mixing matrix is

$$
\begin{aligned}
\mathcal{L}_{Higgs} &= +\mu^2_{SM}\Phi^\dagger\Phi - \tfrac{1}{2}\lambda_{SM}(\Phi^\dagger\Phi)^2 \\
\mathcal{L}_{Leptons} &= -f_{SM,ij}\ \overline{L_{iL}}\ \widetilde{\Phi}^\dagger\ l_{jR} + h.c. \\
\mathcal{L}_s &= -m^2_{ij}s_i s_j + \text{quartic terms} \\
\mathcal{L}_{\Phi,s} &= -\lambda_{ij}(\Phi^\dagger\Phi)s_i s_j \\
\mathcal{L}_E &= -m_E\overline{E}E \quad = \quad -m_E\left(\overline{E_L}E_R + \overline{E_R}E_L\right) \\
\mathcal{L}_N &= -\tfrac{1}{2}m_N\left(\overline{N_L}(N_L)^c + \overline{(N_L)^c}N_L\right) \\
\mathcal{L}_D &= -f_D\ \overline{E_R}\ \widetilde{\Phi}\ N_L \qquad\qquad - f_D\ \overline{N_L}\ \widetilde{\Phi}^\dagger\ E_R \\
&= -f_D\left(\overline{E^0_R}\phi^{0*} - \phi^-\overline{E^-_R}\right)N_L - f_D\ \overline{N_L}\left(\phi^0 E^0_R - \phi^+ E^-_R\right) \\
\mathcal{L}_f &= f_i\ \overline{L_{iL}}\ E_R\ s_i \qquad\qquad + f_i\ \overline{E_R}\ L_{iL}\ s_i \\
&= f_i\ \left(\overline{\nu_{iL}}E^0_R + \overline{e_{iL}}E^-_R\right)s_i + f_i\ \left(\overline{E^0_R}\nu_{iL} - \overline{E^-_R}e_{iL}\right)s_i
\end{aligned}
$$

Table 3.2: Lagrangian terms in the scotogenic neutrino mass model.

given by

$$\mathcal{L}_{N+E+D} \supset - \left(\overline{(E_R^0)^c}, \overline{E_L^0}, \overline{N_L}\right) \begin{pmatrix} 0 & m_E & f_D v/\sqrt{2} \\ m_E & 0 & 0 \\ f_D v/\sqrt{2} & 0 & m_N \end{pmatrix} \begin{pmatrix} E_R^0 \\ (E_L^0)^c \\ (N_L)^c \end{pmatrix} + h.c. \tag{3.3}$$

where the identities $\overline{E_L^0} E_R^0 = \overline{(E_R^0)^c}(E_L^0)^c$ and $\overline{N_L} E_R^0 = \overline{(E_R^0)^c}(N_L)^c$ have been used. Let $m_D = f_D v/\sqrt{2}$. Assuming that $m_N$ is much less than $m_D, m_E$, the mass eigenvalues of the mixing matrix are

$$\begin{aligned} m_1 &= \frac{m_E^2 m_N}{m_E^2 + m_D^2} \\ m_2 &= \sqrt{m_E^2 + m_D^2} + \frac{m_D^2 m_N}{2(m_E^2 + m_D^2)} \\ m_3 &= -\sqrt{m_E^2 + m_D^2} + \frac{m_D^2 m_N}{2(m_E^2 + m_D^2)} \end{aligned} \tag{3.4}$$

Taking the limit when $m_N \to 0$ shows that $m_2 = -m_3$. This indicates that $E_R^0$ pairs up with $E_L^0 \cos\theta + N_L \sin\theta$ to form one Dirac fermion with a mass of $\sqrt{m_E^2 + m_D^2}$, where $\sin\theta = m_D/\sqrt{m_E^2 + m_D^2}$. In this limit, the self-energy is easily computed from Fig. 3.1 by writing out the fermion sequence of one Dirac propagator, a mass insertion proportional to

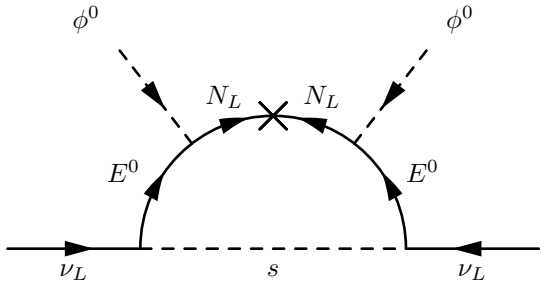


Figure 3.1: Radiative scotogenic neutrino mass.

$m_N$ denoted by the cross, and another Dirac propagator. Including the scalar propagator and integrating over the loop momentum gives the result

$$\begin{aligned} m_\nu &= \frac{f^2 m_D^2 m_N}{16\pi^2(m_E^2+m_D^2-m_s^2)}\left[1-\frac{m_s^2\ln((m_E^2+m_D^2)/m_s^2)}{(m_E^2+m_D^2-m_s^2)}\right] \\ &= \frac{f^2}{16\pi^2}\frac{m_D^2 m_N}{(m_E^2+m_D^2)}F(x) \end{aligned} \tag{3.5}$$

where

$$\begin{aligned} x &= m_s^2/(m_E^2+m_D^2) \\ F(x) &= \frac{1}{1-x}\left[1+\frac{x\ln x}{1-x}\right] \end{aligned} \tag{3.6}$$

Note $F(0)=1$ and $F(x)\to 0$ as $x\to\infty$. The second expression for $m_\nu$ is extremely suggestive of the inverse seesaw relationship. In the denominator, when $m_D$ can be neglected compared to $m_E$, the ratio

$$\frac{m_D^2 m_N}{m_E^2} \tag{3.7}$$

is exactly the well-known expression for the inverse seesaw neutrino mass, which is small because of the combination of a small Majorna mass $m_N$ and a small ratio of the Dirac mass to the invariant mass $(m_D/m_E)^2$.

## 3.2 Three Generations

With three scalar mass eigenstates $s_{1,2,3}$, three generations of neutrino masses can be obtained. A realistic model must also obtain the neutrino mixing matrix $U_{PMNS}$. To this end, a discrete flavor symmetry may be used, for example the Abelian group $Z_3$. This

will restrict the Lagrangian terms listed previously in Table 3.2. Under $Z_3$, let the particle assignments be given by

$$\begin{aligned} \Phi, N_L, E_{L,R} &\sim \mathbf{1} \\ l_{iR} &\sim \mathbf{1}, \mathbf{1}', \mathbf{1}'' \\ L_{iL} &\sim \mathbf{1}, \mathbf{1}', \mathbf{1}'' \\ s_1 &\sim \mathbf{1} \\ (s_2 + is_3)/\sqrt{2} &\sim \mathbf{1}' \\ (s_2 - is_3)/\sqrt{2} &\sim \mathbf{1}'' \end{aligned} \tag{3.8}$$

where $s_{1,2,3}$ denote the mass eigenstates determined by the allowed scalar Lagrangian terms. The three cubic roots of unity are essentially the three group elements of $Z_3$ described by the notation of $\mathbf{1}, \mathbf{1}', \mathbf{1}''$. The $Z_3$ symmetry restricts the scalar mass terms to be given by $\mathcal{L}_s \supset -{m_s}^2 s_1^2 - {m'_s}^2(s_2^2 + s_3^2)$. It also restricts the quartic couplings to be given by $\mathcal{L}_{\Phi,s} = -(\Phi^\dagger\Phi)\left(\lambda s_1^2 + \lambda'(s_2^2 + s_3^2)\right)$ which generates mass terms after electroweak symmetry breaking, but these can be absorbed into the mass eigenvalues $m_s$ and $m'_s, m'_s$ for the mass eigenstates $s_1$ and $s_2, s_3$ respectively. Using a shorthand notation, the scalar interaction states defined by the $Z_2$ assignments above are $U_{ij}s_j$ where

$$U = \begin{pmatrix} 1 & 0 & 0 \\ 0 & 1/\sqrt{2} & i/\sqrt{2} \\ 0 & 1/\sqrt{2} & -i/\sqrt{2} \end{pmatrix} \tag{3.9}$$

The $Z_3$ symmetry restricts the SM charged lepton Higgs Yukawa terms to be diagonal $\mathcal{L}_{Leptons} = -f_{SM,ii}\ \overline{L_{iL}}\ \widetilde{\Phi}^\dagger\ l_{iR} + h.c.$ with $i = e, \mu, \tau$ so the tree-level charged

fermion mass matrix will be diagonal after electroweak symmetry breaking. This means the neutrino mixing matrix is given by

$$U_{PMNS} \;=\; U_L^l U_L^\nu \;\;=\;\; U_L^\nu \tag{3.10}$$

and it remains to determine $U_L^\nu$.

The radiative neutrino mass matrix $\mathcal{M}_\nu$ in the $Z_3$ basis is

$$(\overline{\nu_{eL}}, \overline{\nu_{\mu L}}, \overline{\nu_{\tau L}})\, \mathcal{M}_\nu \begin{pmatrix} (\nu_{eL})^c \\ (\nu_{\mu L})^c \\ (\nu_{\tau L})^c \end{pmatrix} \quad + \quad h.c. \tag{3.11}$$

where each entry of the $3 \times 3$ matrix involves a loop integral of the same form as Eq. (3.5). The matrix $\mathcal{M}_\nu$ corresponds to $(\nu_{iL})^c \to \nu_{jL}$ and the hermitian conjugate term with the matrix $\mathcal{M}_\nu^\dagger$ corresponds to $\nu_{iL} \to (\nu_{jL})^c$.

The couplings $f_i$ between the $Z_3$ interaction states $\nu_{iL}$ and $U_{ij}s_j$ form a diagonal matrix. Using a shorthand notation where the matrix $f = diag(f_e, f_\mu, f_\tau)$ and the row vector $\overline{\nu_L} = (\overline{\nu_{eL}}, \overline{\nu_{\mu L}}, \overline{\nu_{\tau L}})$ and the column vector $s = (s_1, s_2, s_3)^T$, the allowed Yukawa terms for the calculation of the radiative neutrino mass loop diagrams are

$$\begin{aligned} \mathcal{L}_f \;&\supset\; \overline{\nu_L}\; f\; U s\; E_R^0 \quad + \quad h.c. \\ &=\; \overline{(E_R^0)^c}\; s^T U^T f\; (\nu_L)^c \quad + \quad h.c. \end{aligned} \tag{3.12}$$

where in the last line $\overline{\nu_L} E_R^0 = \overline{(E_R^0)^c}(\nu_L)^c$ and $f^T = f$ were used. Then reading off the

matrices from this expression gives

$$\begin{aligned}\mathcal{M}_\nu &= f\,U \begin{pmatrix} I(m_s) & 0 & 0 \\ 0 & I(m'_s) & 0 \\ 0 & 0 & I(m'_s) \end{pmatrix} U^T f \\ &= \begin{pmatrix} f_e^2 I(m_s) & 0 & 0 \\ 0 & 0 & f_\mu f_\tau I(m'_s) \\ 0 & f_\mu f_\tau I(m'_s) & 0 \end{pmatrix} \end{aligned} \tag{3.13}$$

where the loop integral $I(m_s)$ is given by Eq. (3.5) with $f^2$ removed.

This $\mathcal{M}_\nu$ is not realistic, but it can be made realistic. Let $Z_3$ be broken softly by arbitrary but suitable Lagrangian terms $(\mathcal{M}^2)_{ij} s_i s_j$ so that the new mass eigenvalues are $m_{s_1}, m_{s_2}, m_{s_3}$ corresponding to the new mass eigenstates $s'_{1,2,3}$ given by $s'_i = \mathcal{O}_{ij} s_j$ where $\mathcal{O}$ is an orthogonal matrix. This gives

$$\mathcal{M}_\nu = f\,U\,\mathcal{O}^T \begin{pmatrix} I(m_{s_1}) & 0 & 0 \\ 0 & I(m_{s_2}) & 0 \\ 0 & 0 & I(m_{s_3}) \end{pmatrix} \mathcal{O}\,U^T f \tag{3.14}$$

Since $f$ is diagonal, this identifies $U_L^{\nu\,\dagger} = U\,\mathcal{O}^T$, which determines $U_{PMNS}$. The couplings $f_e, f_\mu, f_\tau$ may be taken to be real by absorbing their phases into the arbitrary relative phases between $\nu_{eL}, \nu_{\mu L}, \nu_{\tau L}$ and $E_R^0$. Consider the case $f_\mu = f_\tau$, which results in the interesting

pattern

$$\mathcal{M}_\nu = \begin{pmatrix} A & C & C^* \\ C & D^* & B \\ C^* & B & D \end{pmatrix} \tag{3.15}$$

where $A, B$ are real but $C, D$ remain complex. This pattern is protected by a symmetry $e \to e$ and $\mu \leftrightarrow \tau$ with $CP$ conjugation [33–35]. This means that the neutrino mixing matrix $U_{PMNS}$ will have maximal mixing of $\theta_{23} = \pi/4$ and maximal $CP$ violation of $\exp(-i\delta_{CP}) = \pm i$ while $\theta_{13}$ may be nonzero and arbitrary.

For charged leptons, there are corresponding radiative contributions to the muon anomalous magnetic moment $\Delta a_\mu$ and rare decays such as $\mu \to e\gamma$. The values $f_{e,\mu,\tau} \sim 0.1$, $m_N \sim 10$ MeV, $m_D \sim 10$ GeV, $m_E \sim 1$ TeV, $m_{s_{1,2,3}} \lesssim m_E$ give negligible contributions to $\Delta a_\mu$ and satisfy the experimental bound of $\mu \to e\gamma$. They also give realistic neutrino masses $m_\nu \sim 0.1$ eV.

To summarize, this chapter has examined a new model of radiative neutrino mass based on the inverse seesaw that accommodates dark matter. In the next chapter, the model will be slightly modified by enlarging both the particle content and the discrete symmetry.

# Chapter 4

# Radiative Masses with $A_4$ Symmetry

## 4.1 Outline of the Model

This chapter discusses a comprehensive radiative model for the entire lepton sector, and is based on the work previously published in Ref. [3]. The full symmetry group is the based on the SM gauge group, but incorporates two discrete symmetries

$$SU(3)_C \times SU(2)_L \times U(1)_Y \times Z_{2\,dark} \times A_4 \tag{4.1}$$

The discrete symmetry $Z_{2\,dark}$ is used to stabilize dark matter and is therefore assumed to be exactly conserved. The main purpose of the discrete flavor symmetry $A_4$ is to forbid the Higgs Yukawa coupling to charged fermions at tree-level, but to permit its realization in one-loop. To obtain a realistic neutrino mixing matrix $U \equiv U_{PMNS} = U_L^l \, U_L^{\nu\,\dagger}$ the method of Ref [36] will be used, which is motivated by real scalar dark matter and is partially

based on the model in the previous chapter for radiative inverse seesaw neutrino mass. The rotation $U_L^\nu$ will be an orthogonal matrix that will come from an orthogonal rotation $\mathcal{O}$ required for non-degenerate neutrino masses. The rotation $U_L^l$ will come from the soft breaking of $A_4$ required for the existence of charged lepton radiative masses. The rotation $U_L^l$ is based on the unitary matrix

$$U_\omega = \begin{pmatrix} 1 & 1 & 1 \\ 1 & \omega & \omega^2 \\ 1 & \omega^2 & \omega \end{pmatrix} \tag{4.2}$$

where $\omega = \exp(2\pi i/3)$ is the cubic root of 1. Although $U_\omega$ is familiar from the group $A_4$, it is mostly used here as a bridge between the charged lepton and neutrino sectors. It also accommodates $Z_3$ lepton triality [37] because the use of $U_\omega$ for the soft-breaking described in the next section breaks $A_4$ to its subgroup $Z_3$.

Details of the group muliplication rules for $A_4$ are given at the end of the chapter. In brief, the non-Abelian discrete symmetry $A_4$ allows an irreducible triplet representation $\mathbf{3}$ and three inequivalent one-dimensional representations $\mathbf{1}, \mathbf{1}', \mathbf{1}''$, with the basic multiplication rule

$$\mathbf{3} \times \mathbf{3} = \mathbf{1} + \mathbf{1}' + \mathbf{1}'' + \mathbf{3} + \mathbf{3} \tag{4.3}$$

This makes $A_4$ ideally suited as a flavor symmetry for three generations. The particle content of the model is shown in Table 4.1. All new particles belong to the dark sector. The particles $N_{L,R}$ have no gauge interactions so they do not contribute to the gauge anomaly. The fermions $E^0_{L,R}$, $E^-_{L,R}$ form vector-like electroweak doublets, so their contributions to the gauge anomaly cancel. Hence this model is anomaly-free. Radiative masses for charged

| Particle | | | $(SU(3)_C, SU(2)_L, Y)$ | $Z_{2\ dark}$ | $A_4$ |
|---|---|---|---|---|---|
| $L_{iL}$ | = | $\begin{pmatrix}\nu_{eL}\\ l_{iL}\end{pmatrix}$ | $(\mathbf{1},\mathbf{2},-1/2)$ | + | $\mathbf{3}$ |
| | | $l_{iR}$ | $(\mathbf{1},\mathbf{1},-1)$ | + | $\mathbf{1},\mathbf{1}',\mathbf{1}''$ |
| $\Phi$ | = | $\begin{pmatrix}\phi^+\\ \phi^0\end{pmatrix}$ | $(\mathbf{1},\mathbf{2},+1/2)$ | + | $\mathbf{1}$ |
| $E_{L,R}$ | = | $\begin{pmatrix}E^0\\ E^-\end{pmatrix}_{L,R}$ | $(\mathbf{1},\mathbf{2},-1/2)$ | − | $\mathbf{1}$ |
| | | $N_{L,R}$ | $(\mathbf{1},\mathbf{1},0)$ | − | $\mathbf{1}$ |
| $x_i$ | = | $x_i^-$ | $(\mathbf{1},\mathbf{1},-1)$ | − | $\mathbf{3}$ |
| $y_i$ | = | $y_i^-$ | $(\mathbf{1},\mathbf{1},-1)$ | − | $\mathbf{1},\mathbf{1}',\mathbf{1}''$ |
| | | $s_i$ | $(\mathbf{1},\mathbf{1},0)$ | − | $\mathbf{3}$ |

Table 4.1: Particle content in the $A_4$ model.

lepton masses use the electrically charged scalars $x_{1,2,3}$ and $y_{1,2,3}$. Radiative masses for neutrinos use the real scalars $s_{1,2,3}$ the lightest combination of which is dark matter. Although not listed, lepton number may be defined as $L = +1$ for $E$,$N$ and the SM leptons, and $L = +2$ for $x_i$, $y_i$. All other SM particles have $(Z_{2\ dark}, A_4) = (+, \mathbf{1})$ and are therefore not affected by the imposition of the extra discrete symmetry.

The allowed Lagrangian terms before electroweak symmetry breaking are listed in Table 4.2 for the Yukawa and pure fermion terms, and in Table 4.3 for the pure scalar terms. The form of the scalar mass terms for $x_i$, $y_i$, $s_i$ follow from the $A_4$ symmetry. For the new fermions the general mass terms $m_A\overline{E_L}E_R$ and $m_B\overline{E_R}E_L$ are allowed, but adding their hermitian conjugates simply leads to $m_E = (m_A + m_B)$, and similarly for the singlets $N_{L,R}$ and $m_N$. For the hard Yukawa terms in $\mathcal{L}_D$, there are similar terms allowed under $A_4$ with $N_R$ replaced by $(N_L)^c$ and $f_D$ replaced by a different coupling, but these

Terms that respect $A_4$

$$
\begin{aligned}
\mathcal{L}_E &= -m_E \left( \overline{E_L^0} E_R^0 + \overline{E_L^-} E_R^- + \overline{E_R^0} E_L^0 + \overline{E_R^-} E_L^- \right) \\
\mathcal{L}_N &= -m_N \left( \overline{N_L} N_R + \overline{N_R} N_L \right) - \tfrac{1}{2} m_L \left( \overline{N_L} (N_L)^c + \overline{(N_L)^c} N_L \right) \\
&\qquad - \tfrac{1}{2} m_R \left( \overline{N_R} (N_R)^c + \overline{(N_R)^c} N_R \right) \\
\mathcal{L}_D &= -f_D \, \overline{E_R} \, \widetilde{\Phi} \, N_L - f_D \, \overline{N_L} \, \widetilde{\Phi}^\dagger \, E_R \\
&= -f_D \left( \overline{E_R^0} \phi^{0*} - \phi^- \overline{E_R^-} \right) N_L - f_D \, \overline{N_L} \left( \phi^0 E_R^0 - \phi^+ E_R^- \right) \\
\mathcal{L}_F &= -f_F \, \overline{E_L} \, \widetilde{\Phi} \, N_R - f_F \, \overline{N_R} \, \widetilde{\Phi}^\dagger \, E_L \\
&= -f_F \left( \overline{E_L^0} \phi^{0*} - \phi^- \overline{E_L^-} \right) N_R - f_F \, \overline{N_R} \left( \phi^0 E_L^0 - \phi^+ E_L^- \right) \\
\mathcal{L}_{f'} &= f' \, \overline{L_{iL}} \, \widetilde{(E_L)} \, x_i + f' \, \overline{\widetilde{(E_L)}} \, L_{iL} \, x_i^* \\
&= f' \, \left( \overline{\nu_{iL}} (E_L^-)^c - \overline{e_{iL}} (E_L^0)^c \right) x_i + f' \, \left( \overline{(E_L^-)^c} \nu_{iL} - \overline{(E_L^0)^c} e_{iL} \right) x_i^* \\
\mathcal{L}_{f_l} &= -f_i \, \overline{l_{iR}} \, (N_R)^c y_i - f_i \, \overline{(N_R)^c} \, l_{iR} y_i^* \\
\mathcal{L}_f &= f \, \overline{L_{iL}} \, E_R \, s_i + f \, \overline{E_R} \, L_{iL} \, s_i \\
&= f \, \left( \overline{\nu_{iL}} E_R^0 + \overline{e_{iL}} E_R^- \right) s_i + f \, \left( \overline{E_R^0} \nu_{iL} + \overline{E_R^-} e_{iL} \right) s_i
\end{aligned}
$$

Table 4.2: Yukawa and Fermion Lagrangian terms in the $A_4$ model.

Terms that respect $A_4$

$$
\begin{aligned}
\mathcal{L}_{Higgs} &= +\mu_{SM}^2 \Phi^\dagger\Phi - \tfrac{1}{2}\lambda_{SM}(\Phi^\dagger\Phi)^2 \\
\mathcal{L}_s &= -\tfrac{1}{2}m_s^2\left(s_1^2+s_2^2+s_3^2\right) \quad -\lambda_1\left(s_1^2+s_2^2+s_3^2\right)^2 - \lambda\left(s_1^2+s_2^2+s_3^2\right)(\Phi^\dagger\Phi) \\
\mathcal{L}_x &= -m_x^2\left(x_1^*x_1+x_2^*x_2+x_3^*x_3\right) \quad -\lambda_3\left(x_1^*x_1+x_2^*x_2+x_3^*x_3\right)^2 \\
&\qquad\qquad -\lambda_x\left(x_1^*x_1+x_2^*x_2+x_3^*x_3\right)(\Phi^\dagger\Phi) \\
\mathcal{L}_y &= -m_{y_1}^2 y_1^* y_1 \quad -\lambda_5\left(y_1^*y_1\right)^2 \quad -\lambda_8\left(y_1^*y_1\right)(\Phi^\dagger\Phi) \\
&\quad -m_{y_2}^2 y_2^* y_2 \quad -\lambda_6\left(y_2^*y_2\right)^2 \quad -\lambda_9\left(y_2^*y_2\right)(\Phi^\dagger\Phi) \\
&\quad -m_{y_3}^2 y_3^* y_3 \quad -\lambda_7\left(y_3^*y_3\right)^2 \quad -\lambda_y\left(y_3^*y_3\right)(\Phi^\dagger\Phi) \\
\mathcal{L}_{sx} &= -\lambda_{11}\left(x_1^*s_1+x_2^*s_2+x_3^*s_3\right)\left(x_1s_1+x_2s_2+x_3s_3\right) \\
&\quad -\lambda_{12}\left(x_1^*x_1+x_2^*x_2+x_3^*x_3\right)\left(s_1^2+s_2^2+s_3^2\right) \\
\mathcal{L}_{sy} &= -\lambda_{13}\, y_1^*y_1\left(s_1^2+s_2^2+s_3^2\right) - \left[\,\lambda_{16}\, y_1^*y_2\left(s_1^2+\omega s_2^2+\omega^2 s_3^2\right) + h.c.\,\right] \\
&\quad -\lambda_{14}\, y_2^*y_2\left(s_1^2+s_2^2+s_3^2\right) - \left[\,\lambda_{17}\, y_2^*y_3\left(s_1^2+\omega s_2^2+\omega^2 s_3^2\right) + h.c.\,\right] \\
&\quad -\lambda_{15}\, y_3^*y_3\left(s_1^2+s_2^2+s_3^2\right) - \left[\,\lambda_{18}\, y_1^*y_3\left(s_1^2+\omega^2 s_2^2+\omega s_3^2\right) + h.c.\,\right] \\
\mathcal{L}_{sxy} &= -\lambda_{19}\, y_1\left(x_1^*s_1^2+x_2^*s_2^2+x_3^*s_3^2\right) + h.c. \\
&\quad -\lambda_{20}\, y_2\left(x_1^*s_1^2+\omega x_2^*s_2^2+\omega^2 x_3^*s_3^2\right) + h.c. \\
&\quad -\lambda_{21}\, y_3\left(x_1^*s_1^2+\omega^2 x_2^*s_2^2+\omega x_3^*s_3^2\right) + h.c. \\
\mathcal{L}_{xy} &= \text{Quartic terms} \quad x_i^*x_j y_k^* y_l \quad \text{and} \quad x_i^*x_j^* y_k y_l
\end{aligned}
$$

Terms that break $A_4$

$$
\begin{aligned}
\mathcal{L}_{xy} &= -\mu_i^2\, y_i (U_\omega)_{ij} x_j^* + h.c. \qquad \text{where} \qquad \mu_i^2 = \mu_e^2, \mu_\mu^2, \mu_\tau^2 \\
\mathcal{L}_{ss} &= -s_i m_{ij}^2 s_j + h.c.
\end{aligned}
$$

Table 4.3: Scalar Lagrangian terms in the $A_4$ model.

are not included because they break lepton number. Similar comments apply for $\mathcal{L}_F$ and the use of $N_L$ instead of $(N_R)^c$. The soft breaking of lepton number by the Majorana mass terms $\overline{N_L}(N_L)^c$, $\overline{N_R}(N_R)^c$ is needed for neutrino mass in section 4.6, but these terms can be naturally small because their absence enhances the lepton number symmetry. So in the following sections that deal with charged leptons we will neglect the Majorana mass terms. Also, when writing out the most general Lagrangian, there are additional terms that are similar to those listed in $\mathcal{L}_{Yukawa,f_D}$ with a different coupling, $-f'_D\ \overline{(N_L)^c}\ \Phi^\dagger \widetilde{E_R} + h.c.$, but adding these simply gives $(-f_D + f'_D)\overline{E_R}\ \widetilde{\Phi} N_L + h.c$, so the coefficient is redefined as $-f_D$. Similar comments apply for $\mathcal{L}_F$ and $\mathcal{L}_{f'}$.

As mentioned earlier, there is soft-breaking of the $A_4$ symmetry, and this comes from the scalar terms $y_i x_j^*$ and $s_i s_j$. Most of the other scalar terms listed are not needed in what follows, although at the end of the chapter there are some technical remarks about the quartic terms as they relate to the soft symmetry-breaking terms.

## 4.2 Charged Leptons

Every possible SM Yukawa term $\Phi^0 \overline{L_{iL}} l_{jR}$ is forbidden by the $A_4$ symmetry. This follows from the group multiplication rules given at the end of the chapter. The Higgs $\Phi^0 \sim \mathbf{1}$ is trivial, and the multiplication of $\overline{L_{iL}} \sim \mathbf{3}$ and $l_{jR} \sim \mathbf{1}, \mathbf{1'}, \mathbf{1''}$ yields another $\mathbf{3}$, so the total combination is a $\mathbf{3}$. Therefore these terms are forbidden since they are not a $\mathbf{1}$ under $A_4$. All $x_i^* y_j$ terms are likewise forbidden, since $x_i^* \sim \mathbf{3}$ and $y_j \sim \mathbf{1}, \mathbf{1'}, \mathbf{1''}$. For charged leptons, the one-loop Higgs Yukawa interaction is shown in Fig. 4.1. Connecting $x_i$ with $y_i^*$ requires the breaking of $A_4$. This can be done explicitly or it can be done spontaneously

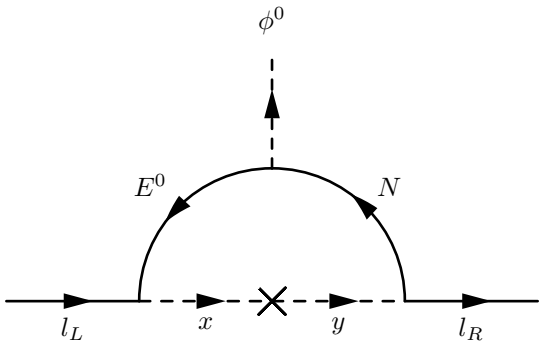


Figure 4.1: Radiative Higgs Yukawa interaction for charged leptons.

using the VEV of another $A_4$ scalar. We choose explicit breaking terms because other $A_4$ scalars would introduce extra contributions to the effective Higgs Yukawa coupling and we want to highlight the SM deviations caused by the underlying radiative mechanism. The soft-breaking indicated by the cross in the figure is assumed to be

$$\mathcal{L}_{xy} \quad = \quad -\mu_i^2 \, y_i (U_\omega)_{ij} x_j^* \quad + \quad h.c. \tag{4.4}$$

which as mentioned earlier is chosen for the method of obtaining the neutrino mixing matrix. These terms can be interpreted as a rotation from $x_i$ to $z_i$, that is

$$\begin{aligned} z_i^* &= (U_\omega)_{ij} x_j^* \\ x_i &= (U_\omega)_{ij} z_j \end{aligned} \tag{4.5}$$

where in the last line the property $U_\omega = U_\omega^T$ has been used. This is a convenient rotation because going to the basis of $z_i$ and $y_i$ will make the scalar mixing matrix block-diagonal

$$-\mathcal{L}_{xy} = (z_1^*, y_1^*, z_2^*, y_2^*, z_3^*, y_3^*) \begin{pmatrix} m_x^2 & \mu_e^2 & 0 & 0 & 0 & 0 \\ \mu_e^2 & m_{y_1}^2 & 0 & 0 & 0 & 0 \\ 0 & 0 & m_x^2 & \mu_\mu^2 & 0 & 0 \\ 0 & 0 & \mu_\mu^2 & m_{y_2}^2 & 0 & 0 \\ 0 & 0 & 0 & 0 & m_x^2 & \mu_\tau^2 \\ 0 & 0 & 0 & 0 & \mu_\tau^2 & m_{y_3}^2 \end{pmatrix} \begin{pmatrix} z_1 \\ y_1 \\ z_2 \\ y_2 \\ z_3 \\ y_3 \end{pmatrix} \tag{4.6}$$

For example, the electron block has mass eigenstates $\zeta_{1e}, \zeta_{2e}$ with masses $m_{1e}, m_{2e}$ and mixing angle $\theta_e$

$$\begin{pmatrix} z_1^- \\ y_1^- \end{pmatrix} = \begin{pmatrix} \cos\theta_e & -\sin\theta_e \\ \sin\theta_e & \cos\theta_e \end{pmatrix} \begin{pmatrix} \zeta_{1e}^- \\ \zeta_{2e}^- \end{pmatrix} \tag{4.7}$$

where the new parameters $m_{1e}, m_{2e}, \theta_e$ are related to the old parameters $m_\eta, m_\chi, \mu_e$ by

$$\mu_e^2 = \sin\theta_e \cos\theta_e (m_{1e}^2 - m_{1e}^2) \tag{4.8}$$

$$m_\eta^2 = \cos\theta_e m_{1e}^2 + \sin\theta_e m_{1e}^2 \tag{4.9}$$

$$m_\chi^2 = \sin\theta_e m_{1e}^2 + \cos\theta_e m_{1e}^2 \tag{4.10}$$

and similarly for the blocks corresponding to $\mu$ and $\tau$.

## 4.3 Radiative Mass

The one-loop Higgs Yukawa interactions in the previous Fig. 4.1 generates radiative masses for all three charged leptons when the electroweak symmetry is spontaneously

broken. The Higgs VEV induces the mixing of $N$ and $E^0$, which comes from the diagonal mass terms $\mathcal{L}_N$, $\mathcal{L}_E$ and the off-diagonal $f_D$, $f_F$ Yukawa terms $\mathcal{L}_D$, $\mathcal{L}_F$. The mixing matrix

$$\mathcal{L}_{N+E+D+F} \supset - \left(\overline{N_L}, \overline{E_L^0}\right) \begin{pmatrix} m_N & f_D v/\sqrt{2} \\ f_F v/\sqrt{2} & m_E \end{pmatrix} \begin{pmatrix} N_R \\ E_R^0 \end{pmatrix} + h.c. \tag{4.11}$$

is diagonalized by a rotation of the left-handed fields $N_L, E_L^0$ and a separate rotation of the right-handed fields $N_R, E_R^0$ into the two physical Dirac particles $n_1 = n_{1L} + n_{1R}$ and $n_2 = n_{2L} + n_{2R}$ with mass eigenvalues $m_1$ and $m_2$. For the left-handed fields

$$\begin{pmatrix} N_L \\ E_L^0 \end{pmatrix} = \begin{pmatrix} \cos\theta_L & -\sin\theta_L \\ \sin\theta_L & \cos\theta_L \end{pmatrix} \begin{pmatrix} n_{1L} \\ n_{2L} \end{pmatrix} \tag{4.12}$$

and for the right-handed fields

$$\begin{pmatrix} N_R \\ E_R^0 \end{pmatrix} = \begin{pmatrix} \cos\theta_R & -\sin\theta_R \\ \sin\theta_R & \cos\theta_R \end{pmatrix} \begin{pmatrix} n_{1R} \\ n_{2R} \end{pmatrix} \tag{4.13}$$

The four new parameters $m_1, m_2, \theta_L, \theta_R$ are related to the four old parameters $m_N, m_E, f_D, f_F$ by the four equations

$$\begin{aligned} m_N &= m_1 \cos\theta_L \cos\theta_R + m_2 \sin\theta_L \sin\theta_R \\ m_E &= m_2 \cos\theta_L \cos\theta_R + m_1 \sin\theta_L \sin\theta_R \\ f_D v/\sqrt{2} &= m_1 \cos\theta_L \sin\theta_R - m_2 \cos\theta_R \sin\theta_L \\ f_F v/\sqrt{2} &= m_1 \cos\theta_R \sin\theta_L - m_2 \cos\theta_L \sin\theta_R \end{aligned} \tag{4.14}$$

In the case when $\theta_L = \theta_R$ the last two lines above are the same and give $f_D = f_F$, and so there are only three equations. The three new parameters $m_1, m_2, \theta_L$ are related to the

three old parameters $m_N, m_E, f_D$ by the three equations

$$\begin{aligned} m_N &= m_1 \cos^2\theta_L + m_2 \sin^2\theta_L \\ m_E &= m_2 \cos^2\theta_L + m_1 \sin^2\theta_L \\ f_D v/\sqrt{2} &= (m_1 - m_2)\cos\theta_L \sin\theta_L \end{aligned} \tag{4.15}$$

The previous rotation from $x_i$ to $z_i$ affects the other $f'$ Yukawa interactions of the left-handed charged leptons

$$\begin{aligned} \mathcal{L}_{f'} &\supset f' \left( \overline{l_{iL}} (E_L^0)^c x_i + \overline{(E_L^0)^c} l_{iL} x_i^* \right) \\ &= f' \left( \overline{e_{jL}} (E_L^0)^c z_j + \overline{(E_L^0)^c} e_{jL} z_j^* \right) \end{aligned} \tag{4.16}$$

which identifies the linear combinations of the $A_4$ basis states $l_{iL}$

$$\begin{aligned} \overline{e_{jL}} &= \overline{l_{iL}} (U_\omega)_{ij} \\ e_{jL} &= l_{iL} (U_\omega^\dagger)_{ij} = (U_\omega^\dagger)_{ji} l_{iL} \end{aligned} \tag{4.17}$$

that diagonalize the radiative mass matrix

$$(\overline{e_L}, \overline{\mu_L}, \overline{\tau_L}) \begin{pmatrix} m_e & 0 & 0 \\ 0 & m_\mu & 0 \\ 0 & 0 & m_\tau \end{pmatrix} \begin{pmatrix} e_R \\ \mu_R \\ \tau_R \end{pmatrix} \tag{4.18}$$

so that the physical Dirac field of charged lepton $e_i$ is $e_i = e_{iL} + e_{iR}$. The right-handed charged leptons have the Yukawa terms

$$\mathcal{L}_{fl} = f_i \, \overline{l_{iR}} \, (N_R)^c y_i + f_i \, \overline{(N_R)^c} \, l_{iR} y_i^* \tag{4.19}$$

and since $y_i$ is not rotated, the $A_4$ basis states $l_{iR}$ already correspond to the mass-diagonal

states $e_{iR}$.

The calculation of the electron mass is shown schematically in Fig. 4.2. It is similar to the calculation in Chapter 2, and as before the projection operators may be separated from the fields. Because the conjugate fields $n^c$ propagate in the loop, we use $(n_L)^c = (n^c)_R = P_R(n^c)$, $(n_R)^c = (n^c)_L = P_L(n^c)$. This allows contractions to made between $n_i^c$ and $\overline{n_i^c}$ to give propagators. Expressing the fields $E^0$, $N$ in terms of the mass eigenstates $n_1$, $n_2$ and the fields $z_1$, $y_1$ in terms of the mass eigenstates $\zeta_{1e}$, $\zeta_{2e}$ we have

$$\mathcal{L}_{f'+f_l} = \sum_{i,k} \overline{e} \left[ a_{ik} f' P_R + b_{ik} f_e P_L \right] n_i^c \zeta_k^- + \overline{n_i^c} \left[ a_{ik} f' P_L + b_{ik} f_e P_R \right] e \zeta_k^+ \qquad (4.20)$$

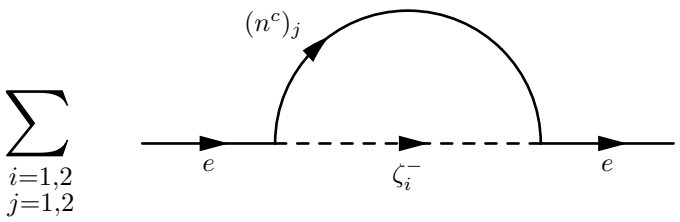


Figure 4.2: Radiative electron mass in the $A_4$ model.

with the shorthand notation

$$a_{ik} \;=\; \begin{array}{c|cc} & \zeta_1 & \zeta_2 \\ \hline n_1^c & s_L c & -s_L s \\ n_2^c & c_L c & -c_L s \end{array}$$

$$b_{ik} \;=\; \begin{array}{c|cc} & \zeta_1 & \zeta_2 \\ \hline n_1^c & c_R s & c_R c \\ n_2^c & -s_R s & -s_R c \end{array} \tag{4.21}$$

where $c = \cos\theta_e,\ s = \sin\theta_e,\ c_L = \cos\theta_L,\ s_L = \sin\theta_L,\ c_R = \cos\theta_R,\ s_R = \sin\theta_R$. Let the arrows in Fig. 4.2 dictate the flow of momentum. Then the momenta for $e, n_i^c, \zeta_k^-$ are $p, k, p-k$ respectively, and we set $p$ to zero. Then the loop integral for the self-energy is

$$-im_e \;=\; i^4 \sum_{i,k} \int \frac{d^4k}{(2\pi)^4} \left[ \frac{numerator}{(k^2 - m_{ke}^2)(k^2 - m_i^2)} \right] \tag{4.22}$$

where the factor of $i^4 = 1$ is from the two propagators and the two vertices, and the numerator is

$$\begin{aligned} numerator &= \left[a_{ik} f' P_R + b_{ik} f_e P_L\right] \left[\not{k} + m_i\right] \left[a_{ik} f' P_L + b_{ik} f_e P_R\right] \\ &= f' f_e a_{ik} b_{ik} m_i (P_L^2 + P_R^2) \\ &= f' f_e a_{ik} b_{ik} m_i \end{aligned} \tag{4.23}$$

which has been simplified as before, since the term linear in $k$ will integrate to zero, and

the projectors make some terms vanish. Then using $a_{ik}$ and $b_{ik}$, we have

$$-im_e = f'f_e \int \frac{d^4k}{(2\pi)^4} \begin{bmatrix} \frac{(s_L c)(c_R s)m_1}{(k^2-m_1^2)(k^2-m_{1e}^2)} + \frac{(-s_L s)(c_R c)m_1}{(k^2-m_1^2)(k^2-m_{2e}^2)} \\ \\ \frac{(c_L c)(-s_R s)m_2}{(k^2-m_2^2)(k^2-m_{1e}^2)} + \frac{(-c_L s)(-s_R c)m_2}{(k^2-m_2^2)(k^2-m_{2e}^2)} \end{bmatrix}$$

$$= f'f_e \int \frac{d^4k}{(2\pi)^4} \begin{bmatrix} \frac{sc\; s_L c_R\, m_1\, (m_{1e}^2 - m_{2e}^2)}{(k^2-m_1^2)(k^2-m_{1e}^2)(k^2-m_{2e}^2)} \\ \\ \frac{-sc\; c_L s_R\, m_2\, (m_{1e}^2 - m_{2e}^2)}{(k^2-m_2^2)(k^2-m_{1e}^2)(k^2-m_{2e}^2)} \end{bmatrix} \tag{4.24}$$

In the first equation, each term diverges, but the sum is finite, as shown in the second equation by putting terms over common denominators. Using the integrals from Chapter 2, the radiative mass is

$$\begin{aligned} -im_e &= f'f_e \frac{-i}{16\pi^2} sc \left[ s_L c_R\, m_1\, \left[H(x_{1e,1}) - H(x_{2e,1})\right] - c_L s_R\, m_2\, \left[H(x_{1e,2}) - H(x_{2e,2})\right]\right] \\ &= f'f_e \frac{-i}{16\pi^2} sc \begin{bmatrix} s_L c_R\, m_1\, \left[H(x_{1e,1}) - H(x_{2e,1})\right] \\ \\ -c_L s_R\, m_2\, \left[H(x_{1e,2}) - H(x_{2e,2})\right] \end{bmatrix} \end{aligned} \tag{4.25}$$

where the notation $x_{c,d}$ denotes the scalar-to-fermion ratios of mass-squared $x_{ie,1} = m_{ie}^2/m_1^2$ and $x_{ie,2} = m_{ie}^2/m_2^2$.

## 4.4 Anomalous Higgs Yukawa Couplings

Consider now the heaviest charged lepton tau. There are three contributions to the effective $h\overline{\tau}\tau$ coupling

$$g_\tau = g_\tau^{(1)} + g_\tau^{(2)} + g_\tau^{(3)} \tag{4.26}$$

First we will calculate the primary contribution $g_\tau^{(1)}$ shown in Fig. 4.3. There are two Higgs connections at the top which come from the $f_D$ and $f_F$ Yukawa terms in $\mathcal{L}_D$ and $\mathcal{L}_F$

$$\begin{aligned} \mathcal{L}_D &\supset -f_D \frac{h}{\sqrt{2}} \left[ \overline{E_R^0} N_L + \overline{N_L} E_R^0 \right] \\ \mathcal{L}_F &\supset -f_F \frac{h}{\sqrt{2}} \left[ \overline{E_L^0} N_R + \overline{N_R} E_L^0 \right] \end{aligned} \tag{4.27}$$

We express $E_{L,R}^0$, $N_{L,R}$ in terms of the mass eigenstates $(n_1)_{L,R}$, $(n_2)_{L,R}$ and then use $(n_L)^c = (n^c)_R = P_R(n^c)$, $(n_R)^c = (n^c)_L = P_L(n^c)$ to allow contractions to made between

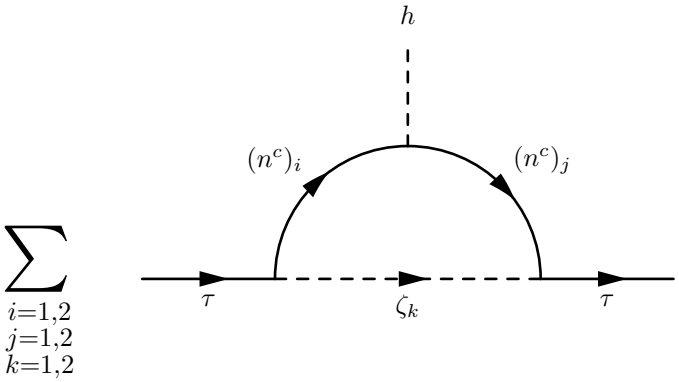


Figure 4.3: First contribution to $h\overline{\tau}\tau$ in the $A_4$ model.

$n_i^c$ and $\overline{n_i^c}$ to give propagators. This gives

$$\begin{aligned}
\mathcal{L}_{D+F} \quad \supset \quad & -hA\,\overline{n_1^c} n_1^c \\
& -hB\,\overline{n_2^c} n_2^c \\
& -h\overline{n_1^c}\,[\,CP_L + DP_R\,]\,n_2^c \\
& -h\overline{n_2^c}\,[\,DP_L + CP_R\,]\,n_1^c
\end{aligned} \tag{4.28}$$

where

$$\begin{aligned}
A &= (\quad f_D c_L s_R + f_F s_L c_R)/\sqrt{2} \\
B &= (-f_D s_L c_R - f_F c_L s_R)/\sqrt{2} \\
C &= (\quad f_D c_L c_R - f_F s_L s_R)/\sqrt{2} \\
D &= (-f_D s_L s_R + f_F c_L c_R)/\sqrt{2}
\end{aligned} \tag{4.29}$$

Let the arrows in Fig. 4.3 dictate the flow of momentum. Assuming that $m_h^2$ is small compared to $m_{1,2}^2$ and $m_{\tau 1,2}^2$, the momenta for $\tau, n_i^c, n_j^c, \zeta_k^-$ are $p, k, k, p-k$ respectively, and we set $p$ to zero. Then the loop integral for the primary effective Yukawa coupling is

$$-ig_\tau^{(1)} \quad = \quad i^6 \sum_{i,j,k} \int \frac{d^4k}{(2\pi)^4} \left[ \frac{numerator}{(k^2 - m_i^2)(k^2 - m_j^2)(k^2 - m_{\tau k}^2)} \right] \tag{4.30}$$

where the factor of $i^6 = -1$ is from the three propagators and the three vertices. For the numerator, consider the four cases $numerator_{ji}$ corresponding to $\overline{n_j^c} n_i^c$. For the two cases

when $i = j$ we have

$$\begin{aligned} numerator_{11} &= \left[a_{1k}f'P_R + b_{1k}f_\tau P_L\right]\left[\not{k} + m_1\right]\left[-A\right]\left[\not{k} + m_1\right]\left[a_{1k}f'P_L + b_{1k}f_\tau P_R\right] \\ numerator_{22} &= \left[a_{2k}f'P_R + b_{2k}f_\tau P_L\right]\left[\not{k} + m2\right]\left[-B\right]\left[\not{k} + m_2\right]\left[a_{2k}f'P_L + b_{2k}f_\tau P_R\right] \end{aligned} \tag{4.31}$$

The terms linear in $k$ integrate to zero and the projection operators each of these simplifies

$$\begin{aligned} numerator_{11} &= -f'f_\tau A\; a_{1k}b_{1k}\left[m_1^2 + k^2\right] \\ numerator_{22} &= -f'f_\tau B\; a_{2k}b_{2k}\left[m_2^2 + k^2\right] \end{aligned} \tag{4.32}$$

For the two cases when $i \neq j$ we have

$$\begin{aligned} numerator_{21} &= \left[a_{2k}f'P_R + b_{2k}f_\tau P_L\right]\left[\not{k} + m_2\right]\left[-DP_L - CP_R\right]\left[\not{k} + m_1\right]\left[a_{1k}f'P_L + b_{1k}f_\tau P_R\right] \\ numerator_{12} &= \left[a_{1k}f'P_R + b_{1k}f_\tau P_L\right]\left[\not{k} + m_1\right]\left[-CP_L - DP_R\right]\left[\not{k} + m_2\right]\left[a_{2k}f'P_L + b_{2k}f_\tau P_R\right] \end{aligned} \tag{4.33}$$

Together, these two equations combine to give

$$\begin{aligned} numerator_{21+21} &= -f'f_\tau m_1 m_2 \begin{bmatrix} [a_{2k}b_{1k}CP_R + b_{2k}a_{1k}DP_L] \\ +[a_{1k}b_{2k}DP_R + b_{1k}a_{2k}CP_L] \end{bmatrix} \\ & \quad -f'f_\tau \quad k^2 \quad \begin{bmatrix} [a_{2k}b_{1k}DP_R + b_{2k}a_{1k}CP_L] \\ +[a_{1k}b_{2k}CP_R + b_{1k}a_{2k}DP_L] \end{bmatrix} \\ &= -f'f_\tau m_1 m_2 \left[a_{2k}b_{1k}C + b_{2k}a_{1k}D\right] \\ & \quad -f'f_\tau \quad k^2 \quad \left[a_{2k}b_{1k}D + b_{2k}a_{1k}C\right] \end{aligned} \tag{4.34}$$

Then using $a_{ik}$ and $b_{ik}$, we have

$$-ig_\tau^{(1)} = +f'f_\tau \int \frac{d^4k}{(2\pi)^4} \left[ \begin{array}{c} \frac{s_L c_R\, sc\, A\,(m_1^2+k^2)}{(k^2-m_1^2)^2(k^2-m_{1\tau}^2)} - \frac{s_L c_R\, sc\, A\,(m_1^2+k^2)}{(k^2-m_1^2)^2(k^2-m_{2\tau}^2)} \\ -\frac{c_L s_R\, sc\, B\,(m_2^2+k^2)}{(k^2-m_2^2)^2(k^2-m_{1\tau}^2)} + \frac{c_L s_R\, sc\, B\,(m_2^2+k^2)}{(k^2-m_2^2)^2(k^2-m_{2\tau}^2)} \\ +\frac{(c_L c_R\, sc\, C - s_L s_R\, sc\, D)(m_1 m_2)}{(k^2-m_1^2)(k^2-m_2^2)(k^2-m_{1\tau}^2)} \\ -\frac{(c_L c_R\, sc\, C - s_L s_R\, sc\, D)(m_1 m_2)}{(k^2-m_1^2)(k^2-m_2^2)(k^2-m_{2\tau}^2)} \\ +\frac{(c_L c_R\, sc\, D - s_L s_R\, sc\, C)(k^2)}{(k^2-m_1^2)(k^2-m_2^2)(k^2-m_{1\tau}^2)} \\ -\frac{(c_L c_R\, sc\, D - s_L s_R\, sc\, C)(k^2)}{(k^2-m_1^2)(k^2-m_2^2)(k^2-m_{2\tau}^2)} \end{array} \right] \tag{4.35}$$

The integrals involving $m_i m_j$ are finite, and the integral has already been done. The integrals involving $k^2$ diverge, but can be put over a common denominator with a neighbouring term to give a finite result. So this reduces to

$$-ig_\tau^{(1)} = +f'f_\tau sc \left[ \begin{array}{c} s_L c_R\, A\, m_1^2 (I_{1,1,1\tau} - I_{1,1,2\tau}) \\ -c_L s_R\, B\, m_2^2 (I_{2,2,1\tau} - I_{2,2,2\tau}) \\ +(c_L c_R\, C\, - s_L s_R\, D) m_1 m_2 (I_{1,2,1\tau} - I_{1,2,2\tau}) \\ +s_L c_R\, A\,(m_{1\tau}^2 - m_{2\tau}^2) K_{1,1,1\tau,2\tau} \\ -c_L s_R\, B\,(m_{1\tau}^2 - m_{2\tau}^2) K_{2,2,1\tau,2\tau} \\ +(c_L c_R\, D\, - s_L s_R\, C)(m_{1\tau}^2 - m_{2\tau}^2) K_{1,2,1\tau,2\tau} \end{array} \right] \tag{4.36}$$

where

$$
\begin{aligned}
I_{a,b,c} &= I(m_a, m_b, m_c) \\
&= \frac{-i}{16\pi^2}\left[\frac{m_a^2\ln(m_a^2/M^2)}{(m_a^2-m_b^2)(m_a^2-m_c^2)} + \frac{m_b^2\ln(m_b^2/M^2)}{(m_b^2-m_a^2)(m_b^2-m_c^2)} + \frac{m_c^2\ln(m_c^2/M^2)}{(m_c^2-m_a^2)(m_c^2-m_b^2)}\right]
\end{aligned}
$$

$$
\begin{aligned}
K_{a,b,c,d} &= K(m_a, m_b, m_c, m_d) \\
&= \int \frac{d^4k}{(2\pi)^4}\frac{k^2}{(k^2-m_a^2)(k^2-m_b^2)(k^2-m_c^2)(k^2-m_d^2)} \\
&= \frac{-i}{16\pi^2}\left[\begin{array}{l}
\dfrac{m_a^4\ln(m_a^2/M^2)}{(m_a^2-m_b^2)(m_a^2-m_c^2)(m_a^2-m_d^2)} \\
+\dfrac{m_b^4\ln(m_b^2/M^2)}{(m_b^2-m_a^2)(m_b^2-m_c^2)(m_b^2-m_d^2)} \\
+\dfrac{m_c^4\ln(m_c^2/M^2)}{(m_c^2-m_a^2)(m_c^2-m_b^2)(m_c^2-m_d^2)} \\
+\dfrac{m_d^4\ln(m_d^2/M^2)}{(m_d^2-m_a^2)(m_d^2-m_b^2)(m_d^2-m_c^2)}
\end{array}\right]
\end{aligned}
\tag{4.37}
$$

The factors of $-i$ cancel and $g_\tau^{(1)}$ is real. Here the mass scale $M$ is arbitrary. It appears if we choose to put the loop integrals into dimensionless form before doing the momentum integration. For convenience we choose $M = m_1$ as described at the end of this section.

The second and third contributions $g_\tau^{(2)}$ and $g_\tau^{(3)}$ to the effective Higgs Yukawa

coupling come from the scalar interactions

$$\begin{aligned} \mathcal{L}_x &\supset -(\lambda_x v)h\,(x_1^* x_1 + x_2^* x_2 + x_3^* x_3) \\ \mathcal{L}_y &\supset -(\lambda_y v)h\,(y_3^* y_3) \end{aligned} \tag{4.38}$$

respectively. Putting this in terms of the mass eigenstates $\zeta_i = \zeta_{1,2}$ gives the diagrams shown schematically in Fig. 4.4 Looking back to Chapter 2, this is the same type of diagram as Fig. 2.3 so the integrals have been done and it is straightforward to adapt those results, so the expressions for $g_\tau^{(2)}$ and $g_\tau^{(3)}$ are not written here for brevity.

Adding all three contributions, the effective Higgs Yukawa coupling will deviate from the SM prediction when

$$\frac{g_\tau v}{m_\tau} = \frac{[g_\tau^{(1)} + g_\tau^{(2)} + g_\tau^{(3)}]v}{m_\tau} \tag{4.39}$$

deviates from unity. To simplify the analysis, we focus on $\theta_L = \theta_R$, in which case $f_D = f_F$. We use the relation $f_D v/\sqrt{2} = s_L c_L(m_1 - m_2) = s_L c_L m_1(1 - m_2/m_1)$ from fermion mixing Eq. (4.15) to define $m_1$ as a function of $\theta_L$ for a constant ratio $m_2/m_1 = 2.2$ and coupling $f_D/\sqrt{4\pi} = -0.19$. In this parameterization, the combination $s_L c_L m_1$ remains constant,

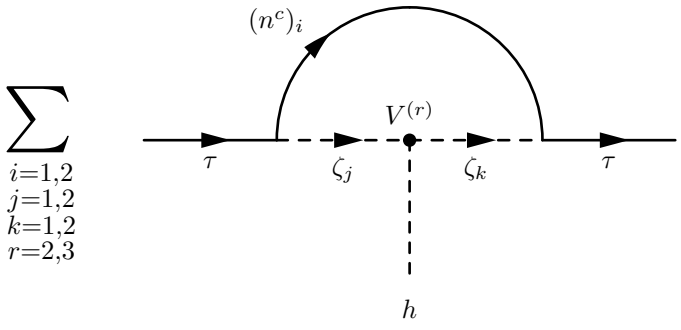


Figure 4.4: Second and third contributions to $h\overline{\tau}\tau$ in the $A_4$ model.

and also appears in the radiative mass formula for each charged lepton. In addition, we use the value $f'/\sqrt{4\pi} = -0.6$. For the scalars in the tau sector, we choose fixed mass ratios $m_{1\tau}/m_1 = 5.7$ and $m_{2\tau}/m_1 = 1.1$. To satisfy the mass formula, we verify that the product $f_\tau \sin 2\theta_\tau$ is not too large. We have checked that the values used here also allow solutions for the muon and electron radiative masses. In Fig. 4.5 we plot the ratio $(g_\tau v/m_\tau)^2$ from Eq. (4.39) as a function of $\theta_L$, using the values $f_\tau/\sqrt{4\pi} = -0.54$, $\theta_\tau = 0.8$ for the $\lambda_{x,y}$ curves. We see that a significant deviation from the SM prediction is possible. This is

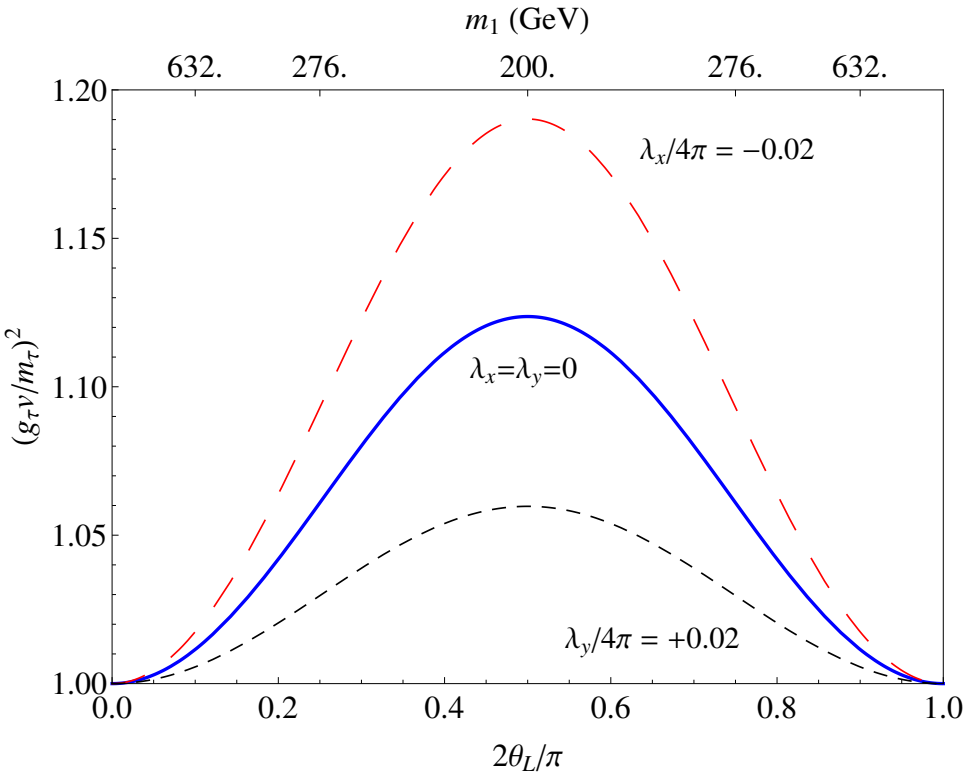


Figure 4.5: The ratio $(g_\tau v/m_\tau)^2$ plotted against $\theta_L$ with various $\lambda_{x,y}$ for the case $\theta_L = \theta_R$.

consistent with the bounds from LHC measurements by ATLAS [21] and CMS [22]

$$\begin{aligned} \mu(h \to \tau\tau)|_{\text{ATLAS}} &= 1.43^{+0.43}_{-0.37} \\ \mu(h \to \tau\tau)|_{\text{CMS}} &= 0.91 \pm 0.28 \end{aligned} \tag{4.40}$$

Note that in this model, lepton flavor is not violated by the effective Higgs Yukawa couplings. A recent preliminary measurement [38] of the branching fraction $BR(h \to \tau\mu) \sim 0.01$ is only at the 2 sigma level, but if it is confirmed by future experiments this model will need to be adjusted.

## 4.5 Muon Anomalous Magnetic Moment

Turning now to the muon, there are three contributions to the anomalous magnetic moment. The electromagnetic interaction shown in Fig. 4.6 has the same structure as Fig. 2.7 from Chapter 2, and those results are easily adapted. Similar to the previous model, the dominant contribution is

$$\Delta a_\mu = \frac{m_\mu^2}{m_1 m_2}\left\{ \frac{s_L c_R m_2[G(x_{1\mu,1}) - G(x_{2\mu,1})] + s_R c_L m_1[G(x_{2\mu,2}) - G(x_{1\mu,2})]}{s_L c_R m_1[H(x_{1\mu,1}) - H(x_{2\mu,1})] + s_R c_L m_2[H(x_{2\mu,2}) - H(x_{1\mu,2})]} \right\} \tag{4.41}$$

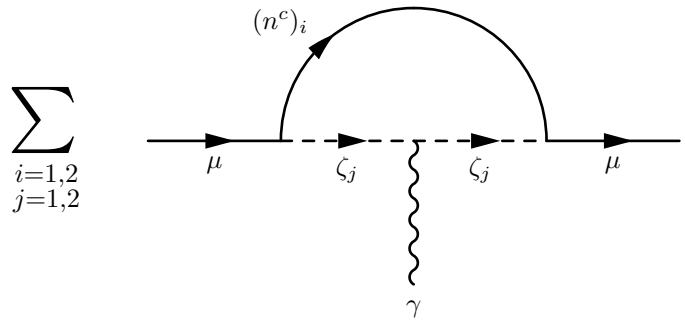


Figure 4.6: First and second contributions to the muon magnetic moment.

where $x_{i\mu,j} = (m_{i\mu}/m_j)^2$ and

$$G(x) = \frac{2x \ln x}{(x-1)^3} - \frac{x+1}{(x-1)^2} \tag{4.42}$$

The second, subdominant contribution is negative as expected

$$(\Delta a_\mu)' = -\frac{-m_\mu^2}{32\pi^2} \left( \begin{array}{c} f'^2 \left[ \frac{s_L^2}{m_1^2} \left( c_\mu^2 J(x_{1\mu,1}) + s_\mu^2 J(x_{2\mu,1}) \right) + \frac{c_L^2}{m_2^2} \left( c_\mu^2 J(x_{1\mu,2}) + s_\mu^2 J(x_{2\mu,2}) \right) \right] \\ + f_\mu^2 \left[ \frac{c_R^2}{m_1^2} \left( s_\mu^2 J(x_{1\mu,1}) + c_\mu^2 J(x_{2\mu,1}) \right) + \frac{s_R^2}{m_2^2} \left( s_\mu^2 J(x_{1\mu,2}) + c_\mu^2 J(x_{2\mu,2}) \right) \right] \end{array} \right)$$

where

$$J(x) = \frac{x \ln x}{(x-1)^4} + \frac{x^2 - 5x - 2}{6(x-1)^3}. \tag{4.43}$$

The third contribution from exchange of $s_{1,2,3}$ is also subdominant, and it will be discussed in the next section.

In the simplifying case we are considering, Eq. 4.41 is independent of $\theta_L = \theta_R$. In Fig. 4.7 we plot $m_{1\mu}$ against $m_1$ for various ratios $m_{2\mu}/m_{1\mu}$ in order to show the values of $m_1$ and $m_{1,2\mu}$ which can account for the discrepancy between the experimental measurement [25] and the SM prediction [26]

$$\Delta a_\mu = 39.35 \pm 5.21_{\text{th}} \pm 6.3_{\text{exp}} \times 10^{-10} \tag{4.44}$$

We have combined the experimental and theoretical uncertainties in quadrature, which corresponds to the curved limits of the shaded regions. The lower limit of 200 GeV for $m_1$ corresponds to $\theta_L = \pi/4$.

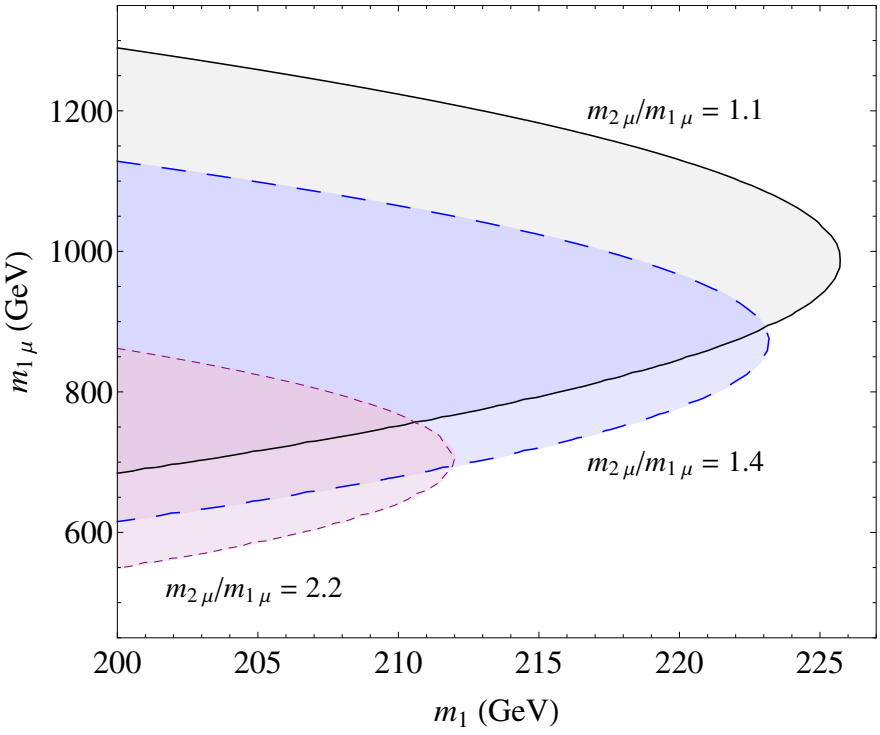


Figure 4.7: Values of $m_1$, $m_{1\mu}$ and $m_{2\mu}$ which can explain $\Delta a_\mu$ for the case $\theta_L = \theta_R$.

## 4.6 Neutrinos and Rare Lepton Decays

The radiative neutrino mass diagram comes from the four-point diagram shown in Fig. 4.8. It is almost the same as Fig. 3.1 from the previous Chapter, except that here $N_R$ is also present. The cross indicates the breaking of lepton number by the Majorana mass terms

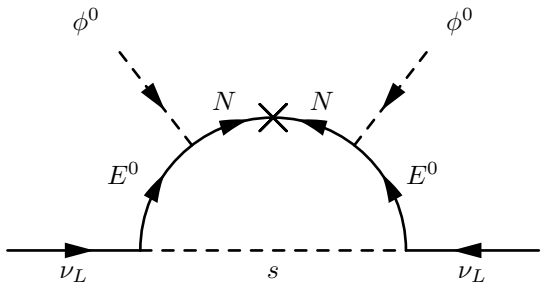


Figure 4.8: Radiative neutrino mass in the $A_4$ model.

for $N_R$ and $N_L$. All interactions in this diagram respect the $A_4$ symmetry. Furthermore, if $A_4$ were unbroken, then $s_{1,2,3}$ have the same mass from $\mathcal{L}_s \supset -\frac{1}{2}m_s^2\left(s_1^2+s_2^2+s_3^2\right)$. The $A_4$ symmetry is also responsible for the one-to-one correspondence between $\nu_{iL}$ and $s_i$ from $\mathcal{L}_f = f\ \overline{L_{iL}}\ E_R\ s_i$. But as mentioned at the beginning of this chapter, the terms $\mathcal{L}_{ss} = -s_i m_{ij}^2 s_j$ arbitrarily break $A_4$ so that a realistic neutrino mixing matrix can be obtained and also allows nonzero neutrino mass differences. Let the physical mass states be $s'_i = \mathcal{O}_{ij}s_j$. Because the orthogonal matrix $\mathcal{O}$ is arbitrary due to the arbitrary mass matrix $m_{ij}^2$, it does not preserve the $Z_3$ lepton triality which exists in the charged lepton sector.

Because $\mathcal{L}_f$ is written with $A_4$ basis states, the interaction $\overline{\nu_{iL}}\ E_R^0\ s_i$ corresponds to $\overline{\nu_{iL}}\left(\mathcal{O}^T\right)_{ij} s'_j$ where $s'_j$ are mass eigenstates with masses $m_{s_i}$. This identifies $\nu'_{iL} = \mathcal{O}_{ij}\nu_{jL}$ as the physical neutrino mass states. Together with the charged lepton rotation mentioned earlier $e_{iL} = (U_\omega^\dagger)_{ij} l_{jL}$, the neutrino mixing matrix is $U = U_\omega^\dagger \mathcal{O}^T$.

Corresponding to Fig. 4.8 for neutrinos is Fig. 4.9 for charged leptons. It describes contributions to the muon magnetic moment as well as the rare process $\mu \to e\gamma$. For charged leptons, because $\mathcal{L}_f$ is written with $A_4$ basis states, the interaction $\overline{l_{iL}}\ E_R^-\ s_i$ corresponds

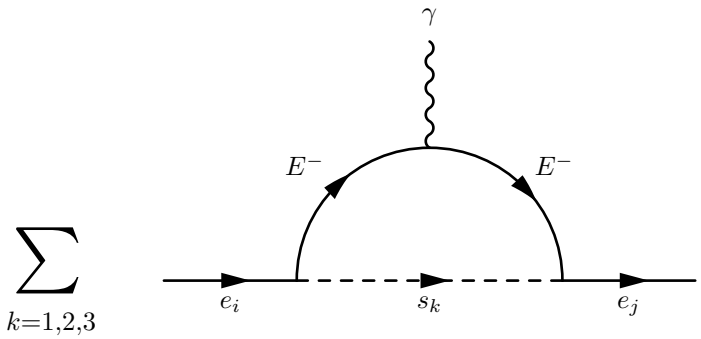


Figure 4.9: One-loop diagram for $e_i \to e_j\gamma$.

to $\overline{e_{iL}}(U_\omega^\dagger)_{ij}\ E_R^-\ \left(\mathcal{O}^T\right)_{jk} s'_k$ where $s'_k$ are mass eigenstates. The resulting combination of $U_\omega^\dagger \mathcal{O}^T$ is the neutrino mixing matrix $U$ as explained above, so the vertex factors for diagrams involving mass eigenstates are determined by the known values of $U$.

One such diagram is $\mu \to \mu\gamma$ with a virtual photon, which is the third contribution to $\Delta a_\mu$ mentioned in the previous section, and this contribution is

$$(\Delta a_\mu)'' = -\sum_{i=1}^{3} \frac{f^2 |U_{\mu i}|^2 m_\mu^2}{16\pi^2 m_E^2} G_\gamma(x_i), \tag{4.45}$$

where $x_i = m_{s_i}^2/m_E^2$ and

$$G_\gamma(x) = \frac{2x^3 + 3x^2 - 6x^2 \ln x - 6x + 1}{6(x-1)^4} < \frac{1}{6}. \tag{4.46}$$

Due to our parameterization for the fermion mixing of $N$ and $E^0$, the mass of $E^-$ has a lower limit of $m_E \simeq 300$ GeV. Hence $(\Delta a_\mu)''$ is less than $10^{-10} f^2$, which for $f < 1$ is below the present experimental sensitivity of $10^{-9}$ and thus can be neglected.

This diagram also applies to the rare decay $\mu \to e\gamma$, which has the amplitude

$$A_{\mu e} = \frac{e f^2 m_\mu}{32\pi^2 m_E^2} \sum_i U_{ei}^* U_{\mu i} G_\gamma(x_i), \tag{4.47}$$

For small $x_i$ and $x_1 \simeq x_2$

$$|\sum_i U_{ei}^* U_{\mu i} G_\gamma(x_i)| = \frac{s_{13} c_{13}}{3\sqrt{2}} |x_3 - x_2| \tag{4.48}$$

where $s_{13} = \sin\theta_{13}$, $c_{13} = \cos\theta_{13}$, and we have taken $\sin\theta_{23} = 1/\sqrt{2}$. This gives the branching fraction

$$B = \frac{\alpha s_{13}^2 c_{13}^2}{384\pi} \left( \frac{f^2 |x_3 - x_2|}{G_F m_E^2} \right)^2 \tag{4.49}$$

The lower limit mentioned earlier of $m_E \simeq 300$ GeV is numerically equivalent to $G_F m_E^2 \simeq 1$.

Let $f = 0.2$, $|x_3 - x_2| \simeq 0.05$, then $B = 5.6 \times 10^{-13}$, which is just below the experimental constraint [39] given by $5.7 \times 10^{-13}$.

This diagram also applies to another possible rare decay is $\mu^- \to e^- e^+ e^-$, which has one set of contributions from the processes $\mu^- \to e^-(\gamma, Z) \to e^- e^+ e^-$. The process with a virtual photon is obtained by adding $\gamma \to e^+ e^-$, and the amplitude for this process is

$$\begin{aligned} i\mathcal{M}_\gamma &= \frac{-ie^2 f^2}{32\pi^2 m_E^2} \sum_{i=1}^{3} U_{ei}^* U_{\mu i} \bar{u}(p_1) \left[ G_e(x_i) \left( \gamma^\alpha - \frac{q^\alpha \not{q}}{q^2} \right) P_L - i m_\mu G_\gamma(x_i) \frac{\sigma^{\alpha\beta} q_\beta}{q^2} P_R \right] \\ &\qquad \times u_\mu(p) \bar{u}(p_2) \gamma_\alpha v(p_3) \\ &\quad -(p_1 \leftrightarrow p_2) \end{aligned} \tag{4.50}$$

where the spinors indicate the particles and their momenta, $q = p - p_1$, and

$$G_e(x) = \frac{7 - 36x + 45x^2 - 16x^3 + 6x^2(2x-3)\ln x}{18(x-1)^4}. \tag{4.51}$$

The amplitude for the process with a virtual $Z$ boson has a similar form because $E_{L,R}$ is vector-like, but it is further suppressed by $m_Z^2$.

With the same specific parameters already chosen, we find that the dominant set of contributions to $\mu^- \to e^- e^+ e^-$ comes from the box diagrams given in Fig. 4.10 and Fig. 4.11. In these diagrams, the muon has momentum $p$, and the outgoing electron connected to it by the fermion line has momentum $p_1$. The other outgoing electron has momentum $p_2$ and the outgoing positron has momentum $p_3$. In the limit of zero external lepton masses, all diagrams have the same loop momentum integrals. We calculate the total amplitude from

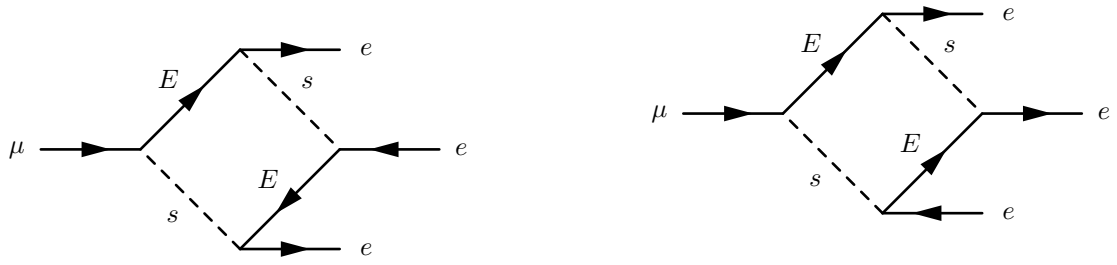


Figure 4.10: First and second box diagrams for $\mu \to eee$ in the $A_4$ model.

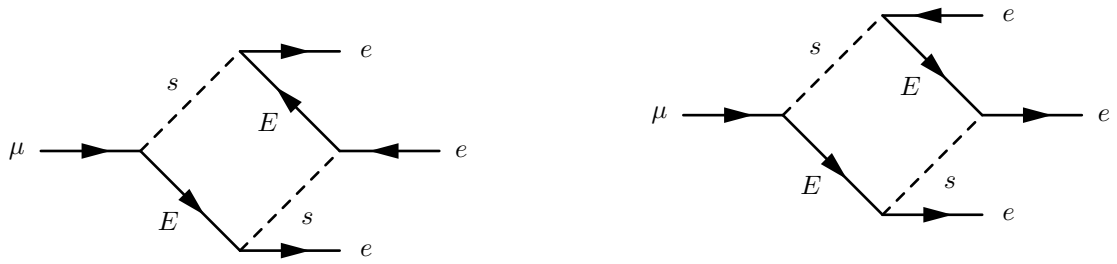


Figure 4.11: Third and fourth box diagrams for $\mu \to eee$ in the $A_4$ model.

all the box diagrams to be

$$i\mathcal{M}_B = \frac{if^4[\bar{u}(p_1)\gamma_\alpha P_L u_\mu(p)\bar{u}(p_2)\gamma^\alpha P_L v(p_3) - (p_1 \leftrightarrow p_2)]}{64\pi^2 m_E^2} \sum_{i,j=1}^{3} U_{\mu i}U_{ej}^*[U_{ei}U_{ej}^* - U_{ej}U_{ei}^*]B_{ij} \tag{4.52}$$

where

$$B_{ij} = \frac{B(x_i) - B(x_j)}{x_i - x_j} \quad i \neq j, \quad B_{ii} = \frac{x_i^2 - 2x_i \ln x_i - 1}{(x_i - 1)^3}, \quad B(x) = \frac{x^2 \ln x}{(x-1)^2} - \frac{1}{x-1} \tag{4.53}$$

There are four different ways to make field contractions, and so there are four basic diagrams. The first and second diagrams shown in Fig. 4.10 have the same relative sign. They differ in the reversal of the fermion line with one electron and one positron. Similarly, the third and fourth diagrams shown in Fig. 4.11 have the same relative sign. However, there is a relative sign between the diagrams in Fig. 4.10 and Fig. 4.11. This is the sign that appears

inside the summation symbol in $\mathcal{M}_B$. In addition, there are copies of all diagrams with a relative sign due to fermion statistics. This is the reason for the $p_1 \leftrightarrow p_2$ in $\mathcal{M}_B$ and $\mathcal{M}_\gamma$.

Since the box diagram contribution is dominant, the $\mu \to eee$ branching fraction is

$$B' = \frac{f^8}{2(8\pi)^4 m_E^4 G_F^2} \left| \sum_{i,j=1}^{3} U_{\mu i} U_{ej}^* [U_{ei} U_{ej}^* - U_{ej} U_{ei}^*] B_{ij} \right|^2 \tag{4.54}$$

For small $x_i$ we have

$$B' = \frac{f^8}{2(8\pi)^4 m_E^4 G_F^2} \frac{\sin^2(4\theta_{13})}{8} \tag{4.55}$$

Using $G_F m_E^2 \simeq 1$, $f = 0.2$ we have $B' = 1.35 \times 10^{-13}$ which is comfortably below the bound [40] of $1.0 \times 10^{-12}$.

## 4.7 Dark Matter Properties

The real scalar dark matter particle in this model is taken to be $s$, which is the lightest mass eigenstate of $s_{1,2,3}$ in the physical basis. The only direct connections of $s$ with SM particles is through the Higgs and the left-handed charged leptons. If the Yukawa coupling $f$ to leptons is small, then the coupling $\lambda$ in the $\lambda v h s^2$ interaction with the Higgs will determine both the dark matter relic density and the elastic cross section off nuclei. This places a strong constraint on the mass of $s$ to be in a small region near $m_s < m_h/2$ according a recent study [41]. This difficulty was solved in Ref. [42] by the radiative mixing between the Higgs and another scalar. The strategy is to increase the channels for dark matter annihilation without affecting the scattering off nuclei through $h$ exchange. We

therefore augment the particle content of our model with a complex electroweak singlet $\chi$ with $(SU(3)_C, SU(2)_L, Y; Z_{2\,dark}, A_4) = (\mathbf{1}, \mathbf{1}, 0; +, \mathbf{1}')$. The additional Lagrangian terms are listed in Table 4.4. Since $\chi, y_2 \sim \mathbf{1}'$ under $A_4$, the new interactions are analogous to those of $y_2$ listed in the previous Table 4.3 but with fewer allowed terms since $\chi$ has $(+)_{dark}$ and $y_2$ has $(-)_{dark}$. Also, new cubic terms $\mathcal{L}_{cubic}$ are allowed, which are needed for the dark matter annihilation channels shown in Fig. 4.12. as well as the radiative mixing shown in Fig. 4.13. The soft-breaking of $A_4$ involving $\chi$ is assumed to occur only through the dimension-two terms $\mathcal{L}_{breaking} = \mu^2\chi^2 + (\mu^*)^2(\chi^*)^2$, which split $\chi$ into its real and imaginary components $\chi_R$ and $\chi_I$.

In the physical mass basis, let the masses of $\chi_{R,I}$ be denoted by $m_{R,I}$. For illustration, we assume $m_R < m_s < m_I$, and take the $\chi_I\chi_R^2$ coupling to be zero, so that the

| Terms that respect $A_4$ |
|---|
| $\mathcal{L}_\chi = -m_\chi^2\chi^*\chi \quad - \lambda_6' (\chi^*\chi)^2 \quad - \lambda_9' (\chi^*\chi)(\Phi^\dagger\Phi)$ |
| $\mathcal{L}_{s\chi} = -\lambda_{13}' \chi^*\chi \left(s_1^2 + s_2^2 + s_3^2\right)$ |
| $\mathcal{L}_{x\chi} =$ Quartic terms $\quad x_i^* x_j \chi^*\chi \quad$ and $\quad x_i^* x_j^* \chi\chi$ |
| $\mathcal{L}_{y\chi} =$ Quartic terms $\quad y_i^* y_j \chi^*\chi \quad$ and $\quad y_i^* y_j^* \chi\chi$ |
| $\mathcal{L}_{cubic} = \mu_\chi\chi^3 + \mu_\chi^*(\chi^*)^3 + \mu_s \left(s_1^2 + \omega s_2^2 + \omega^2 s_3^2\right)\chi + \mu_s^* \left(s_1^2 + \omega^2 s_2^2 + \omega s_3^2\right)\chi^*$ |
| Terms that break $A_4$ |
| $\mathcal{L}_{breaking} = \mu^2\chi^2 + (\mu^*)^2(\chi^*)^2$ |

Table 4.4: Additional Scalar Lagrangian terms in the $A_4$ model.

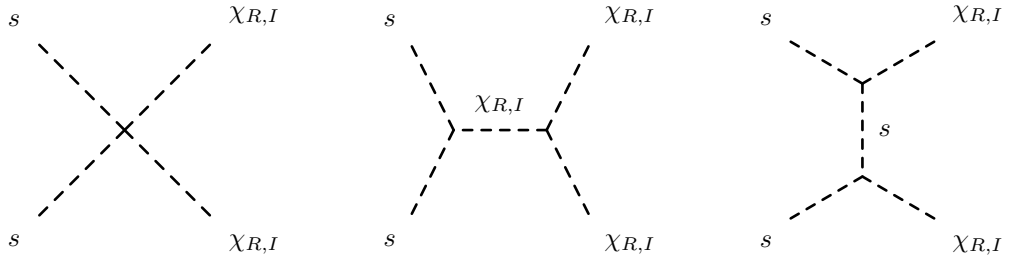


Figure 4.12: Dark matter annihilation channels for $ss$ to $\chi_{R,I}$ mass eigenstates.

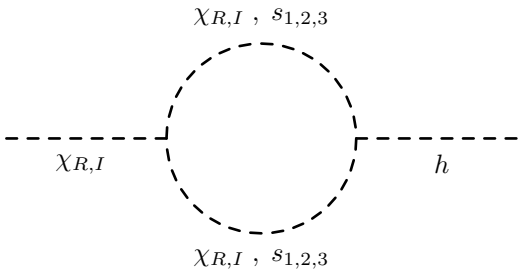


Figure 4.13: Radiative mixing of $\chi_{R,I}$ and $h$.

dark matter annihilations $ss \to \chi_R \chi_R$ are controlled by the interaction terms

$$-\mathcal{L}_{int} = \frac{\lambda'}{4} s^2 \chi_R^2 + \frac{g}{2} s^2 \chi_R + \frac{g'}{3!} \chi_R^3 \tag{4.56}$$

As a result, the annihilation cross section times relative velocity is given by

$$\sigma \times v_{rel} = \frac{\sqrt{1-(m_R/m_s)^2}}{64\pi m_s^2} \left( \lambda' + \frac{g' g}{4m_s^2 - m_R^2} - \frac{g^2}{2m_s^2 - m_R^2} \right)^2 \tag{4.57}$$

Since $s$ is a real scalar, we use [43] the value $\sigma \times v_{rel} = 2.2 \times 10^{-26} \mathrm{cm}^3 \mathrm{s}^{-1}$ and with

$m_s = 200$ GeV and $m_R = 150$ GeV, we find

$$\lambda' + 0.073 \left( \frac{\sqrt{g'g}}{100\,\mathrm{GeV}} \right)^2 - 0.174 \left( \frac{g}{100\,\mathrm{GeV}} \right)^2 = 0.1514 \tag{4.58}$$

Recall that $\chi_R$ mixes radiatively with $h$, so that the dark matter annihilation to SM particles is achieved from $ss \to \chi_R \chi_R \to h \to SM$.

As mentioned earlier, the spin-independent elastic cross section proceeds through the interaction $\lambda v h s^2$ and $h$ exchange with nuclei. The cross section is

$$\sigma_{SI} = \frac{\lambda^2 f_N^2 \mu^2 m_N^2}{\pi m_h^4 m_s^2} \tag{4.59}$$

where $\mu = m_N m_s/(m_N + m_s)$ is the DM-nucleon reduced mass, $m_N = (m_p + m_n)/2 = 938.95\,\mathrm{MeV}$ is the nucleon mass, and $f_N = 0.3$ is the Higgs-nucleon coupling factor [44]. The LUX bound [45] for $m_s = 200\,\mathrm{GeV}$ is $\sigma \approx 1.5$ zb , which implies

$$\lambda < 3.3 \times 10^{-4} \tag{4.60}$$

The next two sections are supplementary to the main results already discussed. To summarize this chapter, we have reaffirmed the important idea that the effective Higgs Yukawa couplings to SM charged fermions can have measurable effects which may point to new physics across the entire lepton sector.

## 4.8 Quartic Terms and the Soft-breaking of $A_4$

There is a subtle issue concerning the scalar Lagrangian terms that has tacitly been postponed in the previous sections. Table 4.3 includes the dimension-four terms that respect $A_4$

$$\mathcal{L}_{sx} \supset -\lambda_{11} \left(x_1^* s_1 + x_2^* s_2 + x_3^* s_3\right) \left(x_1 s_1 + x_2 s_2 + x_3 s_3\right) \tag{4.61}$$

as well as the dimension-two terms that arbitrarily break $A_4$

$$\mathcal{L}_{ss} \supset -s_i m_{ij}^2 s_j \tag{4.62}$$

Together, these will induce the dimension-two term shown in Fig. 4.14, which is a logarithmic divergence. This is a radiative correction to the tree-level term $x_1 x_2^*$ which by construction is not present due to the method used to derive the neutrino mixing matrix $U$. This method assumes that there are only two sources of soft-breaking of $A_4$. The first source comes from the $s_i s_j$ terms above for neutrino mass, and the second source comes from the $y_i x_j^*$ terms for charged lepton mass

$$\mathcal{L}_{xy} \supset -\mu_i^2 \; y_i (U_\omega)_{ij} x_j^* \tag{4.63}$$

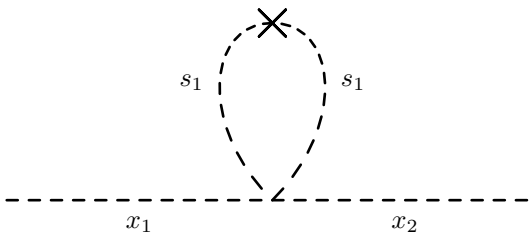


Figure 4.14: Radiative $x_1 x_2^*$ term.

A consistent treatment requires that the tree-level term for $x_1 x_2^*$ be present so that the one-loop divergence can be absorbed in the context of renormalization. This compromises the validity of deriving $U$ from the soft-breaking matrices $U_\omega$ and $\mathcal{O}$.

This is an aspect of the technical difficulty inherent in $A_4$ models. In the original works, the most general Higgs potential allowed by $A_4$ alone makes it difficult to align three different scalar VEVs in different directions [46]. In some cases [47] it is expected that more elaborate frameworks, such as extra dimensions or supersymmetry, are needed to solve this so-called sequestering problem.

In our model, if the quartic couplings are small, then the problem is mitigated, with the understanding that the analysis of the previous sections is valid only in the energy range where the couplings have negligible flow under the renormalization group. In a similar model with a comparable particle content, the $A_4$ obstacle has just recently been overcome [48], where essentially an enlarged symmetry group is used to forbid the troublesome quartic term.

## 4.9 The Group $A_4$ and its Subgroup $Z_3$

The non-Abelian discrete symmetry $A_4$ is the symmetry of the tetrahedron. It has 12 elements and is the smallest group which admits an irreducible **3** representation. It also has three one-dimensional representations $\mathbf{1}, \mathbf{1}', \mathbf{1}''$. The group $A_4$ has two generating elements $S$ and $T$. For the singlets $\mathbf{1}, \mathbf{1}', \mathbf{1}''$, $S$ and $T$ are given by $S = 1, 1, 1$ and $T = 1, \omega, \omega^2$ respectively. Here $\omega = \exp(2\pi i/3)$ is the cubic root of 1, and satisfies $\omega^2 = \omega^*$ and $1 + \omega + \omega^2 = 0$. For a triplet **3**, a convenient representation of $S$ and $T$ due to Ma and

Rajasekaran [49] is

$$S = \begin{pmatrix} 1 & 0 & 0 \\ 0 & -1 & 0 \\ 0 & 0 & -1 \end{pmatrix} \quad , \quad T = \begin{pmatrix} 0 & 1 & 0 \\ 0 & 0 & 1 \\ 1 & 0 & 0 \end{pmatrix} \tag{4.64}$$

The basic multiplication rule given earlier

$$\mathbf{3} \times \mathbf{3} = \mathbf{1} + \mathbf{1}' + \mathbf{1}'' + \mathbf{3} + \mathbf{3}$$

has the explicit multiplication of two triplets $(a_1, a_2, a_3) \sim \mathbf{3}$ and $(b_1, b_2, b_3) \sim \mathbf{3}$ as follows

$$\begin{aligned} a_1b_1 + a_2b_2 + a_3b_3 &\sim \mathbf{1} \\ a_1b_1 + \omega^2 a_2b_2 + \omega a_3b_3 &\sim \mathbf{1}' \\ a_1b_1 + \omega a_2b_2 + \omega^2 a_3b_3 &\sim \mathbf{1}'' \\ (\ a_2b_3\ ,\ a_3b_1\ ,\ a_1b_2\ ) &\sim \mathbf{3} \\ (\ a_3b_2\ ,\ a_1b_3\ ,\ a_2b_1\ ) &\sim \mathbf{3} \end{aligned} \tag{4.65}$$

Instead of the two **3**'s given above, it is often useful to employ the symmetric and antisymmetric combinations

$$\begin{aligned} (\ a_2b_3 + a_3b_2\ ,\ a_3b_1 + a_1b_3\ ,\ a_1b_2 + a_2b_1\ ) &\sim \mathbf{3}_{symmetric} \\ (\ a_2b_3 - a_3b_2\ ,\ -a_3b_1 + a_1b_3\ ,\ a_1b_2 - a_2b_1\ ) &\sim \mathbf{3}_{anitsymmetric} \end{aligned} \tag{4.66}$$

Other multiplication rules [50]. For the multiplication of one singlet $a$ and one triplet $(b_1, b_2, b_3)$ we have

$$\begin{aligned} \mathbf{1} \times \mathbf{3} &\sim \mathbf{3} & a\,(\,b_1\,,\,b_2\,,\,b_3\,) &\sim \mathbf{3} \\ \mathbf{1}' \times \mathbf{3} &\sim \mathbf{3} & a\,(\,b_1\,,\,\omega b_2\,,\,\omega^2 b_3\,) &\sim \mathbf{3} \\ \mathbf{1}'' \times \mathbf{3} &\sim \mathbf{3} & a\,(\,b_1\,,\,\omega^2 b_2\,,\,\omega b_3\,) &\sim \mathbf{3} \end{aligned} \tag{4.67}$$

The multiplication of two singlets $a$ and $b$ is just $ab$ for the trivial combinations

$$\begin{aligned} \mathbf{1} \times \mathbf{1} &\sim \mathbf{1} & a\,b &\sim \mathbf{1} \\ \mathbf{1} \times \mathbf{1}' &\sim \mathbf{1}' & a\,b &\sim \mathbf{1}' \\ \mathbf{1} \times \mathbf{1}'' &\sim \mathbf{1}'' & a\,b &\sim \mathbf{1}'' \end{aligned} \tag{4.68}$$

as well as for the nontrivial combinations

$$\begin{aligned} \mathbf{1}' \times \mathbf{1}'' &\sim \mathbf{1} & a\,b &\sim \mathbf{1} \\ \mathbf{1}'' \times \mathbf{1}'' &\sim \mathbf{1}' & a\,b &\sim \mathbf{1}' \\ \mathbf{1}' \times \mathbf{1}' &\sim \mathbf{1}'' & a\,b &\sim \mathbf{1}'' \end{aligned} \tag{4.69}$$

The generators $S$ and $T$ only acts on the states $l_{1,2,3}$ in the $A_4$ basis. The subgroup $Z_3$ of $A_4$ is generated solely by the action of the $T$ generator [51]. As a first example, consider the mass eigenstates of charged leptons. The right-handed projections of the mass eigenstates are $e_{iR} = l_{iR}$, which transform as singlets $\mathbf{1}, \mathbf{1}', \mathbf{1}''$ so under the action of $T$ they transform as

$$\begin{aligned} e_R &\to e_R \\ \mu_R &\to \omega\,\mu_R \\ \tau_R &\to \omega^2\,\tau_R \end{aligned} \tag{4.70}$$

as described at the beginning of this section. For the $A_4$ triplet of left-handed charged leptons in the $A_4$ basis, the action of $T$ is

$$T \begin{pmatrix} l_{1L} \\ l_{2L} \\ l_{3L} \end{pmatrix} = \begin{pmatrix} 0 & 1 & 0 \\ 0 & 0 & 1 \\ 1 & 0 & 0 \end{pmatrix} \begin{pmatrix} l_{1L} \\ l_{2L} \\ l_{3L} \end{pmatrix} = \begin{pmatrix} l_{2L} \\ l_{3L} \\ l_{1L} \end{pmatrix} \tag{4.71}$$

which is simply the permutation $l_{1L} \to l_{2L}, l_{2L} \to l_{3L}, l_{3L} \to l_{1L}$. The left-handed projections of the mass eigenstates are $e_{iL} = (U_\omega^\dagger)_{ij}\, l_{jL}$, so we have

$$\begin{aligned} e_L &= l_{1L} + l_{2L} + l_{3L} \\ \mu_L &= l_{1L} + \omega^2\, l_{2L} + \omega\, l_{3L} \\ \tau_L &= l_{1L} + \omega\, l_{2L} + \omega^2\, l_{3L} \end{aligned} \tag{4.72}$$

and under the action of $T$ on $l_{1,2,3}$ this becomes

$$\begin{aligned} e_L &\to l_{2L} + l_{3L} + l_{1L} &&= e_L \\ \mu_L &\to l_{2L} + \omega^2\, l_{3L} + \omega\, l_{1L} &&= \omega \left[ l_{1L} + \omega^2\, l_{2L} + \omega\, l_{3L} \right] = \omega\, \mu_L \\ \tau_L &\to l_{2L} + \omega\, l_{3L} + \omega^2\, l_{1L} &&= \omega^2 \left[ l_{1L} + \omega\, l_{2L} + \omega^2\, l_{3L} \right] = \omega^2\, \tau_L \end{aligned} \tag{4.73}$$

Thus the left- and right-handed fields transform the same way, which must be true for the mass eigenstates to obey the $Z_3$ lepton triality. In this model, the assignment is $e, \mu, \tau \sim 1, \omega, \omega^2$.

As second example, consider the scalars. The fields $y_i$ transform as singlets $\mathbf{1}, \mathbf{1}', \mathbf{1}''$

so under the action of $T$ they transform as

$$\begin{aligned} y_1 &\rightarrow y_1 \\ y_2 &\rightarrow \omega\, y_2 \\ y_3 &\rightarrow \omega^2\, y_3 \end{aligned} \tag{4.74}$$

as described at the beginning of this section. For the $A_4$ triplet $x_i^*$ in the $A_4$ basis, the action of $T$ is

$$T \begin{pmatrix} x_1^* \\ x_2^* \\ x_3^* \end{pmatrix} = \begin{pmatrix} 0 & 1 & 0 \\ 0 & 0 & 1 \\ 1 & 0 & 0 \end{pmatrix} \begin{pmatrix} x_1^* \\ x_2^* \\ x_3^* \end{pmatrix} = \begin{pmatrix} x_2^* \\ x_3^* \\ x_1^* \end{pmatrix} \tag{4.75}$$

which is simply the permutation $x_1^* \rightarrow x_2^*, x_2^* \rightarrow x_3^*, x_3^* \rightarrow x_1^*$. The rotated states $z_i^*$ are $z_i^* = (U_\omega)_{ij}\, x_j^*$ so we have

$$\begin{aligned} z_1^* &= x_1^* + x_2^* + x_3^* \\ z_2^* &= x_1^* + \omega\, x_2^* + \omega^2\, x_3^* \\ z_3^* &= x_1^* + \omega^2\, x_2^* + \omega\, x_3^* \end{aligned} \tag{4.76}$$

and under the action of $T$ on $x_{1,2,3}^*$ this becomes

$$\begin{aligned} z_1^* &\rightarrow x_2^* + x_3^* + x_1^* &&= z_1^* \\ z_2^* &\rightarrow x_2^* + \omega\, x_3^* + \omega^2\, x_1^* &&= \omega^2 \left[x_1^* + \omega^2\, x_2^* + \omega\, x_3^*\right] = \omega^2\, z_2^* \\ z_3^* &\rightarrow x_2^* + \omega^2\, x_3^* + \omega\, x_1^* &&= \omega \left[x_1^* + \omega\, x_2^* + \omega^2\, x_3^*\right] = \omega\, z_3^* \end{aligned} \tag{4.77}$$

So under the action of $T$ the soft terms that break $A_4$ to $Z_3$ transform as

$$\begin{aligned} \mu_e^2 &: \; y_1 z_1^* \to y_1 z_1^* \\ \mu_\mu^2 &: \; y_2 z_2^* \to \omega \; y_2 \; \omega^2 \; z_2^* = y_2 z_2^* \\ \mu_\tau^2 &: \; y_3 z_3^* \to \omega^2 \; y_3 \; \omega \; z_3^* = y_3 z_3^* \end{aligned} \tag{4.78}$$

so these Lagrangian terms are invariant under $Z_3$ lepton triality.

# Part II

# Related Phenomena Beyond the Standard Model

# Chapter 5

# Higgs Triplet Scalar Extension

## 5.1 Neutrino Mass

This chapter considers the phenomenology of a particular type of Higgs triplet model. The motivation is to obtain the radiative Majorana neutrino mass shown in Fig. 5.1, For simplicity, it shows only a single neutrino $\nu_L$ and a single scalar mass eigenstate $s$. The emphasis will be on an interesting collider signature, and also on dark matter constraints from relic density. The constraints from direct detection are accommodated in a simple way and so a comprehensive analysis is not needed. This chapter is based on the work previously published in Ref. [4].

The full symmetry group is the based on the SM gauge group

$$SU(3)_C \times SU(2)_L \times U(1)_Y \tag{5.1}$$

but also incorporates a discrete symmetry which is assumed to be exactly conserved since

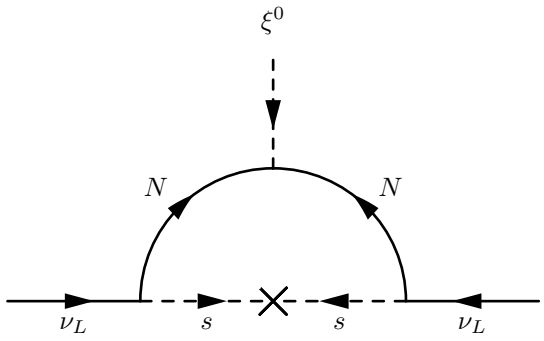

Figure 5.1: Radiative neutrino mass.

its purpose is to stabilize dark matter. This dark $Z_2$ symmetry (dark parity) functions in the same way as $Z_{2\ dark}$ used in the previous chapters, but here it is actually derivable from the concept of lepton parity [52] according to

$$Z_{2\ dark} = (-1)^{L+2j} \tag{5.2}$$

where $L$ is lepton number and $j$ is particle spin. Lepton number corresponds to a global $U(1)_L$ symmetry, which in this model is the symmetry used to to forbid the Higgs triplet coupling to neutrinos at tree-level but to permit its realization in one-loop. The particle content is shown in Table 5.1. The Higgs triplet consists of the complex scalars $\xi^{++}, \xi^{+}, \xi^{0}$ which are arranged for convenience into a $2 \times 2$ matrix. The dark sector includes new fermions $N_{L,R}$ and $E^{-}_{L,R}$ arranged in electroweak doublets, which are vector-like so the model is anomaly-free. The dark sector also includes three complex scalars $s_i$ which are electroweak singlets and carry lepton number. The lightest physical $s_i$ is taken to be the dark matter candidate in this model.

The allowed Lagrangian terms are listed in Table 5.2 before spontaneous symmetry breaking. Conservation of lepton number is imposed on all hard terms. The SM charged

| Particle | | | $(SU(3)_C, SU(2)_L, Y)$ | $Z_{2\ dark}$ | $L$ |
|---|---|---|---|---|---|
| $L_{iL}$ | $=$ | $\begin{pmatrix}\nu_{iL}\\ l_{iL}\end{pmatrix}$ | $(\mathbf{1},\mathbf{2},+1/2)$ | $+$ | 1 |
| | | $l_{iR}$ | $(\mathbf{1},\mathbf{1},-1)$ | $+$ | 1 |
| $\Phi$ | $=$ | $\begin{pmatrix}\phi^+\\ \phi^0\end{pmatrix}$ | $(\mathbf{1},\mathbf{2},+1/2)$ | $+$ | 0 |
| $\psi_{L,R}$ | $=$ | $\begin{pmatrix}N_{L,R}\\ E^-_{L,R}\end{pmatrix}$ | $(\mathbf{1},\mathbf{2},+1/2)$ | $-$ | 0 |
| $\xi$ | $=$ | $\begin{pmatrix}\xi^+/\sqrt{2} & \xi^{++}\\ \xi^0 & -\xi^+/\sqrt{2}\end{pmatrix}$ | $(\mathbf{1},\mathbf{3},+1)$ | $+$ | 0 |
| | | $s_i$ | $(\mathbf{1},\mathbf{1},-1)$ | $-$ | 1 |

Table 5.1: Particle content in the Higgs triplet model.

fermions have the usual Higgs Yukawa interactions and will obtain masses as in the SM after electroweak symmetry breaking. The conservation of lepton number forbids the hard Yukawa term $\overline{\nu_{iL}}\ \xi\ (\nu_{iL})^c$ which would otherwise be allowed. This term would have produced a Type II tree-level Majorana neutrino mass from the interaction $\overline{(\nu_{iL})^c}\ \xi^0\ \nu_{jL}$ when $\xi^0$ gets a VEV. As mentioned at the beginning of Chapter 3, this effective term must still be realized at one-loop in order to obtain the Weinberg operator. As shown in Fig. 5.1, the connection with $\xi^0$ at the top of the loop is achieved with the help of the new fermions $N_{L,R}$. The soft-breaking of lepton number comes from the following scalar terms which in general split the complex $s_i$ into their real and imaginary components

$$\mathcal{L}_{breaking} = \frac{1}{2}(\Delta m_s^2)_{ij} s_i s_j \quad + \quad h.c. \tag{5.3}$$

This is indicated by the cross in the figure and allows completion of the loop.

| Terms that respect $U(1)_L$ |
|---|
| $\mathcal{L}_{Leptons} = -f_{SM,ij}\ \overline{L_{iL}}\ \widetilde{\Phi}^\dagger\ l_{jR} + h.c.$ |
| $\mathcal{L}_{\psi} = -m_E\overline{\psi}\psi \quad = \quad -m_E\left(\overline{E_L}E_R + \overline{N_L}N_R + h.c.\right)$ |
| $\mathcal{L}_{f_s} = \overline{\psi_R}\ L_{iL}\ (f_s)_{ij}\ s_j^* + h.c.$ |
| $\mathcal{L}_{\psi,\xi} = f_L\overline{\widetilde{\psi_L}}\ \xi\ \psi_L \quad + \quad h.c.$<br>$+f_R\overline{\widetilde{\psi_R}}\ \xi\ \psi_R \quad + \quad h.c.$ |
| $-\mathcal{L}_{\Phi,\xi} = m^2\Phi^\dagger\Phi + M^2Tr(\xi^\dagger\xi) + \frac{1}{2}\lambda_1(\Phi^\dagger\Phi)^2$<br>$+\frac{1}{2}\lambda_2[Tr(\xi^\dagger\xi)]^2 + \frac{1}{2}\lambda_3 Tr[(\xi^\dagger\xi)^2]$<br>$+\lambda_4(\Phi^\dagger\Phi)Tr(\xi^\dagger\xi) + \frac{1}{2}\lambda_5\Phi^\dagger\xi\xi^\dagger\Phi$<br>$+\mu(\Phi^\dagger\xi\widetilde{\Phi}) + h.c.$ |
| $-\mathcal{L}_{\Phi,s} = m_{ij}^2 s_i^* s_j + \lambda_{ij}(\Phi^\dagger\Phi)s_i^* s_j + \lambda_{abcd}s_a^* s_b^* s_c s_d \quad + \quad h.c.$ |
| $-\mathcal{L}_{\xi,s} = \lambda_{ij}Tr(\xi\xi^\dagger)s_i^* s_j \quad + \quad h.c.$ |
| Terms that break $U(1)_L$ |
| $-\mathcal{L}_{breaking} = \frac{1}{2}(\Delta m_s^2)_{ij}s_i s_j + h.c.$ |

Table 5.2: Lagrangian terms in the Higgs triplet model.

After electroweak symmetry breaking, the mass-squared matrix $(\mathcal{M}_s^2)_{ij}$ spanning $s_i^* s_j$ is given by

$$(\mathcal{M}_s^2)_{ij} = m_{ij}^2 + \lambda_{ij}v^2 \tag{5.4}$$

where the effects of $\mathcal{L}_{breaking}$ have been neglected for the moment since they are small. In general, there are the allowed Yukawa interactions

$$\begin{aligned}\mathcal{L}_{f_s} &= \overline{\psi_R}\ L_{iL}\ (f_s)_{ij}\ s_j^* \quad + \quad h.c. \\ &= \left(\overline{N_R}\ \nu_{iL} + \overline{E_R^-}\ l_{iL}\right)(f_s)_{ij}\ s_j^* \quad + \quad h.c.\end{aligned} \tag{5.5}$$

We can rotate the $s_j$ into the physical basis $s'_j$ so that the general scalar mass terms $(\mathcal{M}_s^2)_{ij} s_i^* s_j$ become diagonal in the physical basis $(\mathcal{M}'^2_s)_{ij}\ s'^*_i\, s'_j$. The new primed coupling matrix is $(f_s)'_{ij}$. We assume that the primed coupling matrix is diagonal $(f_s)'_{ij} = f'_s \delta_{ij}$. We also assume that the neutrino states $\nu_{iL}$ are mass eigenstates, which means that rotating charged lepton states $l_{iL}$ with the neutrino mixing matrix $U_{PMNS}$ will give the physical states $e_{iL}, \mu_{iL}, \tau_{iL}$.

The first term in parentheses in the second line of the preceding equation is the neutrino Yukawa term in Fig. 5.1. The other allowed Yukawa terms at the top of the figure come from the Higgs triplet

$$\begin{aligned}
\mathcal{L}_{\psi,\xi} \quad &\supset \quad f_L \overline{\widetilde{\psi_L}}\, \xi\, \psi_L \quad + \quad h.c. \\
&= \quad f_L \begin{pmatrix} \overline{(E_L)^c}, -\overline{(N_L)^c} \end{pmatrix} \begin{pmatrix} \xi^+/\sqrt{2} & \xi^{++} \\ \xi^0 & -\xi^+/\sqrt{2} \end{pmatrix} \begin{pmatrix} N_L \\ E_L \end{pmatrix} \quad + \quad h.c. \\
&= \quad f_L \begin{bmatrix} \overline{(E_L)^c}\, (\xi^+/\sqrt{2})\, N_L \quad + \quad \overline{(E_L)^c}\, \xi^{++}\, E_L \\ -\overline{(N_L)^c}\, \xi^0 N_L \quad + \quad \overline{(N_L)^c}\, (\xi^+/\sqrt{2})\, E_L \end{bmatrix} \quad + \quad h.c. \qquad (5.6)
\end{aligned}$$

where $\widetilde{\psi}_L$ is the dual of $\psi_L$ and similarly for the $f_R$ terms. The top of the radiative loop involves the $\overline{(N_L)^c}\, \xi^0 N_L$ and $\overline{(N_R)^c}\, \xi^0 N_R$ terms.

Evaluating the radiative mass involves minimizing the scalar potential after electroweak symmetry breaking. The VEV of $\phi^0$ induces a VEV for $\xi^0$ from the $\mu(\Phi^\dagger \xi \widetilde{\Phi})$ term in $\mathcal{L}_{\Phi,\xi}$. For the self-energy calculation, there are two sequences of propagators. The sequence along the fermion line is a propagator for $N$, followed by a mass insertion proportional to $\langle \xi^0 \rangle$, followed by another propagator for $N$. The sequence along the scalar line is

a propagator for $s$, followed by a mass insertion proportional to $\Delta m_s^2$, followed by another propagator for $s$. We can obtain very reasonable neutrino masses of order 0.1 eV using the values

$$\begin{aligned} \langle \xi^0 \rangle &\sim 0.1 \text{ GeV} \\ m_s^2/m_E^2 &\sim 0.1 \\ f_R &\sim 0.1 \\ f_L &\sim 0.1 \\ \Delta m_s^2/m_s^2 &\sim 0.1 \\ f_s &\sim 0.01 \end{aligned}$$

For the rest of this chapter, we will treat $s_{1,2,3}$ as complex scalars since the effects of $\mathcal{L}_{breaking}$ are small.

## 5.2 Collider Signature

In this model, the VEV of $\xi^0$ is not too small. However, the effective coupling of $\xi$ to leptons is very small, which is different from the tree-level Type II seesaw model, where the decay of $\xi^{++}$ to same-sign dileptons is expected to be dominant. Here, the $\xi^{++}$ term in $\mathcal{L}_{\psi,\xi}$ written out in the previous section is responsible for the decay $\xi^{++} \to E^+E^+$ which is possible when $m(\xi^{++}) > 2m_E$. In Fig. 5.2 we plot the LHC production cross section for

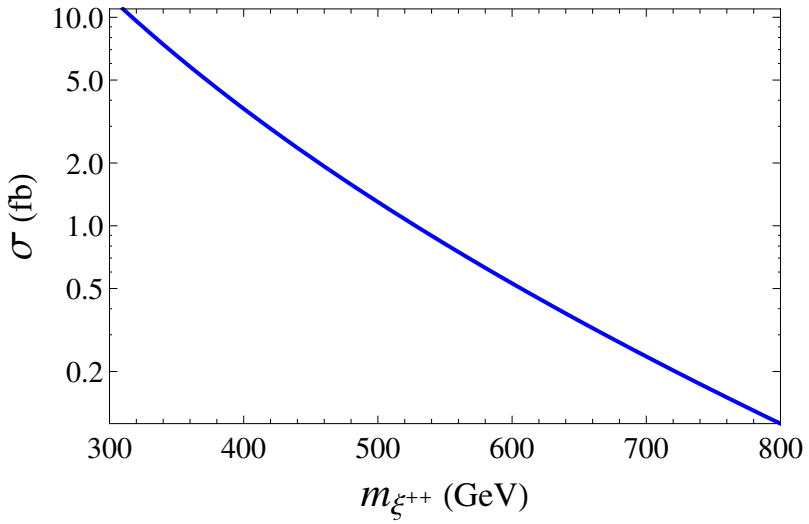


Figure 5.2: LHC production cross section of $\xi^{++}\xi^{--}$ at 13 TeV.

$\xi^{++}\xi^{--}$ for 13 TeV. The subsequent decays after $\xi^{++}\xi^{--}$ production are

$$\begin{aligned} \xi^{++} &\rightarrow E^+E^+ \rightarrow (l^+s)(l^+s) \\ \xi^{--} &\rightarrow E^-E^- \rightarrow (l^-s^*)(l^-s^*) \end{aligned} \tag{5.7}$$

where the second set of decays follows from the terms in $\mathcal{L}_{f_s}$ as written out in the previous section

$$\begin{aligned} E^+ &\rightarrow l^+s \\ E^- &\rightarrow l^-s^* \end{aligned} \tag{5.8}$$

This yields the interesting collider signature of a final state of four charged leptons ${l_a}^+{l_b}^+{l_c}^-{l_d}^-$ and missing energy due to $sss^*s^*$. We assume that $\xi^+$ and $\xi^0$ are heavier than $\xi^{++}$ so that we can focus only on the decay products of $\xi^{++}$ and $\xi^{--}$. We also assume that the lightest $s$ is $s_1$, which is the dark matter candidate discussed in the next section.

Recent LHC searches for multilepton signatures at 8 TeV by CMS and ATLAS are consistent with SM expectations, and are potential restrictions on our model. In particular, the CMS study includes rare SM events such as $e^+e^+\mu^-\mu^-$ and $e^+e^+\mu^-$. Due to the absence of opposite-sign, same-flavor (OSSF) $l^+l^-$ pairs, both events are classified as OSSF0 where lepton $l$ refers to electron, muon, or hadronically decaying tau. Leptonic tau decays contribute to the electron and muon counts, and this determines the OSSF$n$ category. Details from CMS are shown in Table 5.2 for $\geq 3$ leptons and $N_{\tau\text{had}} = 0$.

The CMS study estimates a negligible SM background for SR1-SR3, and in our simulation we use the same selection criteria. We impose the cuts on transverse momentum $p_T > 10$ GeV and psuedorapidity $|\eta| < 2.4$ for each charged lepton, with at least one lepton $p_T > 20$ GeV. In order to be isolated, each lepton with $p_T$ must satisfy $\sum_i p_{Ti} < 0.15 p_T$, where the sum is over all objects within a cone of radius $\Delta R = 0.3$ around the lepton direction. We implement our model with FeynRules 2.0. Using the CTEQ6L1 parton distribution functions, we generate events using MadGraph5, which includes the Pythia

| Selected CMS results OSSF0 $N_{\tau\text{had}} = 0$ , $N_b = 0$ | | | | | |
|---|---|---|---|---|---|
| signal regions | | $H_T > 200$ GeV | | $H_T < 200$ GeV | |
| $\geq 4$ leptons | $\not{E}_T$ (GeV) | Obs. | Exp.(SM) | Obs. | Exp.(SM) |
| SR1 | $(100, \infty)$ | 0 | $0.01^{+0.03}_{-0.01}$ | 0 | $0.11^{+0.08}_{-0.08}$ |
| SR2 | $(50, 100)$ | 0 | $0.00^{+0.02}_{-0.00}$ | 0 | $0.01^{+0.03}_{-0.01}$ |
| SR3 | $(0, 50)$ | 0 | $0.00^{+0.02}_{-0.00}$ | 0 | $0.01^{+0.02}_{-0.01}$ |
| 3 leptons | $\not{E}_T$ (GeV) | Obs. | Exp.(SM) | Obs. | Exp.(SM) |
| SR4 | $(100, \infty)$ | 5 | $3.7 \pm 1.6$ | 7 | $11.0 \pm 4.9$ |
| SR5 | $(50, 100)$ | 3 | $3.5 \pm 1.4$ | 35 | $38 \pm 15$ |
| SR6 | $(0, 50)$ | 4 | $2.1 \pm 0.8$ | 53 | $51 \pm 11$ |

Table 5.3: Events observed by CMS at 8 TeV with integrated luminosity 19.5 fb$^{-1}$.

package for hadronization and showering. MadAnalysis is then used with the Delphes card designed for CMS detector simulation. Generated events intially have 4 leptons. About half are detected as 3 lepton events, but the constraints from signal regions SR4-SR6 are less restrictive than SR1-SR3. The number of detected events in the OSSF0 $\geq 4$ lepton category is almost the same as $e^{\pm}e^{\pm}\mu^{\mp}\mu^{\mp}2s_1 2s_1^*$ with very few additional leptons from showering or initial/final state radiation.

To examine the production of $e^{\pm}e^{\pm}\mu^{\mp}\mu^{\mp}$ we take the mass of $s_1$ to be 130 GeV, which allows $s_1$ to be dark matter as discussed in the next section. We use the values $f_R = f_L = 0.1$ and $f_s = 0.01$, although the results are not sensitive to the exact values due to on-shell production and decay. The effects due to the VEV $\langle \xi^0 \rangle \sim 0.1$ GeV may be neglected.

For our model, we scan the mass range of $\xi^{++}$ and $E^+$. In Fig. 5.3 we plot contours showing the expected number of detected events in the OSSF0 $\geq 4$ lepton category for 13 TeV at luminosity 100 fb$^{-1}$ assuming a negligible background as for the 8 TeV case. Although the branching fractions of $E^+$ to $\tau^+ s_1$ or $\mu^+ s_1$ are comparable, we find that most of the contributions from $\tau^{\pm}$ decay to $e^{\pm}$ or $\mu^{\pm}$ in the $\geq 4$ lepton final state are not detected. A similar analysis performed for 8 TeV at 19.5 fb$^{-1}$ has a maximum number of detected events of 0.4 in the plot analogous to Fig. 5.3, which corresponds to a small estimated exclusion at the 15% confidence level.

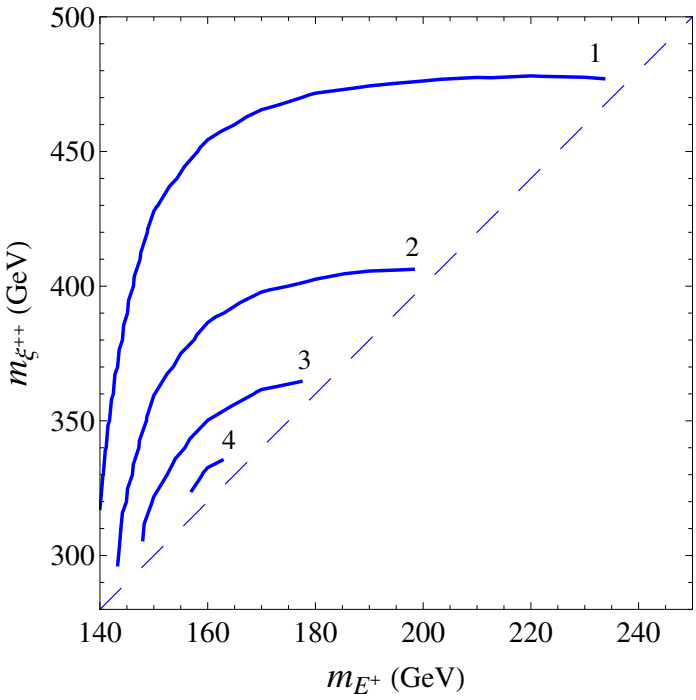


Figure 5.3: Number of $e^{\pm}e^{\pm}\mu^{\mp}\mu^{\mp}2s_1 2s_1^*$ events for 13 TeV at luminosity 100 fb$^{-1}$.

## 5.3 Dark Matter Properties

The complex scalar dark matter particle in this model is taken to be $s_1$, which is the lightest mass eigenstate of $s_{1,2,3}$ in the physical basis. Even though $s_1$ is approximately complex, the comments about real scalar dark matter from Chapter 4 apply here as well. There are only two direct connections of $s_1$ with SM particles, namely, the connection with the Higgs, and the connection with the left-handed charged leptons. The latter will be small since the Yukawa coupling to leptons is small. In this case, the coupling $\lambda$ in the $\lambda vhs^2$ interaction with the Higgs will determine both the dark matter relic density and the elastic cross section off nuclei. This places a strong constraint on the mass of $s$ to be in a small region near $m_s < m_h/2$ according a recent study [41].

In this model, we can make use of $s_{2,3}$. After electroweak symmetry breaking, the

mass-squared matrix $(\mathcal{M}_s^2)_{ij}$ spanning $s_i^* s_j$ is the same expression given earlier

$$(\mathcal{M}_s^2)_{ij} = m_{ij}^2 + \lambda_{ij} v^2 \tag{5.9}$$

Upon diagonalizing $\mathcal{M}_s^2$, the coupling matrix $\lambda_{ij}$ will not be diagonal in general. In the physical basis, $s_1$ will interact with $s_2$ through $h$. This allows the annihilation of $s_1 s_1^*$ to $hh$ through $s_2$ exchange, and contributes to the dark matter relic density without affecting the $s_1$ scattering cross section off nuclei through $h$. This mechanism restores $s_1$ as a dark-matter candidate for $m_s > m_h$.

To demonstrate the scale of the values involved, we consider the simplifying case when $m_{s_2} = m_{s_3}$ and $\lambda_{12} = \lambda_{13}$. The additional choice $m_{s_{2,3}}^2 = m_{s_1}^2 + m_h^2$ ensures that $s_{2,3}$ are heavier than $s_1$, and is convenient because then the relic abundance requirement no longer depends explicitly on $m_{s_{2,3}}^2$. Taking into account that $s_1$ is a complex scalar, we use [43] the value $\sigma \times v_{rel} = 4.4 \times 10^{-26} \mathrm{cm}^3 \mathrm{s}^{-1}$ and in Fig. 5.4 we plot the allowed values for $\lambda_{12}$ and $m_{s_1}$ taking $\lambda_{11} = 0$ for simplicity to satisfy the LUX data.

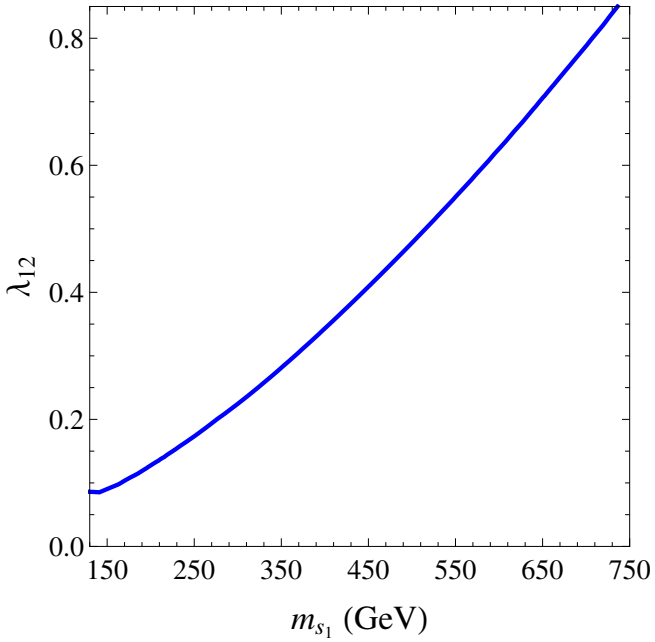


Figure 5.4: Allowed values of $\lambda_{12}$ plotted against $m_{s_1}$ from relic abundance assuming $\lambda_{11} = 0$.

To summarize, this chapter has examined a radiative Higgs triplet model for neutrino mass. It has an interesting verifiable collider signature that also includes the missing energy signature of dark mater.

# Chapter 6

# Vector Dark Matter $SU(2)_N$ Gauge Extension

## 6.1 Outline of the Model

Vector dark matter is somewhat unique compared to fermion or scalar dark matter. Introducing a new massive vector particle requires a Lorentz covariant description of its spin degrees of freedom. This essentially promotes the vector particle to the status of a gauge field, and the mass of the vector boson is generated when the gauge symmetry is spontaneously broken. This is analogous to the SM, where the massive vector gauge bosons $W^{\pm}$ and $Z$ obtain masses after spontaneous breaking of the electroweak gauge symmetry. This chapter is based on the work previously published in Ref. [5]. Similar to the earlier versions [53, 54] of the model, there is an extra global symmetry $U(1)_{S'}$, but here it used to define a conserved dark charge $S$. Another difference is that in this model, all the SM

fermions are singlets under the extra gauge symmetry $SU(2)_N$. This extension of the SM is similar to other works [55, 56] which use an extra $U(1)$ gauge symmetry to obtain vector dark matter and an extra $Z_2$ discrete symmetry to stabilize it. Other possibilities for vector dark matter include considerations of the Littlest Higgs [57] or extra dimensions [58].

The full symmetry group of our model before spontaneous symmetry breaking is

$$SU(3)_C \times SU(2)_L \times U(1)_Y \times SU(2)_N \times U(1)_{S'} \tag{6.1}$$

The first factor is the extra local $SU(2)_N$ gauge symmetry, whose new gauge bosons will be the source of vector dark matter. As in the SM, when the $Q = 0$ component of $\Phi$ gets a VEV and spontaneously breaks the local electroweak symmetry $SU(2)_L \times U(1)_Y$ down to the local $U(1)_Q$, the electric charge $Q$ of all particles remains exactly conserved

$$Q = T_3 + Y \tag{6.2}$$

In this model there is a somewhat similar construction, except that $U(1)_S$ is a global symmetry rather than a local symmetry. Some of the new particles carry charge global $S$ defined by

$$S = T_{3N} + S' \tag{6.3}$$

which will also remain exactly conserved when the $S = 0$ components of the new scalars $\chi, \zeta, \Delta$ get VEVs and spontaneously break the $SU(2)_N$ symmetry. In this model, particles with charge $S \neq 0$ belong to the dark sector, and the lightest mass eigenstate with $Q = 0$ is expected to be the dark matter candidate. Here $T_{3N}$ and $S'$ are analogous to $T_3$ and hypercharge $Y$ respectively in the SM. In this model, the imposed $U(1)_{S'}$ is global symmetry without any corresponding gauge field. This global $U(1)_{S'}$ is the second extra factor in the

full symmetry group. It is chosen in such a way that $S$ is exactly conserved after $SU(2)_N$ and the electroweak symmetry have both been completely broken, as described above. Note this means the new scalars that get VEVs must have both $S = 0$ and $Q = 0$.

The particle content is listed in Table 6.1. Also listed are the charges $S'$ and $S$ corresponding to $U(1)_{S'}$ and $U(1)_S$. Before the spontaneous symmetry breaking of $SU(2)_N$, there are three real gauge fields $X_1, X_2, X_3$ but only the complex combinations $X, \overline{X}$ of $X_1, X_2$ carry $S$ charge. Under $SU(2)_N$, all SM particles are neutral gauge singlets with $T_{3N} = 0$ and $S' = 0$. In contrast, all new particles carry $SU(2)_N$ gauge charges $T_{3N} \neq 0$ and $S' \neq 0$. There is one complex doublet $\chi$ and one complex triplet $\Delta$. There is also one complex bidoublet $\zeta$, which transforms vertically under $SU(2)_L \times U(1)_Y$ and horizontally under $SU(2)_N$. The new fermions come in three generations $n, n', n''$. Each of these is a vector-like doublet under $SU(2)_N$ so their contributions to the $SU(2)_N$ gauge anomaly cancel, hence this model is anomaly-free. Although not listed, lepton number may be defined as $L = +1$ for $n, n', n''$ and the SM leptons, and $L = -2$ for the triplet particles $\Delta$.

The notation for the VEVs and their approximate hierarchy is

$$\begin{aligned} \langle \chi_2 \rangle &= u_2 \sim \text{TeV} \\ \langle \phi^0 \rangle &= v_1 \sim 100\ \text{GeV} \\ \langle \zeta_2^0 \rangle &= v_2 \sim \text{GeV} \\ \langle \Delta_3 \rangle &= u_3 \sim \text{keV}, \text{MeV} \end{aligned} \tag{6.4}$$

This means that $SU(2)_N$ is mostly broken by the largest VEV of $\langle \chi_2 \rangle = u_2$. Note this is slightly higher than the scale of electroweak symmetry breaking. The electroweak symmetry

| Particle | $(SU(3)_C, SU(2)_L, Y)$ | $SU(2)_N$ | $S'$ | $S$ |
|---|---|---|---|---|
| $L_{iL} = \begin{pmatrix}\nu_{iL}\\ l_{iL}\end{pmatrix}$ | $(\mathbf{1},\mathbf{2},-1/2)$ | $\mathbf{1}$ | 0 | 0 |
| $l_{iR}$ | $(\mathbf{1},\mathbf{1},-1)$ | $\mathbf{1}$ | 0 | 0 |
| $\Phi = \begin{pmatrix}\phi^+\\ \phi^0\end{pmatrix}$ | $(\mathbf{1},\mathbf{2},+1/2)$ | $\mathbf{1}$ | 0 | 0 |
| $\begin{pmatrix} X = (X_1 - iX_2)/\sqrt{2} \\ \overline{X} = (X_1 + iX_2)/\sqrt{2} \\ X_3 \end{pmatrix}$ | $(\mathbf{1},\mathbf{1},0)$ | $\mathbf{3}$ | 0 | $\begin{pmatrix}+1\\ -1\\ 0\end{pmatrix}$ |
| $\zeta = \begin{pmatrix}\zeta_1^0 & \zeta_2^0\\ \zeta_1^- & \zeta_2^-\end{pmatrix}$ | $(\mathbf{1},\mathbf{2},-1/2)$ | $\mathbf{2}$ | $-1/2$ | $\begin{pmatrix}-1 & 0\\ -1 & 0\end{pmatrix}$ |
| $\chi = \begin{pmatrix}\chi_1\\ \chi_2\end{pmatrix}$ | $(\mathbf{1},\mathbf{1},0)$ | $\mathbf{2}$ | $+1/2$ | $\begin{pmatrix}+1\\ 0\end{pmatrix}$ |
| $n_{L,R} = \begin{pmatrix}n_1\\ n_2\end{pmatrix}_{L,R}$ | $(\mathbf{1},\mathbf{1},0)$ | $\mathbf{2}$ | $+1/2$ | $\begin{pmatrix}+1\\ 0\end{pmatrix}$ |
| $n'_{L,R} = \begin{pmatrix}n'_1\\ n'_2\end{pmatrix}_{L,R}$ | $(\mathbf{1},\mathbf{1},0)$ | $\mathbf{2}$ | $+1/2$ | $\begin{pmatrix}+1\\ 0\end{pmatrix}$ |
| $n''_{L,R} = \begin{pmatrix}n''_1\\ n''_2\end{pmatrix}_{L,R}$ | $(\mathbf{1},\mathbf{1},0)$ | $\mathbf{2}$ | $+1/2$ | $\begin{pmatrix}+1\\ 0\end{pmatrix}$ |
| $\Delta = \begin{pmatrix}\Delta_2/\sqrt{2} & \Delta_3\\ \Delta_1 & -\Delta_2/\sqrt{2}\end{pmatrix}$ | $(\mathbf{1},\mathbf{1},0)$ | $\mathbf{3}$ | $-1$ | $\begin{pmatrix}-1 & 0\\ -2 & -1\end{pmatrix}$ |

Table 6.1: Particle content in the vector dark matter model.

is mostly broken by $\langle \phi^0 \rangle = v_1$. This is close to the SM value, and is part of the reason why the SM Higgs will be approximately $Re(\phi^0)$ with a small admixture of the other new scalars. This small mixing is also partly due to the small value of $\langle \zeta_2^0 \rangle = v_2$ relative to $v_1$. The VEV of $\zeta_2^0$ breaks both the electroweak and $SU(2)_N$ symmetries because $\zeta$ is a bidoublet. In this model, the bidoublet is an important link between the SM and the dark sector. Without it, the only link would be the Higgs portal from other scalar interactions [59, 60]. The bidoublet is also important for neutrino mass, in combination with the smallest VEV of $\langle \Delta_3 \rangle = u_3$, which is needed to implement the inverse seesaw mechanism [28–30].

The allowed Lagrangian terms before spontaneous symmetry breaking are listed in Table 6.2, where the duals of the fields are

$$\begin{aligned} \widetilde{\Phi} &= \begin{pmatrix} \phi^{0*} \\ -\phi^- \end{pmatrix} \\ \widetilde{\chi} &= \begin{pmatrix} \chi_2^* \\ -\chi_1^* \end{pmatrix} \\ \widetilde{\zeta} &= \begin{pmatrix} \zeta_2^+ & -\zeta_1^+ \\ -\zeta_2^{0*} & \zeta_1^{0*} \end{pmatrix} \\ \widetilde{n_L} &= \begin{pmatrix} (n_{2L})^c \\ -(n_{1L})^c \end{pmatrix} \end{aligned} \tag{6.5}$$

and similarly for $\widetilde{n_R}$, $\widetilde{n'_{L,R}}$ and $\widetilde{n''_{L,R}}$. The Lagrangian is written in terms of $\Delta$ but not its dual $\widetilde{\Delta}$ because using $\widetilde{\Delta}$ does not give any additional independent terms. Note that because $n, n', n''$ are not gauge singlets under $SU(2)_N$, explicit Majorana mass terms such as $\overline{n_{iL}}(n_{jL})^c$ or $\overline{n_{iR}}(n_{jR})^c$ are forbidden for all combinations of $\overline{n_i}, \overline{n'_i}, \overline{n''_i}$ and $(n_j)^c, (n'_j)^c, (n''_j)^c$.

Fermion and Yukawa Terms

$$
\begin{aligned}
-\mathcal{L}_n &= M_{ab}\,\overline{n_L^a}\,n_R^b \quad + \quad h.c. \qquad\qquad \text{where } n^{a,b} = n, n', n'' \\
-\mathcal{L}_\zeta &= f_i\,\overline{L_{iL}}\,\zeta\,n_R \quad + \quad f_i'\,\overline{L_{iL}}\,\zeta\,n_R' \quad + \quad f_i''\,\overline{L_{iL}}\,\zeta\,n_R'' \quad + \quad h.c. \\
&= f_i\,\left[\overline{\nu_{iL}}\,\left(\zeta_1^0\,n_{1R} + \zeta_2^0\,n_{2R}\right) + \overline{e_{iL}}\,\left(\zeta_1^-\,n_{1R} + \zeta_2^-\,n_{2R}\right)\right] \\
&\quad + f_i'\,\left[\overline{\nu_{iL}}\,\left(\zeta_1^0\,n_{1R}' + \zeta_2^0\,n_{2R}'\right) + \overline{e_{iL}}\,\left(\zeta_1^-\,n_{1R}' + \zeta_2^-\,n_{2R}'\right)\right] \\
&\quad + f_i''\,\left[\overline{\nu_{iL}}\,\left(\zeta_1^0\,n_{1R}'' + \zeta_2^0\,n_{2R}''\right) + \overline{e_{iL}}\,\left(\zeta_1^-\,n_{1R}'' + \zeta_2^-\,n_{2R}''\right)\right] \quad + \quad h.c. \\
-\mathcal{L}_{\Delta,L} &= f_L^{ab}\,\overline{\widetilde{n_L^a}}\,\Delta\,n_L^b \quad + \quad h.c. \\
&= f_L^{ab}\,\left[\overline{(n_{2L}^a)^c}\left(\frac{\Delta_2}{\sqrt{2}}n_{1L}^b + \Delta_3 n_{2L}^b\right) - \overline{(n_{1L}^a)^c}\left(\Delta_1 n_{1L}^b - \frac{\Delta_2}{\sqrt{2}}n_{2L}^b\right)\right] + h.c. \\
-\mathcal{L}_{\Delta,R} &= f_R^{ab}\,\overline{\widetilde{n_R^a}}\,\Delta\,n_R^b \quad + \quad h.c. \\
&= f_R^{ab}\,\left[\overline{(n_{2R}^a)^c}\left(\frac{\Delta_2}{\sqrt{2}}n_{1R}^b + \Delta_3 n_{2R}^b\right) - \overline{(n_{1R}^a)^c}\left(\Delta_1 n_{1R}^b - \frac{\Delta_2}{\sqrt{2}}n_{2R}^b\right)\right] + h.c.
\end{aligned}
$$

Scalar Terms

$$
\begin{aligned}
-\mathcal{L}_{scalars} &= \mu_\zeta^2\,Tr(\zeta^\dagger\zeta) + \mu_\Phi^2\,\Phi^\dagger\Phi + \mu_\chi^2\,\chi\chi^\dagger + \mu_\Delta^2\,Tr(\Delta^\dagger\Delta) \\
&\quad + (\mu_1\widetilde{\Phi}^\dagger\zeta\chi + \mu_2\widetilde{\chi}^\dagger\Delta\chi + h.c.) \\
&\quad + \tfrac{1}{2}\lambda_1[Tr(\zeta^\dagger\zeta)]^2 + \tfrac{1}{2}\lambda_2(\Phi^\dagger\Phi)^2 \\
&\quad + \tfrac{1}{2}\lambda_3 Tr(\zeta^\dagger\zeta\zeta^\dagger\zeta) + \tfrac{1}{2}\lambda_4(\chi^\dagger\chi)^2 + \tfrac{1}{2}\lambda_5[Tr(\Delta^\dagger\Delta)]^2 \\
&\quad + \tfrac{1}{4}\lambda_6\,Tr(\Delta^\dagger\Delta - \Delta\Delta^\dagger)^2 + f_1\chi^\dagger\widetilde{\zeta}^\dagger\,\widetilde{\zeta}\chi \\
&\quad + f_2\chi^\dagger\zeta^\dagger\zeta\chi + f_3\Phi^\dagger\zeta\zeta^\dagger\Phi + f_4\Phi^\dagger\widetilde{\zeta}\,\widetilde{\zeta}^\dagger\Phi \\
&\quad + f_5(\Phi^\dagger\Phi)(\chi^\dagger\chi) + f_6(\chi^\dagger\chi)\,Tr(\Delta^\dagger\Delta) \\
&\quad + f_7\chi^\dagger(\Delta\Delta^\dagger - \Delta^\dagger\Delta)\chi + f_8(\Phi^\dagger\Phi)\,Tr(\Delta^\dagger\Delta) \\
&\quad + f_9\,Tr(\zeta^\dagger\zeta)\,Tr(\Delta^\dagger\Delta) + f_{10}\,Tr[\zeta(\Delta^\dagger\Delta - \Delta\Delta^\dagger)\zeta^\dagger]
\end{aligned}
$$

Table 6.2: Lagrangian terms in the vector dark matter model.

## 6.2 Spontaneous Symmetry Breaking

First consider first the gauge bosons. Their masses are affected by all four of the scalar VEVs. The masses of $W^{\pm}$ and $X, \overline{X}$ are

$$\begin{aligned} m_W^2 &= \frac{1}{2} g_2^2 (v_1^2 + v_2^2) \\ m_X^2 &= \frac{1}{2} g_N^2 [u_2^2 + v_2^2 + 2u_3^2] \end{aligned} \tag{6.6}$$

where $g_2$ and $g_N$ are the gauge couplings. The mass of $W$ is mostly due to $v_1 = \langle \phi^0 \rangle$ and the mass of $X$ is mostly due to $u_2 = \langle \chi_2 \rangle$. The mass matrix that mixes the interaction state gauge bosons $Z$ and $X_3 = Z'$ is

$$m_{Z,Z'}^2 = \frac{1}{2} \begin{pmatrix} (g_1^2 + g_2^2)(v_1^2 + v_2^2) & -g_N \sqrt{(g_1^2 + g_2^2)} v_2^2 \\ -g_N \sqrt{(g_1^2 + g_2^2)} v_2^2 & g_N^2 (u_2^2 + v_2^2 + 4u_3^2) \end{pmatrix} \tag{6.7}$$

which determines the physical mass eigenstate gauge bosons. Unlike other $Z'$ models, this $Z'$ does not couple directly to SM particles, so it will not be easy to detect at the LHC.

Next consider the SM fermions. As in the SM, Dirac mass terms for the charged SM fermions come from the larger Higgs VEV $v_1 = \langle \phi^0 \rangle$. For neutrinos, Dirac mass terms come from the modest VEV $v_2 = \langle \zeta_2^0 \rangle$ and small Majorana mass terms come from the smallest VEV $u_3 = \langle \Delta_3 \rangle$. The relevant Lagrangian terms are

$$-\mathcal{L} \supset \left( \overline{\nu_{eL}} \, , \, \overline{(n_{2R})^c} \, , \, \ldots \right) (\mathcal{M}_{\nu n}) \begin{pmatrix} (\nu_{eL})^c \\ n_{2R} \\ \vdots \end{pmatrix} \tag{6.8}$$

where the neutrino mass matrix $\mathcal{M}_{\nu n}$ has the schematic form

| | $(\nu_{eL})^c$ | $n_{2R}$ | $(n_{2L})^c$ | $(\nu_{\mu L})^c$ | $n'_{2R}$ | $(n'_{2L})^c$ | $(\nu_{\tau L})^c$ | $n''_{2R}$ | $(n''_{2L})^c$ |
|---|---|---|---|---|---|---|---|---|---|
| $\overline{\nu_{eL}}$ | 0 | $f_e v_2$ | 0 | 0 | $f'_e v_2$ | 0 | 0 | $f''_e v_2$ | 0 |
| $\overline{(n_{2R})^c}$ | $f_e v_2$ | $f_R^{11} u_3$ | $M_{11}$ | $f'_e v_2$ | $f_R^{12} u_3$ | $M_{12}$ | $f''_e v_2$ | $f_R^{13} u_3$ | $M_{13}$ |
| $\overline{n_{2L}}$ | 0 | $M_{11}$ | $f_L^{11} u_3$ | 0 | $M_{12}$ | $f_L^{12} u_3$ | 0 | $M_{13}$ | $f_L^{13} u_3$ |
| $\overline{\nu_{\mu L}}$ | 0 | $f_\mu v_2$ | 0 | 0 | $f'_\mu v_2$ | 0 | 0 | $f''_\mu v_2$ | 0 |
| $\overline{(n'_{2R})^c}$ | $f_\mu v_2$ | $f_R^{12} u_3$ | $M_{12}$ | $f'_\mu v_2$ | $f_R^{22} u_3$ | $M_{22}$ | $f''_\mu v_2$ | $f_R^{23} u_3$ | $M_{23}$ |
| $\overline{n'_{2L}}$ | 0 | $M_{12}$ | $f_L^{12} u_3$ | 0 | $M_{22}$ | $f_L^{22} u_3$ | 0 | $M_{23}$ | $f_L^{23} u_3$ |
| $\overline{\nu_{\tau L}}$ | 0 | $f_\tau v_2$ | 0 | 0 | $f'_\tau v_2$ | 0 | 0 | $f''_\tau v_2$ | 0 |
| $\overline{(n''_{2R})^c}$ | $f_\tau v_2$ | $f_R^{13} u_3$ | $M_{13}$ | $f'_\tau v_2$ | $f_R^{23} u_3$ | $M_{23}$ | $f''_\tau v_2$ | $f_R^{33} u_3$ | $M_{33}$ |
| $\overline{n''_{2L}}$ | 0 | $M_{13}$ | $f_L^{13} u_3$ | 0 | $M_{23}$ | $f_L^{23} u_3$ | 0 | $M_{33}$ | $f_L^{33} u_3$ |

(6.9)

The VEV $u_3 = \langle \Delta_3 \rangle$ is naturally small because it breaks lepton number $L$ to $(-1)^L$. The couplings $f_{L,R}^{ab}$ are not naturally small, but the end result is that the products $f_{L,R}^{ab} u_3$ are small Majorana masses.

The simplest case occurs when the following parameters can be neglected compared

to other terms

$$
\begin{aligned}
( f'_e \, , \, f''_e \, ) \, v_2 &\sim 0 \\
( f_\mu \, , \, f''_\mu \, ) \, v_2 &\sim 0 \\
( f_\tau \, , \, f'_\tau \, ) \, v_2 &\sim 0 \\
( f_L^{12} \, , \, f_L^{13} \, , \, f_L^{23} \, ) \, u_3 &\sim 0 \\
( f_R^{12} \, , \, f_R^{13} \, , \, f_R^{23} \, ) \, u_3 &\sim 0 \\
M_{12} \, , \, M_{13} \, , \, M_{23} &\sim 0
\end{aligned}
\tag{6.10}
$$

so that the $9 \times 9$ neutrino mass matrix is block diagonal, and each block takes the well-known form of the inverse seesaw. For the electron block

$$
\mathcal{M}_{\nu n}|_e = \begin{pmatrix} 0 & f_e v_2 & 0 \\ f_e v_2 & f_R^{11} u_3 & M_{11} \\ 0 & M_{11} & f_L^{11} u_3 \end{pmatrix} \tag{6.11}
$$

When $f_L^{11} u_3$ and $f_R^{11} u_3$ are much less than $M_{11}$, this gives the inverse seesaw neutrino mass

$$
m_{\nu_1} \simeq \frac{(f_e v_2)^2 (f_L^{11} u_3)}{M_{11}^2} \tag{6.12}
$$

where the small neutrino mass results from the combination of the small Majorna mass $f_L^{11} u_3$ and the small ratio of the Dirac mass to the invariant mass $(f_e v_2 / M_{11})^2$.

Consider now the scalar particles. Minimizing the scalar potential and taking into

account the hierarchy of the VEVs mentioned earlier, we find the VEVs to be given by

$$\begin{aligned} u_2^2 &\simeq \frac{-\mu_\chi^2}{\lambda_4} \\ v_1^2 &\simeq \frac{-\mu_\Phi^2 - f_5 u_2^2}{\lambda_2} \\ v_2 &\simeq \frac{-\mu_1 v_1 u_2}{\mu_\zeta^2 + f_2 u_2^2} \\ u_3^2 &\simeq \frac{-\mu_2 u_2^2}{\mu_\Delta^2 + (f_6 - f_7) u_2^2} \end{aligned} \tag{6.13}$$

and the physical masses of the scalars to be given by

$$\begin{aligned} m^2(\sqrt{2} Re\ \chi_2) &\simeq 2\lambda_4 u_2^2 \\ m^2(\sqrt{2} Re\ \phi^0) &\simeq 2\lambda_2 v_1^2 \\ m^2(\zeta_2^0) &\simeq \mu_\zeta^2 + f_2 u_2^2 + f_4 v_1^2 \\ m^2(\zeta_2^-) &\simeq \mu_\zeta^2 + f_2 u_2^2 + f_3 v_1^2 \\ m^2(\zeta_1^0) &\simeq \mu_\zeta^2 + f_1 u_2^2 + f_4 v_1^2 \\ m^2(\zeta_1^-) &\simeq \mu_\zeta^2 + f_1 u_2^2 + f_3 v_1^2 \\ m^2(\Delta_1) &\simeq \mu_\Delta^2 + (f_6 + f_7) u_2^2 + f_8 v_1^2 \\ m^2(\Delta_3) &\simeq \mu_\Delta^2 + (f_6 - f_7) u_2^2 + f_8 v_1^2 \\ m^2(\Delta_2) &\simeq \mu_\Delta^2 + f_6 u_2^2 + f_8 v_1^2 \end{aligned} \tag{6.14}$$

where the names of the physical particles reflect the dominant component of the scalar mixtures. The five scalar components $Re\chi_1$, $Im\chi_1$, $Re\phi^+$, $Im\phi^+$, $Im\phi^0$ are not listed because they are absorbed to become the five longitudinal components of the massive gauge bosons $W^\pm$, $X$, $\overline{X}$ and the physical gauge boson mixtures of $Z$, $Z'$.

## 6.3 Dark Matter Properties

The particles with dark charge $S \neq 0$ are the fermions $n_1, n_1', n_1''$, the scalars $\Delta_1, \Delta_2, \zeta_1$, and the gauge bosons $X, \overline{X}$. Of these, we assume $X, \overline{X}$ are the lightest, which means they are stable. In this way, we obtain vector dark matter. The new particles with no dark charge $S = 0$ are the fermions $n_2, n_2', n_2''$, the scalars $\Delta_3, \zeta_2, Re\chi_2$, and the interaction gauge boson $X_3 = Z'$. Of these, we assume for illustration that $\zeta_2^0$ and $\zeta_2^-$ are lighter than $X$ so that the dark matter annihilations $X\overline{X} \to \zeta_2^0 \zeta_2^{0*}$ and $X\overline{X} \to \zeta_2^+ \zeta_2^-$ are kinematically allowed and other annihilations are kinematically forbidden. Note that in this model, dark matter does not annihilate directly to SM particles. Subsequent decays such as $\zeta_2 \zeta_2^\dagger \to l^- l^+$ maintain thermal equilibrium with SM particles.

Using the diagrams for the dark matter annihilation shown in Fig. 6.1, we calculate the annihilation cross section times relative velocity to be

$$\sigma \times v_{rel} = \frac{g_N^4}{576\pi m_X^2} \sqrt{1 - \frac{m_{\zeta_2}^2}{m_X^2}} \left( 2 + \left[ 1 + \frac{4(m_X^2 - m_{\zeta_2}^2)}{m_{\zeta_1}^2 + m_X^2 - m_{\zeta_2}^2} \right]^2 \right) \tag{6.15}$$

We use [43] the value $\sigma \times v_{rel} = 4.4 \times 10^{-26} \mathrm{cm}^3 \mathrm{s}^{-1}$ which takes into account that $X$ is

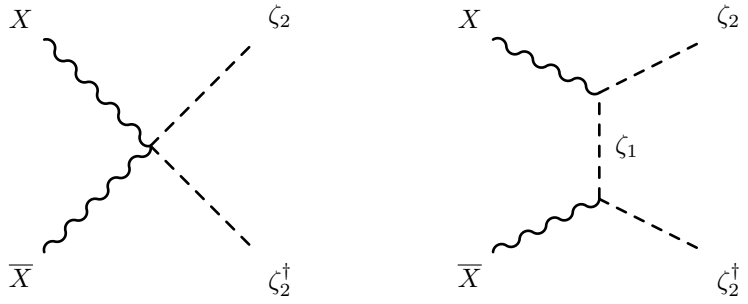


Figure 6.1: Dark matter annihilation of $X\overline{X}$ to $\zeta_2 {\zeta_2}^\dagger$.

a complex vector field, and in Fig. 6.2 we plot the allowed values of $m_X/g_N^2$ versus the parameter $r = m_{\zeta_2}^2/m_X^2$.

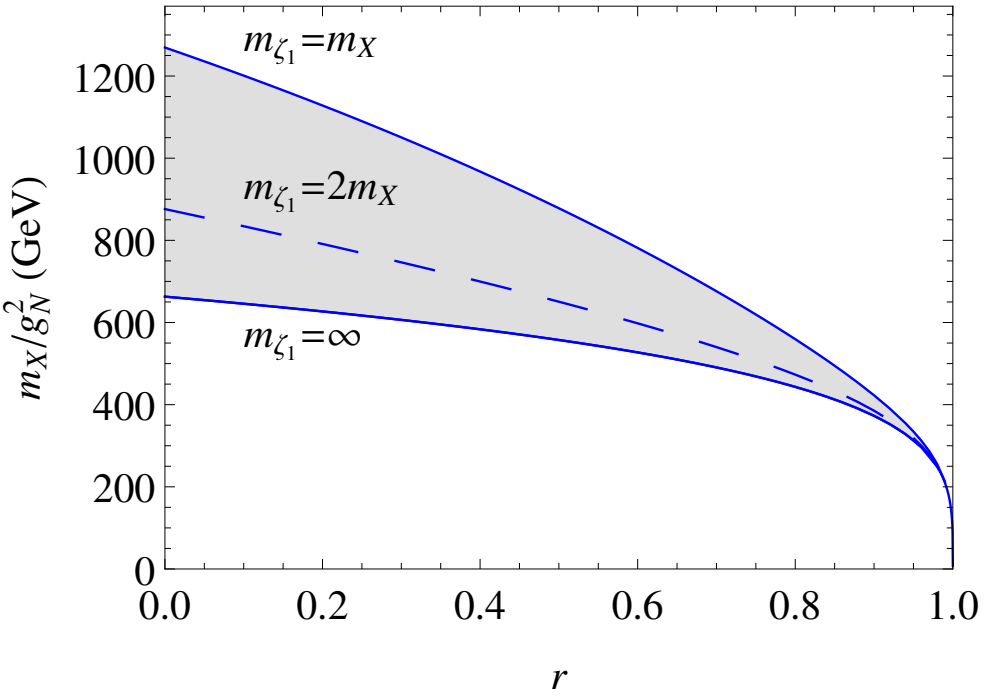


Figure 6.2: Allowed parameter values from relic abundance.

In this model, there is a chance of detecting $X$ from its scattering off nuclei due to $h$ exchange, where $h$ is the 125 GeV particle resulting from a linear combination of $\sqrt{2}Re\phi^0$, $\sqrt{2}Re\zeta_2^0$ and $\sqrt{2}Re\chi_2$. The $hX\overline{X}$ interaction is due primarily to the mixing of $\phi^0$ and $\chi_2$, and is approximately $(g_N^2 v_1/\sqrt{2})(f_5/\lambda_4)$. The Higgs interaction with quarks $hq\overline{q}$ has coupling strength given by $(m_q/\sqrt{2}v_1)$. The spin-independent elastic cross section for scattering off a nucleus of $Z$ protons and $A-Z$ neutrons normalized to one nucleon is given by [61]

$$\sigma_{SI} = \frac{1}{\pi}\left(\frac{m_N}{m_X + Am_N}\right)^2 \left|\frac{Zf_p + (A-Z)f_n}{A}\right|^2 \tag{6.16}$$

where we find

$$\begin{aligned}
\frac{f_p}{m_p} &= -0.075\left[\frac{g_N^2(f_5/\lambda_4)}{4m_\phi^2}\right] - 0.925(3.51)\left[\frac{g_N^2(f_5/\lambda_4)}{54m_\phi^2}\right] \\
\frac{f_n}{m_n} &= -0.078\left[\frac{g_N^2(f_5/\lambda_4)}{4m_\phi^2}\right] - 0.922(3.51)\left[\frac{g_N^2(f_5/\lambda_4)}{54m_\phi^2}\right]
\end{aligned} \tag{6.17}$$

with $m_\phi = 125$ GeV. In Fig. 6.3 we plot maximum allowed value of $g_N^2(f_5/\lambda_4)$ as a function of $m_X$ using the LUX data [62]

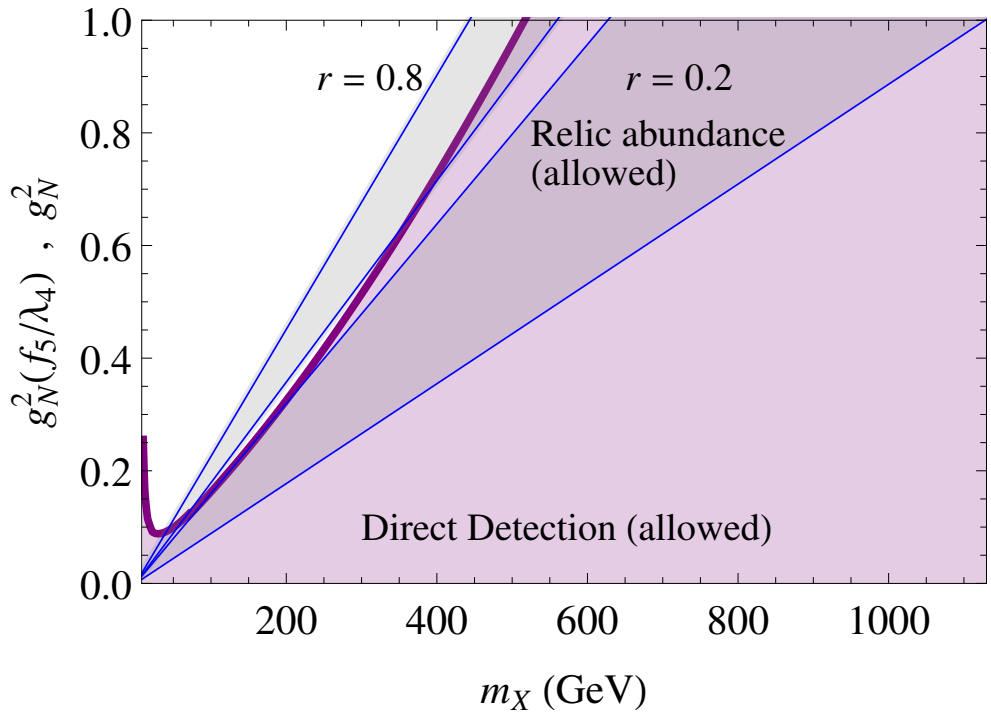


Figure 6.3: Allowed parameter values from relic abundance and direct detection.

Although not considered here, this model includes the interesting possibility that one of the $\Delta$ particles is stable, allowing $\Delta$ to become a significant additional component [63] of dark matter. Consider the interactions based on the Lagrangian terms, neglecting the mixing between scalars. From $\mathcal{L}_{\Delta,L}$ and $\mathcal{L}_{\Delta,R}$ there are possible decays $\Delta \to n^a n^b$. In

general these decays are not suppressed by the couplings $f^{ab}_{L,R}$, but they can be kinematically forbidden by the large invariant masses $M_{ab}$ of $\overline{n^a}n^b$. This is consistent with the inverse seesaw mechanism for neutrino masses outlined in the previous section. There are also possible decays from $\mathcal{L}_{scalars}$, but we assume these are also kinematically forbidden. The remaining possible decays come from gauge interactions. For example, the Lagrangian term $\Delta_3\Delta_1^*\overline{X}\,\overline{X}$ describes the decay $\Delta_3 \to \Delta_1 XX$. Thus $\Delta_3$ is kinematically stable if we have $m(\Delta_3) < 2m_X + m(\Delta_1)$. Similarly, the Lagrangian term $\Delta_1\Delta_3^* XX$ describes the decay $\Delta_1 \to \Delta_3\overline{X}\,\overline{X}$ and $\Delta_1$ is kinematically stable if $m(\Delta_1) < 2m_X + m(\Delta_3)$. Note this stability of $\Delta$ arises from kinematics rather than from any additional modification of the dark symmetry. One indication of this can be seen by comparing the dark charges of the stable particle. In the first case $\Delta_1$ carries dark charge $S = -2$, whereas in the second case $\Delta_3$ does not carry any dark charge $S = 0$.

To summarize, this chapter has examined a realistic model of vector dark matter that includes tree-level neutrino masses based on the inverse seesaw. The 125 GeV particle is an electroweak scalar that mixes only slightly with its scalar counterpart in the dark sector.

# Chapter 7

# Supersymmetric $U(1)_X$ Gauge Extension

## 7.1 Outline of the Model

The original motivation for the analysis of this chapter was the suggestion of a 750 GeV diphoton excess based on preliminary LHC measurements [64, 65]. The importance of this event was the hope that it was the first solid glimpse into physics beyond the SM. Since that time many papers have appeared in response to this issue. Very recent updates [66, 67] report that the intial LHC results were most likely due to statistical fluctuations, which was of course also widely suspected from the begining. Nonetheless, the diphoton analysis for the model considered in this chapter may still be valuable should a similar phenomenon reappear as the LHC run continues. Independent of this aspect, another important outcome of this chapter is the relaxation of the standard supersymmetric constraints on the Higgs

boson mass of 125 GeV. This chapter is based on the work previously published in Ref. [6], where further details may be found that are not included here.

The LHC diphoton data do not show any significant excesses in the dijet, massive diboson or $t\bar{t}$ channels. This strongly suggests that for an explanation due to a resonance, the new particle is neutral under the SM gauge group and has spin 0 or spin 2, with suppressed decays into massive electroweak gauge bosons and SM fermions [68]. For the model outlined in this chapter, this precisely describes the complex scalars $S_{1,2,3}$ and their interactions with the new vectorlike fermions $U, D$ which are colored singlets. These particles are essential ingredients in this model for a unique pattern of anomaly cancellation, and were not invented after the fact to explain the diphoton excess.

For background, recall that the SM is an excellent reference model even though it treats neutrinos as massless. Similarly, the well-known minimal supersymmetric standard model (MSSM) is a popular reference model even though it treats neutrinos as massless. The main appeal of supersymmetric models is their ability to greatly alleviate the hierarchy problem, which is the question of why scalar masses near the electroweak scale should remain small when they receive large radiative corrections from a higher mass scale. In the SM by itself, there is no hierarchy problem because there is no hierarchy, that is, the electroweak scale in the only mass scale the theory. The problem arises when the SM is embedded into any broader framework that introduces a higher mass scale, for example, implementing the canonical or inverse seesaw mechanism for neutrinos introduces a large fermion invariant mass. The most realistic models consider the very high Planck scale, which introduces enormous radiative corrections. In spite of the advantage offered by the

MSSM and other supersymmetric models, there is one shortcoming, which is the $\mu$ problem. This is the question of why the dimensionful $\mu$ coupling in the Higgs sector should be so close the mass scale of soft supersymmetry breaking. On general grounds, these scales are expected to have very different physical origins, and yet for the correct phenomenology they must both be close to the electroweak scale.

The particular model which is the subject of this chapter stems from the original proposal [69] which is a $U(1)$ gauge extension of the SM with supersymmetry. It includes neutrino masses and explains the $\mu$ problem. A specific version of it [70, 71] is the basis of this chapter. Before spontaneous breaking of the gauge symmetry, the gauge group part of the full symmetry group is

$$SU(3)_C \times SU(2)_L \times U(1)_Y \times U(1)_X \tag{7.1}$$

which shows the $U(1)_X$ gauge extension of the SM. The remaining part of the full symmetry group involves the supersymmetric transformations between the bosonic and fermionic fields. Details may be found in Ref. [72], which is also a good source for other aspects that are only briefly covered below.

The particle content of the model is listed in Table 7.1 and grouped by particle type. Listed first are the SM gauge bosons and the new $U(1)_X$ gauge boson, the SM quarks, the SM leptons and new fermions $N$ for neutrino masses, the two scalar Higgs doublets and new scalars $S$, and the new exotic fermions $U$ and $D$. The $R$ parity familiar from the MSSM is defined by $R = (-1)^{2j+3B+L}$ where $j$ is particle spin. The corresponding superpartners and values of $R$ parity are indicated with a tilde. As in the MSSM, $R$ parity is also conserved

| $R$ | Particle | copies | $\widetilde{\text{Particle}}$ | $\widetilde{R}$ | $B$ | $L$ | $SU(3)_C$ | $SU(2)_L$ | $Y$ | $X$ |
|---|---|---|---|---|---|---|---|---|---|---|
| $+$ | $g_a$ | 1 | $\widetilde{g}_a$ | $-$ | 0 | 0 | **8** | **1** | 0 | 0 |
| $+$ | $W_a$ | 1 | $\widetilde{W}_a$ | $-$ | 0 | 0 | **1** | **3** | 0 | 0 |
| $+$ | $B$ | 1 | $\widetilde{B}$ | $-$ | 0 | 0 | **1** | **1** | 0 | 0 |
| $+$ | $B_X$ | 1 | $\widetilde{B}_X$ | $-$ | 0 | 0 | **1** | **1** | 0 | 0 |
| $+$ | $Q = \begin{pmatrix} u \\ d \end{pmatrix}$ | 3 | $\widetilde{Q}_i = \begin{pmatrix} \widetilde{u}_L \\ \widetilde{d}_L \end{pmatrix}$ | $-$ | $1/3$ | 0 | **3** | **2** | $1/6$ | 0 |
| $+$ | $u^c$ | 3 | $\widetilde{u}_R^*$ | $-$ | $-1/3$ | 0 | $\mathbf{3}^*$ | **1** | $-2/3$ | $1/2$ |
| $+$ | $d^c$ | 3 | $\widetilde{d}_R^*$ | $-$ | $-1/3$ | 0 | $\mathbf{3}^*$ | **1** | $1/3$ | $1/2$ |
| $+$ | $L = \begin{pmatrix} \nu \\ e \end{pmatrix}$ | 3 | $\widetilde{L}_i = \begin{pmatrix} \widetilde{\nu}_L \\ \widetilde{e}_L \end{pmatrix}$ | $-$ | 0 | 1 | **1** | **2** | $-1/2$ | $1/3$ |
| $+$ | $e^c$ | 3 | $\widetilde{e}_R^*$ | $-$ | 0 | $-1$ | **1** | **1** | 1 | $1/6$ |
| $+$ | $N^c$ | 3 | $\widetilde{N}_R^*$ | $-$ | 0 | $-1$ | **1** | **1** | 0 | $1/6$ |
| $+$ | $\phi_1 = \begin{pmatrix} \phi_1^0 \\ \phi_1^- \end{pmatrix}$ | 1 | $\widetilde{\phi}_1 = \begin{pmatrix} \widetilde{\phi}_1^0 \\ \widetilde{\phi}_1^- \end{pmatrix}$ | $-$ | 0 | 0 | **1** | **2** | $-1/2$ | $-1/2$ |
| $+$ | $\phi_2 = \begin{pmatrix} \phi_2^+ \\ \phi_2^0 \end{pmatrix}$ | 1 | $\widetilde{\phi}_2 = \begin{pmatrix} \widetilde{\phi}_2^+ \\ \widetilde{\phi}_2^0 \end{pmatrix}$ | $-$ | 0 | 0 | **1** | **2** | $1/2$ | $-1/2$ |
| $+$ | $S_1$ | 3 | $\widetilde{S}_1$ | $-$ | 0 | 0 | **1** | **1** | 0 | $-1/3$ |
| $+$ | $S_2$ | 3 | $\widetilde{S}_2$ | $-$ | 0 | 0 | **1** | **1** | 0 | $-2/3$ |
| $+$ | $S_3$ | 2 | $\widetilde{S}_3$ | $-$ | 0 | 0 | **1** | **1** | 0 | 1 |
| $-$ | $U$ | 2 | $\widetilde{U}_L$ | $+$ | $1/3$ | 1 | **3** | **1** | $2/3$ | $-2/3$ |
| $-$ | $D$ | 1 | $\widetilde{D}_L$ | $+$ | $1/3$ | 1 | **3** | **1** | $-1/3$ | $-2/3$ |
| $-$ | $U^c$ | 2 | $\widetilde{U}_R^*$ | $+$ | $-1/3$ | $-1$ | $\mathbf{3}^*$ | **1** | $-2/3$ | $-1/3$ |
| $-$ | $D^c$ | 1 | $\widetilde{D}_R^*$ | $+$ | $-1/3$ | $-1$ | $\mathbf{3}^*$ | **1** | $1/3$ | $-1/3$ |

Table 7.1: Particle content in the supersymmetric model.

in this model. It serves the same function as the discrete $Z_{2\,dark}$ symmetry in the previous chapters, and the lightest neutral mass eigenstate with odd $R$ parity is the dark matter candidate. The number of copies (generations) is indicated separately. Except for the

vector gauge bosons and their Majorana superpartners, generation indices are suppressed. For the particles with $SU(3)_C \sim \mathbf{3}, \mathbf{3}^*$ an additional color index is understood. The notation used for left- and right-handed fermion fields differs from the previous chapters, and follows the standard convention where all fermion fields are left-handed. For example $e$ is a left-handed electron and $e^c$ is a right-handed positron. Their superpartners are the two complex scalar electrons $e_L$ and $e_R^*$, respectively. It is highly non-trivial to show that in this model, all gauge anomalies cancel.

The supersymmetric Lagrangian terms can be obtained in a lengthy but relatively straightforward way. Alternatively, the formalism of superfields can be used, where the tilde is not written and the context determines whether the tilde is implied or not. For example, the superfield $e$ stands for either $e$ or $\widetilde{e}_L$ and $e^c$ stands for either $e^c$ or $\widetilde{e}_R^*$ depending on the calculation involved. The auxiliary device used to obtain the Lagrangian terms involves the concept of the superpotential. The allowed superpotential terms for this model are listed in Table 7.2, which will be referred to throughout this chapter. The terms affected by the VEVs produce masses for fermions and mass mixings for scalars, as well as interactions. The terms without VEVs produce interactions including decays of the scalar leptoquarks $\widetilde{U}$ and $\widetilde{D}$.

There is currently no direct evidence for the existence of the superpartners, which would have the same mass as the known particles if supersymmetry were exact. Therefore at the low energy scales available in experiments, a valid description must incorporate some kind of supersymmetry breaking. The spontaneous breaking of supersymmetry at some high energy scale is usually considered ideal, but for phenomenological purposes it is

| Superfields | scalar VEV | Particle | $\widetilde{\text{Particle}}$ |
|---|---|---|---|
| $Qu^c\phi_2$ | $\langle\phi_2^0\rangle$ | $uu^c$ Dirac masses | $\widetilde{u}_L\widetilde{u}_R^*$ scalar |
| $Qd^c\phi_1$ | $\langle\phi_1^0\rangle$ | $dd^c$ Dirac masses | $\widetilde{d}_L\widetilde{d}_R^*$ scalar |
| $Le^c\phi_1$ | $\langle\phi_1^0\rangle$ | $ee^c$ Dirac masses | $\widetilde{e}_L\widetilde{e}_R^*$ scalar |
| $LN^c\phi_2$ | $\langle\phi_2^0\rangle$ | $\nu N^c$ Dirac masses | $\widetilde{\nu}_L\widetilde{N}_R^*$ scalar |
| $S_3UU^c$ | $\langle S_3\rangle$ | $UU^c$ Dirac masses | $\widetilde{U}_L\widetilde{U}_R^*$ scalar |
| $S_3DD^c$ | $\langle S_3\rangle$ | $DD^c$ Dirac masses | $\widetilde{D}_L\widetilde{D}_R^*$ scalar |
| $N^cN^cS_1$ | $\langle S_1\rangle$ | $N^cN^c$ Majorana masses | $\widetilde{N}_R^*\widetilde{N}_R^*$ scalar $Re, Im$ |
| $S_1S_2S_3$ | $\langle S_1\rangle, \langle S_2\rangle, \langle S_3\rangle$ | $S_iS_j$ scalar $Re, Im$ | $\widetilde{S}_i\widetilde{S}_j$ Majorana masses |
| $S_3\phi_1\phi_2$ | $\langle S_3\rangle, \langle\phi_1^0\rangle, \langle\phi_2^0\rangle$ | $\phi_1\phi_2$ , $S_3\phi_i$ scalar | $\widetilde{\phi}_i\widetilde{\phi}_j$ fermion masses |
| $u^cN^cU$ | 0 | $\nu u \longleftarrow$ | $\widetilde{U}$ |
| $u^ce^cD$ | 0 | $eu \longleftarrow$ | $\widetilde{D}$ |
| $d^cN^cD$ | 0 | $\nu d \longleftarrow$ | $\widetilde{D}$ |
| $QLD^c$ | 0 | $eu, \nu d \longleftarrow$ | $\widetilde{D}$ |

Table 7.2: Superpotential terms in the supersymmetric model.

customary to parametrize our ignorance of how supersymmetry breaking occurs by including explicit soft breaking terms in the Lagrangian. These soft-breaking terms include tree-level mass terms for the scalar particles and the fermionic gauginos (the superpartners of the gauge bosons). Consistency then requires that corresponding terms should appear in the superpotential. For this model, the superpotential only contains terms that are trilinear in the superfields. Note that in the MSSM, the bilinear superpotential term $\phi_1\phi_2$ is allowed by gauge invariance [73], but here it is forbidden by the $U(1)_X$ gauge charges. So in this model all masses originate from soft supersymmetry breaking. This explains why the VEVs responsible for the spontaneous symmetry breaking scales of $SU(2) \times U(1)_Y$ and $U(1)_X$

are not far from the breaking scale of supersymmetry. In this model, there are five scalar VEVs, two from the Higgses $\phi^0_{1,2}$ and three from the first copies of $S_{1,2,3}$

$$\begin{aligned} v_1 &= \langle \phi^0_1 \rangle \\ v_2 &= \langle \phi^0_2 \rangle \\ u_1 &= \langle S_1 \rangle \\ u_2 &= \langle S_2 \rangle \\ u_3 &= \langle S_3 \rangle \end{aligned} \tag{7.2}$$

## 7.2 Quarks, Leptons and Neutrinos

It is clear from the terms in the superpotential that the SM quarks and leptons receive Dirac masses from the VEVs $v_{1,2}$ as in the MSSM. It is also clear that the neutrino mass matrix for each generation is of the form

$$\mathcal{L}_{\nu N} = - (\nu, N^c) \begin{pmatrix} 0 & m_D \\ m_D & m_N \end{pmatrix} \begin{pmatrix} \nu^c \\ N \end{pmatrix} + h.c. \tag{7.3}$$

where $m_D$ comes from $v_2$ and $m_N$ comes from $u_1$. This is the canonical seesaw, where a small neutrino mass results from a small Dirac mass $m_D$ compared to a large Majorana mass $m_N$.

## 7.3 Gauge Bosons

When the three VEVs $\langle S_{1,2,3} \rangle$ become nonzero, they give the new $Z_X$ gauge boson mass. When the two VEVs $\langle \phi^0_{1,2} \rangle$ become nonzero, they give the $Z$ gauge boson mass, and

give further contributions to $Z_X$ mass, and also produce off-diagonal terms in the mass-squared matrix that mixes $Z$ and $Z_X$. The mass-squared matrix determines the physical vector particles. Precision electroweak measurements require $Z$ and $Z_X$ mixing to be very small [74], which in this model translates to

$$\begin{aligned} v_1 &\simeq v_2 \\ &= (174 \text{ GeV})/\sqrt{2} = 123 \text{ GeV} \end{aligned} \tag{7.4}$$

which will be assumed in the following. As will be mentioned shortly, in the MSSM this corresponds to the parameter choice $\tan\beta \equiv v_2/v_1 \simeq 1$.

There are also experimental limits on the decays $Z_X \to l^- l^+$. To check these, we use the following mass estimates. We take the SM quarks and leptons to be massless, we take all the scalar quarks to have mass 800 GeV, and we take all the scalar leptons to have mass 500 GeV. We take the exotic $U, D$ fermions to have masses 400 GeV so they can explain the diphoton excess, which will be discussed in the last section. We take one of the pseudo-Dirac fermions coming from a linear combination of $\widetilde{S}_1$ and $\widetilde{S}_2$ to have mass 200 GeV so it can be the dark matter candidate, as will be discussed. Finally, we take the $U(1)_X$ coupling to be $g_X \sim 0.5$. This gives [6] a lower bound of $m_{Z_X} \sim 3$ TeV.

## 7.4 Scalars

As mentioned earlier, all scalar particles obtain explicit mass terms due to soft symmetry breaking. Along with the VEVs of spontaneous symmetry breaking, these determine the physical masses after mixing has been taken into account. Consider the scalar

quarks and scalar leptons. The approximate range of their physical masses has been quoted above. Consider the exotic scalars $\widetilde{U}_{L,R}$ and $\widetilde{D}_{L,R}$. They are leptoquarks and decay into ordinary quarks and leptons based on the form of the superpotential terms. Consider the neutral $S$ scalars that do not have any VEV. The second and third copies of $S_{1,2}$ are assumed to be heavy enough so they have not yet been discovered. The second copy of $S_3$ will be the key ingredient to explain the diphoton excess, to be discussed in the next section.

The remaining scalars are examined below. We calculate or estimate the physical particles to be given by approximate linear combinations of the interaction states listed in the particle content Table 7.1. In the following tabular equations, the first entry is the numerical mass or a description. Coefficients are not normalized, and null coefficients are indicated by 0 or left blank. Very small coefficients are indicated by a dot. Coefficients that are generically nonzero are denoted by $x$.

The two charged Higgs scalars give one Goldstone and one physical charged Higgs. For the neutral scalars, the real components will in general mix, but we require that the $Re(\phi^0_{1,2})$ sector be isolated from the $Re(S_{1,2,3})$ sector, which requires

$$u_1 = \sqrt{2}u_2 \tag{7.5}$$

This gives the two physical real scalar Higgses $h, H$ where $h$ is to be identified with the

125 GeV particle, and three other physical real scalars

| | | $\phi_1^+$ | $\phi_2^+$ | $Re(\phi_1^0)$ | $Re(\phi_2^0)$ | $Re(S_1)$ | $Re(S_2)$ | $Re(S_3)$ |
|---|---|---|---|---|---|---|---|---|
| Goldstone | $G^+$ | 1 | 1 | | | | | |
| scalar | $H^+$ | $-1$ | 1 | | | | | |
| 125 GeV | $h$ | | | 1 | 1 | . | . | . |
| heavy | $H$ | | | $-1$ | 1 | . | . | . |
| scalar | | | | . | . | $x$ | $x$ | $x$ |
| scalar | | | | . | . | $x$ | $x$ | $x$ |
| scalar | | | | . | . | $x$ | $x$ | $x$ |

(7.6)

The case when there is small mixing, indicated by the dots, will be referred to later in regards to the direct detection of dark matter.

For the neutral scalars, the five imaginary components give three pseudoscalars and two Goldstones

| | | $Im(\phi_1^0)$ | $Im(\phi_2^0)$ | $Im(S_1)$ | $Im(S_2)$ | $Im(S_3)$ |
|---|---|---|---|---|---|---|
| pseudoscalar | $A$ | $-1$ | 1 | 0 | 0 | 0 |
| pseudoscalar | $A_{12}$ | 0 | 0 | 2 | $-\sqrt{2}$ | 0 |
| pseudoscalar | $A_S$ | 0 | 0 | $u_3$ | $u_3\sqrt{2}$ | $u_2\sqrt{2}$ |
| Goldstone | $G_Z^0$ | 1 | 1 | 0 | 0 | 0 |
| Goldstone | $G_{Z_X}^0$ | $v_1/2$ | $-v_1/2$ | $-u_2\sqrt{2}/3$ | $-u_2 2/3$ | $u_3$ |

(7.7)

which assumes $v_1 \simeq v_2$ is much less than $u_{2,3}$. Note that $A$ is familiar from the MSSM, but

this model has the additional pseudoscalars $A_{12}$ and $A_S$. It is worth mentioning that to correctly achieve only two zero mass eigenvalues for the Goldstone modes it is necessary to include a non-standard but otherwise technically allowed trilnear Lagrangian term of the form given by Eq. (5.2) in Ref. [72].

Based on the physical states above, the physical Higgs mass in this model is

$$m_h^2 \simeq (g_X^2 + 2f^2 + \lambda_2) \left\langle \phi_1^0 \right\rangle^2 \tag{7.8}$$

We see that $m_h = 125$ GeV is determined from three parameters. First, the parameter $g_X = 0.5$ is the gauge coupling as mentioned earlier. Second, the parameter $\lambda_2$ is the well-known one-loop correction from the top quark and the associated physical scalar quarks $\widetilde{t}_1$ and $\widetilde{t}_2$

$$\lambda_2 = \frac{6G_F^2 m_t^4}{\pi^2} \ln\left(\frac{m_{\widetilde{t}_1} m_{\widetilde{t}_2}}{m_t^2}\right) \tag{7.9}$$

Third, the parameter $f$ is the Yukawa coupling of the $fS_3\phi_1\phi_2$ term in the superpotential. Note that the VEV $u_3 = \langle S_3 \rangle$ generates the $\mu$ term

$$\mu = f \langle S_3 \rangle \tag{7.10}$$

whereas in the MSSM $\mu$ is just an explicit coupling with dimension of mass.

Taking $m_{\widetilde{t}_{1,2}} \simeq 1$ TeV and $m_h = 125$ GeV determines $f \simeq 0.5$. Thus the three parameters $g_X, \lambda_2, f$ can easily be chosen in this model to give $m_h = 125$ GeV. This is the relaxation of the supersymmetric constraint on the Higgs mass. That is, the MSSM requires a large value of $\tan\beta$ and must also achieve $m_h = 125$ GeV, and satisfying both of these conditions simultaneously is difficult in the MSSM. Note that the values chosen

for the three parameters $g_X, \lambda_2, f$ are consistent with the earlier constraint $m_{Z_X} \sim 3$ TeV. For example, taking $\langle S_3 \rangle = 2$ TeV and $\langle S_2 \rangle = 4$ TeV gives $m_{Z_X} \sim 3$ TeV directly from the $Z, Z_X$ mass matrix.

The approximate mass range quoted earlier for the scalar leptons includes the scalar neutrinos, but here we make some additional comments. The scalar neutrinos are the only neutral scalars in this model that have odd $R$ parity, so in principle they are scalar dark matter candidates. In the MSSM, scalar neutrinos cannot escape dark matter direct detection bounds due to $Z$ exchange with nucleons. One popular way to avoid this is to introduce mass splitting between the real and imaginary components of the complex scalar neutrino[75]. This is what happens in this model due to lepton number violating terms, which are analogous to the Majorana mass terms $NN^c$ of the fermionic superpartners. Here the complex scalars have corresponding mass terms $\widetilde{N}_R \widetilde{N}_R$, which combine with the $\widetilde{\nu}_L \widetilde{N}_R^*$ terms to determine the physical states of real scalars as linear combinations of $Re(\widetilde{\nu}_L), Im(\widetilde{\nu}_L), Re(\widetilde{N}_R), Im(\widetilde{N}_R)$. However, as already mentioned, we assume the scalar mass eigenvalues are greater than the mass 200 GeV of the lightest pseudo-Dirac dark matter candidate to be discussed in the next section.

## 7.5 New Fermions

Consider first the charged fermions. It is clear from the terms in the superpotential that the exotic fermions $U$ and $D$ receive Dirac masses from the VEV $u_3$. The masses quoted earlier of 400 GeV are in the correct range to explain the diphoton excess, as will be discussed. On the other hand, the mixing of the charged gauginos (winos) and charged

higgsinos

$$\widetilde{W}^+, \widetilde{\phi}_1^+, \widetilde{\phi}_2^+ \tag{7.11}$$

come from gauge interactions rather than the superpotential. Although they are charged, they do not contribute to the diphoton excess because they do not couple to the $S_3$ scalar as discussed in the next section. Similarly, even though the gluinos are colored, they do not couple to the $S_3$ scalar, so they will not contribute to its production from SM gluons at the LHC.

The remaining fermions are neutral and have odd $R$ parity, so they are potential dark matter candidates. Consider first the Majorana fermions $\widetilde{S}$ whose scalar counterparts do not have VEVs. These are the third copies $\widetilde{S}_{1,2}$ and the second copies $\widetilde{S}_{1,2,3}$. As mentioned earlier a specific linear combination of them will be the dark matter candidate. As outlined in Ref. [6], the form of the mass matrix allows us to redefine the interaction states as new linear combinations such that the physical states are

| | | $\widetilde{S}_1$ | $\widetilde{S}_2$ | $\widetilde{S}_1$ | $\widetilde{S}_2$ | $\widetilde{S}_3$ |
|---|---|---|---|---|---|---|
| 200 GeV | $\widetilde{S}$ | 1 | 1 | . | . | . |
| $\gtrsim$ 200 GeV | $\widetilde{S}_{pD}$ | 1 | $-1$ | . | . | . |
| heavy | $\widetilde{S}_{TeV}$ | . | . | $x$ | $x$ | $x$ |
| heavy | $\widetilde{S}'_{TeV}$ | . | . | $x$ | $x$ | $x$ |
| heavy | $\widetilde{S}''_{TeV}$ | . | . | $x$ | $x$ | $x$ |

(7.12)

where the lightest $\widetilde{S}$ is the dark matter candidate, $\widetilde{S}_{pD}$ is its pseudo-Dirac companion, and

the other heavy Majorana fermions are in the TeV range. The value of 200 GeV is chosen in order to accommodate the invisible width of the diphoton resonance, as discussed in the next section.

Since $\widetilde{S}$ is Majorana, there is no chance of direct detection from elastic scattering off nuclei through the $Z_X$ interaction. For a spin-independent cross-section, the only hope for direct detection is from $h$ exchange. As listed previously in the scalar sector, we have taken $h$ to be approximately given by a linear combination of $\phi^0_{1,2}$. It is clear from the superpotential that the desired $\widetilde{S}\widetilde{S}h$ interaction must come from the $S_1S_2S_3$ term, that is, from $\widetilde{S}_i\widetilde{S}_jS_k$ where $S_k$ are the $S$ scalars that have VEV. This means that the previous requirement that the $Re(\phi^0_{1,2})$ sector be isolated from the $Re(S_{1,2,3})$ sector must be relaxed to give $h$ a nonzero $S_k$ component. Details of this are given in Ref. [6], along with analysis of direct detection and relic abundance similar to that already provided for the vector dark matter model in the previous Chapter 6.

Finally, consider the Majorana fermions $\widetilde{S}$ whose scalar counterparts do have VEVs. They mix with the fermionic partner of the $U(1)_X$ gauge boson

$$\widetilde{B}_X, \widetilde{S}_3, \widetilde{S}_2, \widetilde{S}_1 \tag{7.13}$$

and these will mix with the neutral gauginos (bino, wino) and neutral higgsinos

$$\widetilde{B}, \widetilde{W}_3, \widetilde{\phi}^0_1, \widetilde{\phi}^0_2 \tag{7.14}$$

but again we take these mass eigenvalues to be heavier than 200 GeV.

## 7.6 Diphoton Excess

Fig. 7.1 shows the diagram for the loop contributions to explain the 750 GeV diphoton excess based on the parton level process $gg \to S_3 \to \gamma\gamma$. To emphasize the structure, the particle labels show interaction states rather than physical states. The scalar superpartners $\widetilde{U}_{L,R}$ and $\widetilde{D}_{L,R}$ will also contribute in the loop diagrams, but will not be the focus here because the enhancement of the diphoton signal due to fermions is generally stronger[76]. The reason for using $S_3$ is clear from the superpotential terms $S_3 U U^c$ and $S_3 D D^c$, that is, $S_3$ is the only $S$ particle that connects to colored fermions for its production. The extra photonic loop connection to the charged Higgsinos from $S_3 \phi_1 \phi_2$ is a bonus of the model. The physical scalar or pseudoscalar that propagates could come from one of the neutral $S$ scalars that do not have any VEV, which are the second and third copies of $S_{1,2}$ and the second copy of $S_3$. Or it could come from the second copy of $S_3$. We choose the pseudoscalar version of the second copy of $S_3$, with physical state $\chi$. One reason for this choice is that a pseudoscalar will not mix with the SM Higgs. Another reason is that this

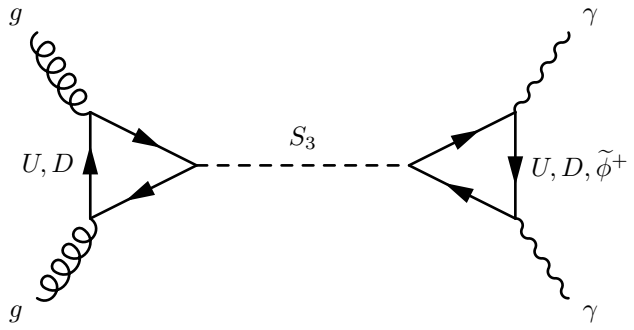


Figure 7.1: Diagram for $gg \to S_3 \to \gamma\gamma$.

allows the physical couplings $f_\phi, f_U, f_D$ for the physical terms $\chi\widetilde{\phi}_1\widetilde{\phi}_2, \chi UU^c, \chi DD^c$ to be independent of these fermion masses. The diphoton cross section for the LHC at 13 TeV is given by [77]

$$\begin{aligned}
\sigma(pp \to \chi \to \gamma\gamma) &= (100 \text{ pb}) \times (\lambda_g \text{ TeV})^2 \times BR(\chi \to \gamma\gamma) \\
\lambda_g &= \frac{\alpha_s}{\pi m_\chi} \sum_Q f_Q F_Q(m_Q^2/m_\chi^2) \\
F(x) &= 2\sqrt{x}\left[\arctan\left(\frac{1}{\sqrt{4x-1}}\right)\right]^2
\end{aligned} \tag{7.15}$$

where $Q = U, D$ and the loop function $F(x)$ has the same origin as the digluon and diphoton loop functions for the Higgs decays covered in Chapter 2. For the diphoton subprocess

$$\begin{aligned}
BR(\chi \to \gamma\gamma) &= \frac{\Gamma(\chi \to \gamma\gamma)}{\Gamma_\chi} \\
\Gamma(\chi \to \gamma\gamma) &= \frac{\lambda_\gamma^2}{64\pi} m_\chi^3 \\
\lambda_\gamma &= \frac{2\alpha}{\pi m_\chi} \sum_\psi N_\psi Q_\psi^2 F_\psi(m_\psi^2/m_\chi^2)
\end{aligned} \tag{7.16}$$

where $\psi = U, D, \widetilde{\phi}^+$. We assume the total width of $\chi$ is dominated by its decay to dark matter $\widetilde{S}$ , which as described in the previous section is the lightest pseudo-Dirac fermion coming from a linear combination of $\widetilde{S}_1$ and $\widetilde{S}_2$

$$\Gamma(\chi \to \widetilde{S}_1\widetilde{S}_2) = \frac{f_S^2}{8\pi}\sqrt{m_\chi^2 - m_S^2} \tag{7.17}$$

where $f_S$ is the $\chi\widetilde{S}_1\widetilde{S}_2$ coupling. Here $m_\chi = 750$ GeV for the resonance explanation of the diphoton excess. If $f_S = 1.2$, then $\Gamma_\chi = 36$ GeV. If $f_S = 0$, then then $\Gamma_\chi \lesssim 1$ GeV is dominated by $\chi$ decay to two gluons. Using the measured value of the cross section $\sigma(pp \to \chi \to \gamma\gamma) = 6.2 \pm 1$ fb for the diphoton resonance[77], In Fig. 7.2 we plot the allowed

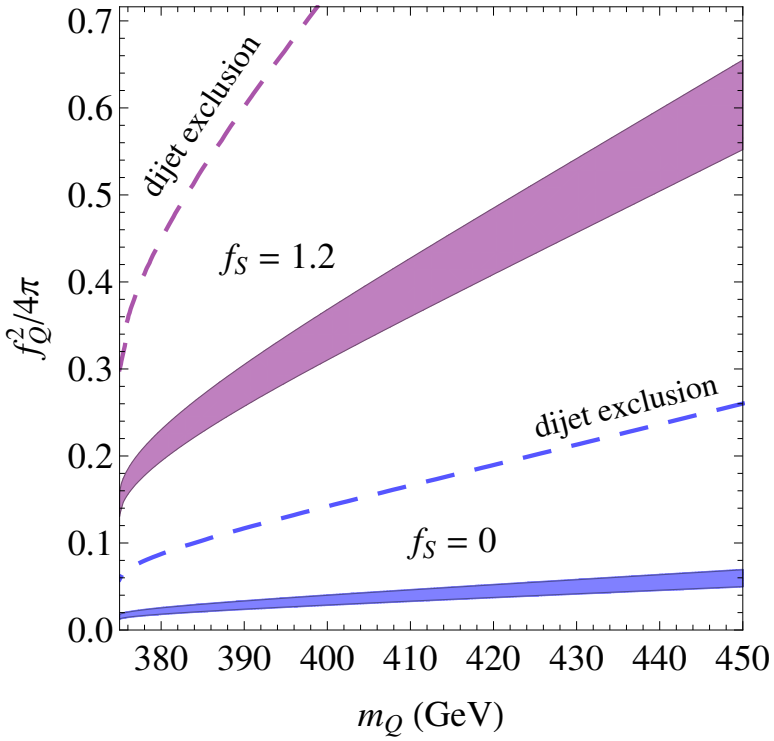


Figure 7.2: Parameters that explain the 750 GeV diphoton excess.

parameters for these two cases. There is also the probability for $\chi$ to decay back into two gluons as shown in Fig. 7.3, so we also plot the most stringent dijet exclusion upper limit of 2 pb from the 8 TeV data. Including important higher-order corrections [78] moves the

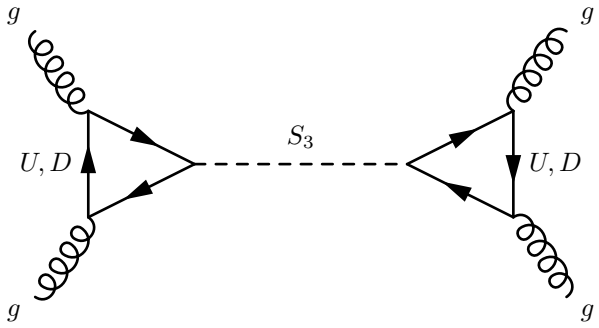


Figure 7.3: Diagram for $gg \to S_3 \to gg$.

dijet exclusion lines toward the allowed regions for the correct cross section but does not compromise this analysis.

To summarize, this chapter has examined a supersymmetric $U(1)_X$ gauge extension of the SM, with an emphasis on explaining the recent LHC diphoton excess and relaxing the supersymmetric constraint on the Higgs mass.

# Part III

# Summary

# Chapter 8

# Conclusion

We have mentioned in Chapter 1 that the SM can accommodate small fermion masses but cannot fully explain or predict them. The radiative models studied in this thesis have taken steps to address this.

In Part I, experimental verification of the $Z_2$ and $A_4$ radiative models studied in Chapters 2 and 4 is expected to come from the heavy fermions due to significant deviations from the SM in the Yukawa sector. This is not the case for leptons, which are all light compared to the electroweak scale, but experimental verification could come from the muon anomalous magnetic moment contributions provided by these models. The very light neutrino masses in Chapter 3 and Chapter 4 are Majorana, so neutrinoless double beta decay is one option for confirmation of these models. There is also the possibility that the new particles could be detected or inferred from other experimental signatures.

Experimental signatures were also important in Part II. An interesting collider signature from new particles was the main result in the Higgs triplet model for radiative

inverse seesaw neutrino mass from Chapter 5. It has a good discovery potential at the LHC. The tentative measurement of the 750 GeV diphoton excess was analyzed based on the new particles from a supersymmetric model in Chapter 7. And for the vector dark matter model in Chapter 6 there is a small cross section to be detected in underground experiments.

Most of the models considered took dark matter to be scalar, as in Chapters 3, 4, 5. Fermionic (Majorana) dark matter was considered in the last Chapter 7, but either fermionic (non-Majorana) or scalar dark matter could have been considered in Chapter 2.

# Bibliography


[1] S. Fraser and E. Ma, "Anomalous Higgs Yukawa Couplings", Europhys. Lett. **108**, 1002 (2014), arXiv:1402.6415 [hep-ph].

[2] S. Fraser, E. Ma, and O. Popov, "Scotogenic Inverse Seesaw Model of Neutrino Mass", Phys. Lett. **B737**, 280–282 (2014), arXiv:1408.4785 [hep-ph].

[3] S. Fraser, E. Ma, and M. Zakeri, "Verifiable Associated Processes from Radiative Lepton Masses with Dark Matter", Phys. Rev. **D93**, 115019 (2016), arXiv:1511.07458 [hep-ph].

[4] S. Fraser, C. Kownacki, E. Ma, and O. Popov, "Type II Radiative Seesaw Model of Neutrino Mass with Dark Matter", Phys. Rev. **D93**, 013021 (2016), arXiv:1511.06375 [hep-ph].

[5] S. Fraser, E. Ma, and M. Zakeri, "$SU(2)_N$ model of vector dark matter with a leptonic connection", Int. J. Mod. Phys. **A30**, 1550018 (2015), arXiv:1409.1162 [hep-ph].

[6] S. Fraser, C. Kownacki, E. Ma, N. Pollard, O. Popov, and M. Zakeri, "Phenomenology of the Utilitarian Supersymmetric Standard Model", Nucl. Phys. **B909**, 644–656 (2016), arXiv:1603.04778 [hep-ph].

[7] E. Ma, "Verifiable radiative seesaw mechanism of neutrino mass and dark matter", Phys. Rev. **D73**, 077301 (2006), arXiv:hep-ph/0601225 [hep-ph].

[8] G. Aad *et al.* (ATLAS Collaboration), "Observation of a new particle in the search for the Standard Model Higgs boson with the ATLAS detector at the LHC", Phys. Lett. **B716**, 1–29 (2012), arXiv:1207.7214 [hep-ex].

[9] S. Chatrchyan *et al.* (CMS Collaboration), "Observation of a new boson at a mass of 125 GeV with the CMS experiment at the LHC", Phys. Lett. **B716**, 30–61 (2012), arXiv:1207.7235 [hep-ex].

[10] K. A. Olive *et al.* (Particle Data Group Collaboration), "Review of Particle Physics", Chin. Phys. **C38**, 090001 (2014).

[11] E. Ma, "Radiative Origin of All Quark and Lepton Masses through Dark Matter with Flavor Symmetry", Phys. Rev. Lett. **112**, 091801 (2014), arXiv:1311.3213 [hep-ph].

[12] M. Drewes, "The Phenomenology of Right Handed Neutrinos", Int. J. Mod. Phys. **E22**, 1330019 (2013), arXiv:1303.6912 [hep-ph].

[13] S. Willenbrock, "Symmetries of the standard model", in Physics in $D \geq 4$. Proceedings, Theoretical Advanced Study Institute in elementary particle physics, TASI 2004, Boulder, USA, June 6-July 2, 2004 (2004), pp. 3–38, arXiv:hep-ph/0410370 [hep-ph].

[14] M. D. Schwartz, *Quantum field theory and the standard model*, Chap. 30, p. 616 (Cambridge University Press, 2014).

[15] K. Symanzik, in *Fundamental interactions at high energies*, edited by A. Perlmutter *et al.* (Gordon and Breach, New York, 1970).

[16] K. Symanzik, in *Cargese lectures in physics*, Vol. 5, edited by D. Bessis (Gordon and Breach, New York, 1972).

[17] C. Itzykson and J.-B. Zuber, *Quantum field theory*, Chap. 11, p. 547 (Courier Corporation, 2006).

[18] T.-P. Cheng and L.-F. Li, *Gauge theory of elementary particle physics*, Chap. 6, p. 188 (Oxford University Press, 1984).

[19] A. Czarnecki and W. J. Marciano, "The Muon anomalous magnetic moment: A Harbinger for 'new physics'", Phys. Rev. **D64**, 013014 (2001), arXiv:hep-ph/0102122 [hep-ph].

[20] E. Ma and M. Maniatis, "Symbiotic Symmetries of the Two-Higgs-Doublet Model", Phys. Lett. **B683**, 33–38 (2010), arXiv:0909.2855 [hep-ph].

[21] G. Aad *et al.* (ATLAS Collaboration), "Measurements of the Higgs boson production and decay rates and coupling strengths using pp collision data at $\sqrt{s} = 7$ and 8 TeV in the ATLAS experiment", Eur. Phys. J. **C76**, 6 (2016), arXiv:1507.04548 [hep-ex].

[22] V. Khachatryan *et al.* (CMS Collaboration), "Precise determination of the mass of the Higgs boson and tests of compatibility of its couplings with the standard model predictions using proton collisions at 7 and 8 TeV", Eur. Phys. J. **C75**, 212 (2015), arXiv:1412.8662 [hep-ex].

[23] B. Swiezewska and M. Krawczyk, "Diphoton rate in the inert doublet model with a 125 GeV Higgs boson", Phys. Rev. **D88**, 035019 (2013), arXiv:1212.4100 [hep-ph].

[24] S. Kanemitsu and K. Tobe, "New physics for muon anomalous magnetic moment and its electroweak precision analysis", Phys. Rev. **D86**, 095025 (2012), arXiv:1207.1313 [hep-ph].

[25] G. W. Bennett *et al.* (Muon g-2 Collaboration), "Final Report of the Muon E821 Anomalous Magnetic Moment Measurement at BNL", Phys. Rev. **D73**, 072003 (2006), arXiv:hep-ex/0602035 [hep-ex].

[26] M. Benayoun, P. David, L. DelBuono, and F. Jegerlehner, "An Update of the HLS Estimate of the Muon g-2", Eur. Phys. J. **C73**, 2453 (2013), arXiv:1210.7184 [hep-ph].

[27] B. A. Dobrescu, G. D. Kribs, and A. Martin, "Higgs Underproduction at the LHC", Phys. Rev. **D85**, 074031 (2012), arXiv:1112.2208 [hep-ph].

[28] D. Wyler and L. Wolfenstein, "Massless Neutrinos in Left-Right Symmetric Models", Nucl. Phys. **B218**, 205–214 (1983).

[29] R. N. Mohapatra and J. W. F. Valle, "Neutrino Mass and Baryon Number Nonconservation in Superstring Models", Phys. Rev. **D34**, 1642 (1986).

[30] E. Ma, "Lepton Number Nonconservation in $E(6)$ Superstring Models", Phys. Lett. **B191**, 287 (1987).

[31] S. Weinberg, "Baryon- and lepton-nonconserving processes", Phys. Rev. Lett. **43**, 1566–1570 (1979).

[32] E. Ma, "Pathways to naturally small neutrino masses", Phys. Rev. Lett. **81**, 1171–1174 (1998), arXiv:hep-ph/9805219 [hep-ph].

[33] W. Grimus and L. Lavoura, "A Nonstandard CP transformation leading to maximal atmospheric neutrino mixing", Phys. Lett. **B579**, 113–122 (2004), arXiv:hep-ph/0305309 [hep-ph].

[34] E. Ma, "The All purpose neutrino mass matrix", Phys. Rev. **D66**, 117301 (2002), arXiv:hep-ph/0207352 [hep-ph].

[35] K. S. Babu, E. Ma, and J. W. F. Valle, "Underlying A(4) symmetry for the neutrino mass matrix and the quark mixing matrix", Phys. Lett. **B552**, 207–213 (2003), arXiv:hep-ph/0206292 [hep-ph].

[36] E. Ma, "Transformative $A_4$ mixing of neutrinos with CP violation", Phys. Rev. **D92**, 051301 (2015), arXiv:1504.02086 [hep-ph].

[37] E. Ma, "Quark and Lepton Flavor Triality", Phys. Rev. **D82**, 037301 (2010), arXiv:1006.3524 [hep-ph].

[38] V. Khachatryan *et al.* (CMS Collaboration), "Search for Lepton-Flavour-Violating Decays of the Higgs Boson", Phys. Lett. **B749**, 337–362 (2015), arXiv:1502.07400 [hep-ex].

[39] J. Adam *et al.* (MEG Collaboration), "New constraint on the existence of the $\mu^+ \to e^+\gamma$ decay", Phys. Rev. Lett. **110**, 201801 (2013), arXiv:1303.0754 [hep-ex].

[40] U. Bellgardt *et al.* (SINDRUM Collaboration), "Search for the Decay $\mu^+ \to e^+e^+e^-$", Nucl. Phys. **B299**, 1–6 (1988).

[41] L. Feng, S. Profumo, and L. Ubaldi, "Closing in on singlet scalar dark matter: LUX, invisible Higgs decays and gamma-ray lines", JHEP **03**, 045 (2015), arXiv:1412.1105 [hep-ph].

[42] E. Ma, "Radiative Mixing of the One Higgs Boson and Emergent Self-Interacting Dark Matter", Phys. Lett. **B754**, 114–117 (2016), arXiv:1506.06658 [hep-ph].

[43] G. Steigman, B. Dasgupta, and J. F. Beacom, "Precise Relic WIMP Abundance and its Impact on Searches for Dark Matter Annihilation", Phys. Rev. **D86**, 023506 (2012), arXiv:1204.3622 [hep-ph].

[44] J. M. Cline, P. Scott, K. Kainulainen, and C. Weniger, "Update on scalar singlet dark matter", Phys. Rev. D **88**, 055025 (2013).

[45] D. S. Akerib *et al.* (LUX Collaboration), "Improved Limits on Scattering of Weakly Interacting Massive Particles from Reanalysis of 2013 LUX Data", Phys. Rev. Lett. **116**, 161301 (2016), arXiv:1512.03506 [astro-ph.CO].

[46] E. Ma, "Dark Scalar Doublets and Neutrino Tribimaximal Mixing from A(4) Symmetry", Phys. Lett. **B671**, 366–368 (2009), arXiv:0808.1729 [hep-ph].

[47] Y. BenTov, X.-G. He, and A. Zee, "An $A_4$ x $Z_4$ model for neutrino mixing", JHEP **12**, 093 (2012), arXiv:1208.1062 [hep-ph].

[48] E. Ma, "Soft $A_4 \to Z_3$ symmetry breaking and cobimaximal neutrino mixing", Phys. Lett. **B755**, 348–350 (2016), arXiv:1601.00138 [hep-ph].

[49] E. Ma and G. Rajasekaran, "Softly broken A(4) symmetry for nearly degenerate neutrino masses", Phys. Rev. **D64**, 113012 (2001), arXiv:hep-ph/0106291 [hep-ph].

[50] R. de Adelhart Toorop, "A flavour of family symmetries in a family of flavour models", PhD thesis (Leiden U., Leiden, Netherlands, 2012).

[51] G. Altarelli and F. Feruglio, "Discrete Flavor Symmetries and Models of Neutrino Mixing", Rev. Mod. Phys. **82**, 2701–2729 (2010), arXiv:1002.0211 [hep-ph].

[52] E. Ma, "Derivation of dark matter parity from lepton parity", Phys. Rev. Lett. **115**, 011801 (2015).

[53] J. L. Diaz-Cruz and E. Ma, "Neutral SU(2) Gauge Extension of the Standard Model and a Vector-Boson Dark-Matter Candidate", Phys. Lett. **B695**, 264–267 (2011), arXiv:1007.2631 [hep-ph].

[54] S. Bhattacharya, J. L. Diaz-Cruz, E. Ma, and D. Wegman, "Dark Vector-Gauge-Boson Model", Phys. Rev. **D85**, 055008 (2012), arXiv:1107.2093 [hep-ph].

[55] T. Abe, M. Kakizaki, S. Matsumoto, and O. Seto, "Vector WIMP Miracle", Phys. Lett. **B713**, 211–215 (2012), arXiv:1202.5902 [hep-ph].

[56] Y. Farzan and A. R. Akbarieh, "VDM: A model for Vector Dark Matter", JCAP **1210**, 026 (2012), arXiv:1207.4272 [hep-ph].

[57] J. Hubisz and P. Meade, "Phenomenology of the littlest Higgs with T-parity", Phys. Rev. **D71**, 035016 (2005), arXiv:hep-ph/0411264 [hep-ph].

[58] G. Servant and T. M. P. Tait, "Is the lightest Kaluza-Klein particle a viable dark matter candidate?", Nucl. Phys. **B650**, 391–419 (2003), arXiv:hep - ph / 0206071 [hep-ph].

[59] T. Hambye, "Hidden vector dark matter", JHEP **01**, 028 (2009), arXiv:0811.0172 [hep-ph].

[60] S. Baek, P. Ko, W.-I. Park, and E. Senaha, "Higgs Portal Vector Dark Matter : Revisited", JHEP **05**, 036 (2013), arXiv:1212.2131 [hep-ph].

[61] J. Hisano, K. Ishiwata, N. Nagata, and M. Yamanaka, "Direct Detection of Vector Dark Matter", Prog. Theor. Phys. **126**, 435–456 (2011), arXiv:1012.5455 [hep-ph].

[62] D. S. Akerib *et al.* (LUX Collaboration), "First results from the LUX dark matter experiment at the Sanford Underground Research Facility", Phys. Rev. Lett. **112**, 091303 (2014), arXiv:1310.8214 [astro-ph.CO].

[63] Q.-H. Cao, E. Ma, J. Wudka, and C. P. Yuan, "Multipartite dark matter", (2007), arXiv:0711.3881 [hep-ph].

[64] The CMS Collaboration, "Search for new physics in high mass diphoton events in proton-proton collisions at 13 TeV", CMS-PAS-EXO-15-004 (2015).

[65] The ATLAS Collaboration, "Search for resonances decaying to photon pairs in 3.2 $\text{fb}^{-1}$ of $pp$ collisions at $\sqrt{s} = 13$ TeV with the ATLAS detector", ATLAS-CONF-2015-081 (2015).

[66] The CMS Collaboration, "Search for resonant production of high mass photon pairs using 12.9 $\text{fb}^{-1}$ of proton-proton collisions at $\sqrt{s} = 13$ TeV and combined interpretation of searches at 8 and 13 TeV", CMS-PAS-EXO-16-027 (2016).

[67] T. A. collaboration, "Search for scalar diphoton resonances with 15.4 $\text{fb}^{-1}$ of data collected at $\sqrt{s}$=13 TeV in 2015 and 2016 with the ATLAS detector", ATLAS-CONF-2016-059 (2016).

[68] M. Bauer and M. Neubert, "Flavor anomalies, the 750 GeV diphoton excess, and a dark matter candidate", Phys. Rev. **D93**, 115030 (2016), arXiv:1512.06828 [hep-ph].

[69] E. Ma, "New U(1) gauge extension of the supersymmetric standard model", Phys. Rev. Lett. **89**, 041801 (2002), arXiv:hep-ph/0201083 [hep-ph].

[70] E. Ma, "Utilitarian Supersymmetric Gauge Model of Particle Interactions", Phys. Rev. **D81**, 097701 (2010), arXiv:1004.0192 [hep-ph].

[71] E. Ma, "Diphoton Revelation of the Utilitarian Supersymmetric Standard Model", (2015), arXiv:1512.09159 [hep-ph].

[72] S. P. Martin, "A Supersymmetry primer", [Adv. Ser. Direct. High Energy Phys.18,1(1998)] (1997) 10.1142/9789812839657_0001,10.1142/9789814307505_0001, arXiv:hep-ph/9709356 [hep-ph].

[73] S. K. Vempati, "Introduction to MSSM", (2012), arXiv:1201.0334 [hep-ph].

[74] J. Erler, P. Langacker, S. Munir, and E. Rojas, "Improved Constraints on Z-prime Bosons from Electroweak Precision Data", JHEP **08**, 017 (2009), arXiv:0906.2435 [hep-ph].

[75] Y.-L. Tang and S.-h. Zhu, "Vectorlike sneutrino dark matter", Phys. Rev. **D93**, 095006 (2016), arXiv:1604.01903 [hep-ph].

[76] J. Kawamura and Y. Omura, "Diphoton excess at 750 GeV and LHC constraints in models with vectorlike particles", Phys. Rev. **D93**, 115011 (2016), arXiv:1601.07396 [hep-ph].

[77] J. Ellis, S. A. R. Ellis, J. Quevillon, V. Sanz, and T. You, "On the Interpretation of a Possible $\sim$ 750 GeV Particle Decaying into $\gamma\gamma$", JHEP **03**, 176 (2016), arXiv:1512.05327 [hep-ph].

[78] F. Staub *et al.*, "Precision tools and models to narrow in on the 750 GeV diphoton resonance", (2016), arXiv:1602.05581 [hep-ph].